Alma Mater Studiorum - Università di Bologna

DOTTORATO DI RICERCA IN

SCIENZE BIOMEDICHE E NEUROMOTORIE

Ciclo 35

Settore Concorsuale: 05/H1 - ANATOMIA UMANA

Settore Scientifico Disciplinare: BIO/16 - ANATOMIA UMANA

CIRCULATING HSA-MIR-5096-5P PREDICTS 18F-FDG PET/CT AND MODULATES
SOMATOSTATIN RECEPTOR-2 EXPRESSION: A CANDIDATE BIOMARKER FOR
PANCREATIC NEUROENDOCRINE TUMORS

Presentata da: Martine Bocchini

Coordinatore Dottorato

Matilde Yung Follo

Supervisore

Massimiliano Mazza

Co-supervisore

Matilde Yung Follo

Esame finale anno 2023

Abbreviations:

ANC: Absolute Neutrophil Count

AUC: Area Under the Curve

CT: Computed Tomography

^{18}F-FDG: 2-deoxy-2-[fluorine-18]fluoro-D-glucose

ENETS: European Neuroendocrine Society

F.E.: Fold Enrichment

GEP-NETs: Gastro-entero-pancreatic NETs

HR: Hazard Ratio

IVD: In Vitro Diagnostic

IHC: Immunohistochemistry

ISH: In situ Hybridization

KM: Kaplan-Meier

NENs: NeuroEndocrine neoplasms

NETs: NeuroEndocrine Tumors

NGS: Next Generation Sequencing

95%CI: 95% confidence interval

OS: Overall Survival

PanNETs: Pancreatic NETs

PD: Progressive Disease

PET: Positron Emission Tomography

PFS: Progression-Free Survival

PCA: Principal Component Analysis

PRRT: Peptide Receptor Radionuclide Therapy

ROC: Receiver Operating Characteristic

RT/qRT/QPCR: Real Time quantitative RT/QPCR

SINETs: Ileal NETs

SSTR: Somatostatin receptor

SUV_{max}: maximum standardized uptake value

3'-UTR: 3'-Untranslated Region

WHO: World Health Organization

Table of contents

Abstract

Gastro-entero-pancreatic neuroendocrine tumors (GEP-NETs) are rare diseases encompassing pancreatic (PanNETs) and ileal NETs (SINETs) and characterized by heterogeneous somatostatin receptors (SSTRs) expression. Treatments for inoperable GEP-NETs are limited, and SSTR-targeted Peptide Receptor Radionuclide Therapy (PRRT) achieves variable responses. Prognostic biomarkers for the management of GEP-NET patients are required. ^{18}F-FDG uptake is a prognostic indicator of aggressiveness in GEP-NETs. This study aims to identify circulating and measurable prognostic miRNAs associated with ^{18}F-FDG-PET/CT status, higher risk, and lower response to PRRT. Whole miRNOme NGS profiling was conducted on plasma samples obtained from well-differentiated advanced, metastatic, inoperable G1, G2 and G3 GEP-NET patients enrolled in the non-randomized clinical trials prior to PRRT (screening set, n= 24). Differential expression analysis was performed between ^{18}F-FDG positive (n=12) and negative (n=12) patients. Validation was conducted by Real-Time quantitative PCR (RT/qPCR) in two distinct well-differentiated GEP-NET validation cohorts, considering the primary site of origin (PanNETs n=38 and SINETs n=30). The Cox regression was applied to assess independent clinical parameters and imaging for progression-free survival (PFS) in PanNETs. In situ RNA hybridization combined with IHC was performed to simultaneously detect miR and protein expression in the same tissue specimens. This novel semi-automated miR-protein protocol was applied in PanNET FFPE specimens (n=8). In vitro functional experiments were performed in PanNET models. A three *miR-signature* (hsa-miR-5096-5p, hsa-let-7i-3p and hsa-miR-4311) was found to correlate with 18F-FDG-PET/CT in PanNETs (p-value:<0.005), thus with tumor metabolism. Statistical analysis has shown that, hsa-miR-5096-5p can distinguish PanNET from SINET patients, predict 6-month PFS (p-value:<0.001) and 12-month Overall Survival upon PRRT treatment (p-value:<0.05), as well as identify 18F-FDG-PET/CT positive PanNETs with worse prognosis after PRRT (p-value:<0.005). Moreover, the statistical analysis revealed that the three-miRNA signature and combined "Predictors" significantly correlates with several clinical parameters (ki-67%; tumor burden and grading). In addition, hsa-miR-5096-5p inversely correlated with both SSTR2 expression in PanNET tissue and with the 68Gallium-DOTATOC captation values (p-value:<0.05), and accordingly it was able to decrease SSTR2 when ectopically expressed in PanNET cells (p-value:<0.01).

The identified three miRNA signature and combined "Predictors" well performs as a biomarker for 18F-FDG-PET/CT status. Hsa-miR-5096-5p is the best candidate biomarkers, since it is expressed both in PanNETs and SINETs and it can distinguish the tumor site of origin and it can be considered an independent predictor of PFS. Moreover, exosome-mediated delivery of hsa-miR-5096-5p may

promote SSTR2 heterogeneity and thus resistance to PRRT. Hence, Hsa-miR-5096-5p interference can be considered as novel therapeutic strategy to sensitize tumor cells to PRRT.

1. Introduction

Gastro-entero-pancreatic neuroendocrine neoplasm (GEP-NENs) are rare and heterogeneous malignancies of epithelial origin arising from cells of diffuse neuroendocrine system. Neuroendocrine disease exhibits variable aggressiveness depending on the site of origin, grade, stage, and functionality (1,2). Among GEP-NENs, pancreatic (PanNENs) show worst prognosis and their outcome is negatively influenced by a deficit of early stage biomarkers and a lack of therapeutic options which are the themes explored by this thesis.

1.1 Gastro-entero-pancreatic neuroendocrine neoplasms (GEP-NENs) biology and epidemiology

1.1.1 Incidence and prevalence of PanNENs

PanNENs are low incidence rare diseases, accounting for about 3% of overall pancreatic malignancies and 8.1% of total NEN cases, but their prevalence is rising (SEER 18) (2-4). PanNENs displaying metastases at diagnosis represent about 60 to 80% of overall PanNEN cases (5).

PanNENs can be classified into functioning (F-PanNENs) from non-functioning neoplasms (NF-PanNENs). Indeed, PanNEN cells can secrete active hormones associated with specific symptomatology resulting in F-PanNEN development. PanNENs can arise as sporadic tumors or in the context of hereditary syndromes, such as multiple endocrine neoplasia type 1 (MEN1) which represent the most common syndrome resulting in PanNEN development in 10% of cases (1-9). Von Hippel–Lindau disease (VHL), neurofibromatosis -1 (NF-1), and tuberous sclerosis (TS) (6-8) are also associated with PanNENs.

1.1.2 Genetic Alterations Promoting PanNENs

Germline and sporadic mutations of PanNEN disease has been mainly identified on the basis of genetic syndromes associated with endocrine neoplasm. Genetic syndromes with recurrent germline mutated genes such as *MEN, VHL, NF1*, and *TS* (2) have been demonstrated to be present in about 10% of all NENs (6). Currently, cyclin-dependent cell cycle regulation and the PI3K/mTOR pathway

9

has been identified as main pathways in PanNENs development associated to MEN-1 and MEN-1, VHL, NF-1, TS sindromes, respectively.

Multiple endocrine neoplasia type 1 (MEN-1) is an autosomal dominant disease, caused by germline-inactivating mutations in the *MEN-1* gene (10, 11) and by somatic loss of the normal allele (12). *MEN-1* can be considered a key regulator in NET biology (13-19) as *MEN- 1* gene alterations have been identified in PanNEN in 60% of patients with MEN-1 syndrome (20) and in 44% of sporadic PanNENs (21). *MEN-1* loss affects a large number of cellular activities, including (a) histone methylation and expression of the CDKN2C/CDKN1B cell cycle inhibitors (22); (b) PI3K/mTOR signaling via Akt (23); (c) homologous recombination (HR) through interactions with DNA repair complexes (e.g., *RAD51* and *BRCA1*; 24, 25). In addition, *MEN-1* mutations have been associated with loss of P27 as an early alteration in NENs development (26).

Von Hippel–Lindau disease, caused by inactivating mutations of the *VHL* gene, which is observed to be inactivated by deletion or methylation also in 25% of sporadic PanNENs (27). *VHL* impairment leads to the activation of the hypoxia induced pro-proliferative signaling (28, 29).

Neurofibromatosis type I disease derives from germline mutations of *NF1* that are associated with NENs development in 10% of patients affected by the syndrome. NF1 protein product is a negative regulator of PI3K/mTOR pathway which holds a key role in NENs tumorigenesis (30). Nevertheless, *NF1* has been rarely reported to be mutated in sporadic PanNENs (27).

Tuberous Sclerosis Complex (TSC), promoted by inactivating mutations in TS lead to TSC syndrome and to sporadic PanNETs in 35% of cases (27). This is caused by inactivation of *TSC1* and *TSC2*, thus inhibiting PI3K/mTOR signaling downstream of AKT1 (31).

Chromosomal and Epigenetic Alterations drive the origin of neuroendocrine transformation in about 50% of cases. There are four PanNENs subtypes, based on chromosomal alterations, according to CNV analysis and whole-genome sequencing (32, 2): (i) chromosome 11q loss (*MEN1* involment); (ii) Recurrent Pattern of whole Chromosomal Loss (RPCL) phenomenon in association with higher mitotic index; (iii) ALT and (iv) ATRX/DAXX inactivation (33, 34–38). In addition, whole-genome mutational analysis, identified 10% of germline mutations in base-excision repair (*MUTYH*) and homologous recombination repair of *BRCA2* and *CHEK2* (13, 31). Epigenetic modification which drives PanNENs development highlights three transcriptional subtypes, resembling A (alpha) or B (beta) cells, enriched for specific mutational profiles, and with prognostic relevance (39;40) and

related to the key pathways of NENs disease: (i) chromatin remodeling pathway results in MEN1-like tumors, (ii) PI3K/mTOR pathway in insulinoma-like tumors and (iii) hypoxia- related pathway drives metastasis-like primary tumors cluster (41). Hyper-methylation of *RASSF1A*, *HIC-1*, *CDKN2A*, *VHL*, and *MGMT* are also found to promote PanNENs (2). In contrast, hypo-methylation of *ALU* and *LINE1*, has been associated with poor prognosis and chromosomal instability (42, 43, 44).

Key genetic alterations have been identified to drive neuroendocrine cells toward PanNETs differentiation or pancreatic neuroendocrine carcinomas (PanNECs), regardless of the grading (45-47). RB1 is a key negative regulator of the cell cycle via p16 and other proteins and it has been reported in 20–44% PanNECs (48, 49-52), while ***TP53* inactivation and/or P53** protein nuclear accumulation have been identified in 20-70% and 65-100% of PanNECs, respectively (2; 53-55). *TP53* and *RB1* combined loss has been confirmed to be driver mutation of PanNECs, representing the 7, 5% of all PanNENs (48). Indeed, PanNECs can be distinguished from G3 NETs with higher Ki-67 percentage and proliferation index, which do not display these mutations (48;56-58). This tumor phenotype is associated with *MEN-1* (10–36%) and/ or *DAXX/ATRXX* (9– 25%) mutations or protein impaired expression (59, 60). Indeed, ATRX and *DAXX* mutations located in the chromatin remodeling compartment (13) or ***ATRX/DAXX* loss** have been identified as driver mutations of PanNETs phenotype in about 23% of cases. In addition, alterations of *ATRX/DAXX* affect PTEN and PI3K/mTOR downstream pathways (13; 32; 61, 62), lead to ALT phenomenon, chromosomal instability and higher tumor stage suggesting this mutation is a late event in the neoplastic transformation (63-65). These alterations, in particular *RB1/TP53* loss, are crucial for diagnosis and prognosis to distinguish NECs from advanced G3 PanNETs, where morphology and immunostaining can be often unreliable markers (46; 60; 66-68). Overview of emerging neuroendocrine tumor features based on genetic and epigenetic signatures is summarized in **Table 1**.

	Non-functional PanNET 1	Non-functional PanNET 2	Non-functional PanNET 3	Insulinoma 1	Insulinoma 2	Insulinoma 3*
Epigenetic similarities	A cell-like	A cell-like > B cell-like	B cell-like/other	B cell-like	B cell-like	A cell-like > B cell-like
Epigenetic signature	Well differentiated	Dedifferentiated	Unknown	Well differentiated	Well differentiated	Dedifferentiated?
MEN1	+ +	+ + +	±	-	−	u
ATRX/DAXX	+	+ + +	-	-	−	+ +
YY1	−	−	−	+ + +	−	u
mTOR	+	+ + +	+	-	−	u
Copy number profiles	Neutral	Amplifications/deletions	Neutral	Neutral	Recurrent amplification[#]	u
Predominant grade	G1	G2	G1	G1	G1	G2
Mean size	3 cm	4 cm	3 cm	<2 cm	<2 cm	>3 cm
Prognosis	Favorable	Poor	Favorable	Favorable	Favorable	Poor

Table 1 Emerging PanNET features based on genetic and epigenetic signatures

PanNET, pancreatic neuroendocrine tumor; G, World Health Organization grade; u, undetermined/unknown [*]Possibly the same as non-functional panNET-2 with acquired symptomatic insulin production [#]In particular chromosome 7 amplifications. From Rindi G, et al. (40)

1.1.3 WHO classification updates: novel molecular classifications for PanNENs

NENs of the digestive tract arise from different organs and epithelial tissues and include heterogeneous entities with different etiologies, morphological aspects, molecular phenotypes, and clinical behaviors. PanNENs, as well, show indolent nature, and wide spectrum of clinical behavior; this prognostic heterogeneity has been defined by the World Health Organization (WHO) classification system. WHO classification is based on cellular proliferation (measured as mitotic count and Ki-67 expression; see **Table 2**) and its 5th edition update concerns classification of tumors of the digestive system including NENs. In addition, the American Joint Committee on Cancer (AJCC), the European Neuroendocrine Tumor Society (ENETS) and the World Health Organization (WHO) identified three independent PanNEN staging systems (2; 40; 69-72).

WHO 2017	G	Mitoses 10 HPF*	Ki-67 Index*	Genetic background	Neoplastic evolution•	8th AJCC/UICC—ENETS consensus for pan NET staging	
Well-differentiated NENs							
NET	G1	< 2	< 3	*ATRX*	G1-G2		
	G2	2-20	3 – 20	*MEN-1*	↓↓	T stage	
	G3	>20	> 20	*DAXX*	G3	T1	Confined to pancreas*, <2 cm
					↓	T2	Confined to pancreas*, 2-4 cm
Poorly-differentiated NENs					↓	T3	Confined to pancreas*, >4 or duodenum or bile duct invasion
NEC	G3	> 20	> 20	*RB*	NEC	T4	Invasion of vessels and contiguous organs
				Tp53			
MiNEN**	G1-G3	NET/NEC + ADC/SCC		Mixed features			

Table 2 WHO grading and 8th AJCC/UICC—ENETS consensus summary for PanNENs

WHO, World Health Organization; NEN, Neuroendocrine Neoplasm; NET/C, Neuroendocrine Tumour/Carcinoma; HPF, Hight Power Field; AJCC, American Joint Committee on Cancer; ENETS, European Neuroendocrine Tumour Society; UICC, Union for International Cancer Control; ADC, Adenocarcinoma; SCC, Squamous cell Carcinoma.
*•Neoplastic evolution Current classification considers the possibility of an evolution with time of a well-differentiated G1-G2 NEN to a higher G3 and, even more rarely, toward a poorly differentiated NEC (13). **MiNENs (Mixed-NENs): may contain of non- neuroendocrine components (e.g., adeno or squamous) and neuroendocrine ones (at least 30% for each component) (11). *Specific parameters for PanNET according to 8th AJCC/UICC-ENETS consensus. From Bocchini M, et al. (2)*

Current classification and the grading novel system for GEP-NENs basically stem from 2017 WHO classification of PanNENs, where well-differentiated NENs are defined as Neuroendocrine Tumors (NETs) regardless the grading, designing three new categories: i) well-differentiated G1 and G2 NETs and ii) well/less - differentiated G3 NET with high Ki-67/mitotic index higher ki-67 % (< 20%); and iii) carcinomas (NECs) , which are G3 and poorly differentiated by definition with poor prognosis and (2, 4; 71, 72). NECs can be further classified on their morphology into large cells (LCNEC) and small cells (SCNEC) (73,74). Finally, a fourth category of mixed tumors (MiNENs) with neuroendocrine and non-neuroendocrine features, has been described (75;76). General features of NENs, including PanNENs, according to most recent updates of WHO 2022 (40) are summarized in **Table 3**.

	Cytology	Histology	IHC profile
NET	Clean smear	Organoid structure (solid, trabecular, glandular, mixed)	CK+
	Cell monomorphism	No necrosis or only spotty	CgA+
	Medium size, round shape	Delicate, highly vascularized stroma	Syn+
	Abundant eosinophilic cytoplasm	Cell monomorphism	INSM1+
	Salt and pepper chromatin	Low nuclear/cytoplasm ratio	SSTR2/5+
	No or very few mitotic figures	Round-oval shape	Hormones+*
		Abundant cytoplasm	Ki67 low
		Salt and pepper chromatin	p53 wild-type staining
		Rare or few mitoses	Rb retained
NEC	Dirty smear—diffuse necrotic debris	Solid/organoid structure	CK+/−(dot-like)
	Cell polymorphism	Abundant necrosis	CgA+/−
	Absent or subtle rim of cytoplasm (SC type)	Abundant fibrous stroma	Syn+
	Evident/abundant cytoplasm (LC type)	Severe cell polymorphism	INSM1+
	Severe nuclear fragility	Round-irregular shape	SSTR2/5−/+
	Salt and pepper chromatin	High nuclear/cytoplasm ratio	Hormones−
	Frequent mitoses often atypical	Scant cytoplasm (SC type)	Ki67 high/very high (typically > 55%)
		Abundant cytoplasm (LC type)	p53 global loss or diffuse positive
		Severe nuclear molding	Rb global loss
		Salt and pepper chromatin	
		Frequent mitoses, often atypical	

Table 3 General features of well-differentiated NETs and PanNETs and poorly differentiated NECs.

*IHC, immunohistochemistry; NET, neuroendocrine tumor; NEC, neuroendocrine carcinoma; SC, small cell; LC, large cell; CK, cytokeratins; CgA, chromogranin A; Syn: synaptophysin; INSM1, insulinoma-associated protein 1; SSTR, somatostatin receptor; *: various, depending on ana- tomical site; p53, Tp53 gene product; Rb, retinoblastoma gene product. From Rindi G, et al. (40)*

The ENETS staging system for PanNENs is based on TNM classification, (3,45) whereas the AJCC draws PanNENs staging on the TNM staging for pancreatic adenocarcinoma (7; 70); Table 2). Few updates for PanNENs, recommends to re-name the "microadenoma" small lesions < 0.5 cm to "neuroendocrine microtumor", since rare cases can promote lymph node invasion (77-79).

As previously reported, beside grading, staging and morphology the novel classification includes molecular driver alteration for PanNEN disease. Indeed, well-differentiated G1 to G3 NETs are defined by *ATRX* and *DAXX* mutations or loss (13); while PanNECs are characterized by *TP53* and *RB1* combined loss. This important update is crucial to facilitate differential diagnosis and prognosis between PanNECs and G3 NETs with higher Ki-67 percentage and proliferation index (46; 60; 66-68). Latest updates extended this molecular classification to NENs of non-endocrine organs leading to a unified approach to classify epithelial NENs from different sites of origin, despite of organ-specific variability (40; 75).

Nowadays, PanNETs can be diagnosed earlier and updated therapeutic algorithms and guidelines have been proposed. Despite novel classification helps the stratification of patients, improving prognosis and response to treatment, substantial differences in clinical behavior and biology still remain, making personalized treatment and prognostication challenging for advanced PanNETs

Over the past two decades, available therapeutic options for patients with advanced PanNETs have been expanded. Systemic treatments for patients with well-differentiated PanNETs include somatostatin receptors ligands (SRLs), peptide receptor radiotherapy (PRRT), cytotoxic chemotherapy regimens, and biologically targeted therapies, in contrast with patients with poorly differentiated NEC. Peptide receptor radionuclide therapy (PRRT), targeting SSTR2, has shown cytoreductive potential and prolonged disease progression-free survival (PFS) in patients with unresectable metastatic disease (17,18). Although PRRT extends PFS, about 15–30% of patients with advanced well-differentiated GEP-NETs progress during treatment or six months to one year after PRRT (19–22). Future optimization of PRRT will depend on improved patient stratification (23,24). Despite these improvements, no clear guidelines exist to address the best treatment schedule. Advances in molecular research and discovery of biomarkers for response allowing a more personalized approach to the multimodality therapy of panNENs are still limited.

In absence of predictive markers and paucity of comparative randomized trials, along with the heterogeneity of PanNENs population, systemic therapy selection in advanced non-resectable disease should be improved thought multidisciplinary approach. The specific clinical context of the patient, with assessment of individual patient clinical and pathological features, SSTRs imaging, must all be considered to address treatment decision making.

1.2 Clinical management of PanNETs: diagnostic and prognostic algorithms

Correct diagnosis and accurate staging are of primary importance for cancer patients and the use of biomarkers can be crucial for tailored treatments. Ideally, biomarkers should display high sensitivity and specificity in predicting tumor aggressiveness (prognostic biomarker) and/or response to treatment (predictive biomarker; 91). In this context, a multi-disciplinary and multi-analyte approach can impact patients' survival, taking into consideration clinical, biochemical, histological, and molecular features of the disease (92). Several clinical parameters, such as tumor localization, size, grade and stage, vascularization, presence of necrotic tissue and the presence of metastases, affect the overall survival (OS) of NENs patients (93, 94). According to the primary tumor site, gastrointestinal

NENs and PanNENs should be separately managed due to their different aggressiveness and clinical behaviors (95; 96).

1.2.1 Functional imaging

Over the years, nuclear medicine has played a central role in the diagnosis of NENs (95). The diagnostic work-up of NENs is based on radiological and nuclear medicine assessment by means of computed tomography (CT) and magnetic resonance imaging (MRI).[68]Gallium-DOTA-somatostatin analogs-positron emission CT (^{68}Ga-DOTA-SSA-PET/CT) and, in selected patients, 2-deoxy-2-[fluorine-18] fluoro-D-glucose (^{18}F-FDG) PET/CT. Recently, radiomics approaches have been suggested as a promising diagnostic and prognostic tool able to predict tumor behavior and patients' clinical outcomes (95; 97).

1.2.1.1 68Gallium-SSA-PET/CT (68Ga-DOTA-SSA-PET/CT) The identification of somatostatin (SST) in 1973, and the discovery of the five somatostatin receptor isoforms (SSTR1 to SSTR5) in the 1990s, provided relevant theragnostic opportunities. Somatostatin receptors (SSTRs) are widely distributed in healthy tissues, with distinct expression throughout the body, but significantly overexpressed in many human solid tumors, especially in GEP-NENs (95; 98 - 102). Since native SST shows poor in vivo stability, synthetic SSA are being developed to improve stability and metabolic properties (103-106). SSTRS scintigraphy (SRS) with 111In-pentetreotide or OctreoScan was the first peptide-based radiopharmaceutical that has been approved by the FDA, in 1994 (Octreoscan®). The internalization and retention mechanism of the radioligand-receptor complex allows SST imaging. Despite the advantages for NENs diagnosis, SRS has many limitations, such as diminished tumor/noise intensity ratio, low spatial resolution, moderate affinity for receptors, and high γ energy, resulting in a high dose of radioactivity and toxicity for the patient. For these reasons, SRS has been replaced by novel radiopharmaceuticals such as next generation of SSA labeled with the positron-emitter radiometal 68Ga, developed for clinical use with PET/CT (103-108). In clinical practice, three 68Ga-labeled radiopharmaceuticals with different pharmacokinetic properties and different affinities for SSTRs subtypes, are available: 68Ga-DOTA-Phe1-Tyr3-Octreotide (DOTA-TOC), 68Ga-DOTA-NaI3-Octreotide (DOTA-NOC), and 68Ga-DOTA-Tyr3-Octreotate (DOTA-TATE) [16]. 68Ga-DOTA-TATE is specific to SSTR2, 68Ga-DOTA-TOC shows higher affinity for SSTR2 and moderate for SSTR5, and 68Ga-DOTA-NOC binds with comparable affinity to SSTR2, SSTR3, and SSTR5 (109-113). Currently, molecular functional imaging with (PET/CT) is used in PanNETs management and updated European Neuroendocrine Society (ENETS) consensus on

Radiological, Nuclear Medicine & Hybrid Imaging recommended 68Ga-DOTA-SSA-PET/CT for tumor staging, preoperative imaging, and re-staging, follow-up, prognostic evaluation, therapy decision-making and monitoring (114, 115). Moreover, imaging with 68Ga-DOTA-SSA-PET/CT shows the highest sensitivity (86–100%) and specificity (79–100%) in localizing PanNENs, as well as other NENs and it has been shown to improve clinical management in 20–55% of patients (96). Although the sensitivity and specificity of SSTR2-specific ^{68}Ga-DOTATOC-PET/CT has been proven, its clinical utility is hampered by heterogeneous SSTR2 expression. Indeed, heterogeneous to low levels of SSTR2 expression challenge ^{68}Ga-DOTA-SSA-PET/CT sensitivity (115), thus eligibility to SSTR2-based therapies, such as Peptide receptor radionuclide therapy PRRT (90,116). Indeed, 68Ga-DOTA-SSA PET/CT shows lower sensitivity in detecting insulinoma compared to other NENs, due to its SSTRs low expression (25–30%) (117, 118), thus making diagnostic work-up challenging (119, 120). Importantly, despite insulinomas being generally benign conditions, about 5–15% of patients display malignant phenotype, characterized by distant metastases, lymph node involvement and direct invasion into surrounding peri-pancreatic tissue, or presence of lymphatic and vascular invasion. Nevertheless, differently from benign insulinomas, malignant insulinomas express SSTRs (121), representing a potential candidate for PRRT therapy (122-123).

Despite high SSTR2 expression can be considered an appropriate predictor of response to PRRT, PET/CT scan with ^{68}Ga-DOTA-SSA alone does not represent a prognostic parameter in terms of PFS (25). Indeed, the basal assessment of the normal biodistribution of the radiopharmaceutical is crucial. In particular, the pancreas can show a variable shade of physiological uptake in the pancreatic uncinate process, during inflammation or hyperplasia and into the intrapancreatic accessory spleen both with a diffuse and focal pattern of distribution (**Figure 1**; 96; 123).
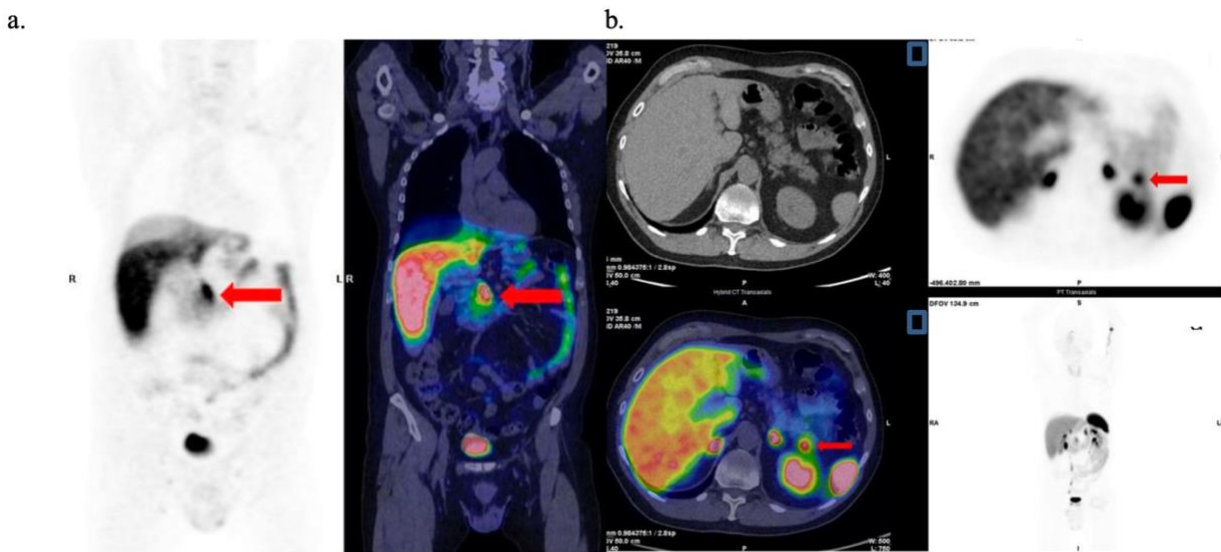
Figure 1 ^{68}Ga-DOTA-TOC PET/CT coronal images and ^{68}Ga-DOTA-TOC PET/CT transaxial images: non-specific uptake.

(a)The red arrows show physiological uptake in the pancreatic head/uncinate process; (b) intrapancreatic spleen: Low-dose CT: PET image-fused PET/CT and maximum intensity projection (MIP). The red arrows in images show focal uptake in the pancreatic tail while restaging patient for small bowel NET (G2, Ki67 3%). Adapted from Prosperi D., et al. (96)

Therefore, functional imaging images must be correctly compared with conventional imaging methods, such as CT or MRI, to achieve sensitivity and specificity for an accurate diagnosis. Artifacts frequent in this abdominal region and can contribute to misinterpretation of pancreatic findings obtained with functional imaging. For those reasons, the pancreatic uptake, displayed by intravenous administration of contrast compounds, should be carefully compared with morphology and conventional imaging methods, such as CT or MRI. Despite the difficulties of data interpretation, ^{68}Ga-DOTA-SSA-PET/CT has improved in the diagnosis of NENs and currently, represents the gold-standard imaging for NENs as well as the method of choice for staging and localization of the disease in patients with non-insulinoma panNENs (96).

1.2.1.2 Deoxy - 2- [fluorine – 18] – fluoro – D - glucose - PET/CT (18F-FDG-PET/CT) is also recommended for high grade well-differentiated GEP-NETs as companion of Somatostatin Receptor based functional Imaging (SRI). ^{18}F-FDG is a glucose analogue retained by neoplastic cells in proportion to their glucose metabolic activity and represents the main radiopharmaceutical used in PET imaging for oncologic management (49). Although 18F-FDG PET/CT has been suggested as an

effective tool for PanNENs management, it still represents a critical issue, especially for the assessment of low-grade tumors (G1- G2 Ki-67 < 10%). Indeed, most panNENs are well-differentiated lesions, characterized by i) SSTRs overexpression at the cell membrane; ii) low Ki-67 and proliferation index and iii) usually do not display increased metabolic pathways. However, disease's progression may lead neoplastic cells to: i) dedifferentiation; SSTRs pattern loss and iii) glucose metabolism increase (50). Guidelines form the European Association of Nuclear Medicine (EANM) and the European Neuro-Endocrine Tumor Society (ENETS) (22, 27, 51) suggest the use of 18F-FDG PET/CT in higher-grade G2 (Ki-67: 10–20%) and G3 NETs and in NECs, which generally show higher glucose metabolism and 18F-FDG avidity. The European Society for Medical Oncology (ESMO) guidelines, published in 2020 (124), included both 18F-FDG and 68Ga-DOTA-SSA-PET/CT assessments as the optimal diagnostic and prognostic work-up for NEN G2–G3 patients. Thus, increased glucose uptake indicates presence of more aggressive clones and correlates worse prognosis, aggressive tumor behavior and resistance to PRRT even in low grade, well-differentiated PanNETs (130) improve patient clinical management (125 – 128) while well-differentiated SINETs, for example, typically show less pronounced uptake of radiolabeled glucose and lower sensitivity at 18F-FDG-PET/CT scan (125). Recently, Magi et al. (126) showed 18F-FDG PET/CT correlated with a worse prognosis and can stratify high-risk patients, who may benefit from more aggressive treatments also in well-differentiated G1 and low-grade G2 (Ki-67 < 10%) setting. Given this, an 18F-FDG scan can be useful for prognostic purposes in GEP-NET G1–G2 where its sensitivity ranges between 40% and 60%, while it increases up to almost 95% in G3 tumors (93,129). Using a combined approach, NENs different features can be defined: 68Ga-DOTA-SSA-PET/CT can provide information about the expression of SSTRs, thus grading, tumor differentiation and personalized therapies assessment. Conversely, 18F-FDG PET/CT can drive prognosis, providing useful information for risk stratification. Indeed, when increased tumor aggressiveness is suspected in patients with well-differentiated metastatic NETS, 18F-FDG PET/CT scans should be always performed. Given this, although the visual assessment provided by functional imaging uptakes is very useful in clinical management of GEP-NENs, including PanNENs, it remains a qualitative assessment. Indeed, despite it is supported by some semi-quantitative parameters such as Maximum and Mean standardized uptake value (SUVmax and SUVmean, respectively) and, more recently, Total Lesion Glycolysis (TLG) and Metabolic Tumor Volume (MTV), their prognostic value in NENs has not been accurately validated yet (125, 126). For those reasons there is still a clinical need for measurable and monitorable prognostic and predictive biomarkers which can supplement grade,

stage, and imaging, improving patient stratification to address more tailored treatments for PanNETs (2).

1.2.2 PanNEN non-specific biomarkers

Biochemical assessment represents the first-line instructive work-up from a diagnostic and prognostic purposes for NENs disease (131). However, the use of the growing number of biochemical tests available must be evidence-driven. Despite quantitative measurement of serum chromogranin A, and the 24-h urinary 5-HIAA metabolite of serotonin are validated and still informative; the performance, yield, and accuracy of circulating metabolites measurements suffers from some limitations. Limitations in measuring peptides in the blood or urine can include availability of the test or its cost. Alternatively, the confounding effect of physio-pathological conditions or interfering medications can prevent reliable assessment. Neuroendocrine markers for biochemical assessment of NENs can be divided into two main groups: non-specific markers that are virtually produced by all NENs (132) and specific markers that are largely produced by Functioning (F-NENs; **Table 4**). Non-specific PanNET biomarkers include chromogranin-A (CHGA), Neuron Specific Enolase (NSE), Pancreatic Polypeptide (PP), Human Chorionic Gonadotropin (HCG), and Alpha Fetoprotein (AFP; **Figure 2**). Biochemical evaluation of these analytes can be achieved from serum/plasma of patients with suspected NENs. Aberrant levels of such non- specific markers drive further diagnostic tests (2).

Biochemical markers			Source	Level	Sens. (%)	Spec. (%)	Combinations improving sens./spec.	Clinical use	References
Non–specific	Chromogranin A	CHGA	Serum	63–14.750 ug/l	60–83	72–85	NSE; PP	For diagnosis and follow up in GEP-NENs and treatment monitoring	(20, 21) (22, 23)
	Neuron-specific enolase	NSE	Plasma	5–92 ug/l	33	73	CHGA	For diagnosis and follow up in GEP-NENs and treatment monitoring	(20, 21) (22, 23)
	Pancreatic-Polipetide	PP	Plasma	480–780 pg/ml	31-63	67	CHGA	For diagnosis and follow up in PanNENs	(23)
	Human Corionic Gonadotropin	HCG	Serum	Increased	na	Na	AFP; CHGA; PP; HCG	Indicative of pancreatic origin	(24)
	Alpha Fetoprotein	AFP	Serum	Increased	na	Na	HCG; CHGA; PP	Indicative of pancreatic origin and de-differentiation	(25, 26)
Specific	Gastrin	GAS	Serum	≥300 pg/mL	94	100	MEN-1; ZES	Diagnostic for Gastrinoma of pancreatic origin	(24, 27)
	Insulin	INS	Serum/ Plasma	≥43• pmol/L	52 - 94	92–100	Whipple's triad	Diagnostic for Insulinoma; suggesting for WD NETs.	(28)
	Glucagon	GCG	Plasma	500–1000 pg/mL	High	High	-	Diagnostic for Glucagonoma; suggesting for WD NETs; Indication for liver metastases	(24)
	Somatostatin	SST	Plasma	Increased°	na	Low	SSoma syndrome°	Diagnostic for SSoma of pancreatic origin;	(24)
	Vasoactive Intestinal Peptide	VIP	Serum/Plasma	75•–200 pg/dL	na	na	Verner Morrison	Diagnostic for ViPoma of pancreatic tail origin.	(29)

Table 4 Overview of biochemical biomarkers for PanNEN diagnosis, prognosis, and treatment monitoring.

PanNENs, Pancreatic Neuroendocrine Neoplasia;GEP-NENs,Gastro-Entero-Pancreatic Neoplasia; WDNETs, welldifferentiatedtumors; Sens.,sensibility;Spec., specificity.•Diagnostic serum/plasma level in association with specific syndrome. ◦Somatostatin increase is very a-specific, increase SS level with SSoma syndrome is suggesting for GEP-NENs. From Bocchini M., et al. (2)

Chromogranin-A (CHGA) is a glycoprotein secreted by neurons and neuroendocrine cells, which is a precursor of bioactive pancreastatin, and vastatins I and II (133). Although all members of the granins family can be secreted by NETs, CHGA is the only one validated for clinical practice. CHGA has a high sensitivity (134) and good specificity (132). Retrieval of increased CHGA in plasma or serum (two to three-fold increase) provides reliable evaluations of tumor progression (135), presence of metastases, tumor burden and response to treatment in PanNETs. Indeed, CHGA decrease in serum can be considered a surrogate marker for treatment efficacy. However, despite CHGA represents a marker for NENs differentiation, also for non-neuroendocrine site of origin; several patho-physiological such as, food intake non-neoplastic endocrine diseases factors can affect diagnosis. For

patients affected by concomitant conditions, CHGA assay specificity may decrease up to 50% and CHGA should be never considered a first-line screening tool (2). Despite the above-mentioned limitations, up to now CHGA is the most used liquid biomarker not only in the diagnosis but also during the follow-up of NEN patients.

Neuron Specific Enolase (NSE) is an enzyme found in neurons and neuroendocrine cells. Even if only 30 to 50% of NENs produce NSE (134, 135) this marker increases in high-grade GEP-NENs (38–40%), including PanNETs also representing a prognostic marker of tumor aggressiveness (136). Indeed, NSE levels have been associated with tumor differentiation, aggressiveness, and size (136, 137) and it was found to correlate with shorter overall survival (OS) and progression-free survival (PFS). NSE has low sensibility but relatively high specificity (see Table 4) since it can be overexpressed by several non-NETs, such as parathyroid cancer, prostate carcinoma, neuroblastoma. For this reason, NSE alone is rarely used for diagnostic purposes or to distinguish NENs from non-endocrine tumors. Up to date, there is no robust evidence of the predictive role of NSE in predicting therapy efficacy and monitoring patients during follow-up. On the other hand, increased CHGA/NSE provide prognostic information on PFS and survival in patients with advanced PanNET treated with the mTOR inhibitor Everolimus (2). Evaluation of both NSE and CHGA concentration increases the reliability of NEN diagnosis; however, given the non-specific nature of these markers, they do not provide information on the primary tumor site and its origin (2).

Pancreatic Polypeptide (PP) PP is a 36 amino acid linear oligopeptide, primarily secreted by the PP cells of Langerhans' islets (42). PP is supposed to regulate pancreatic, GI secretions (132) and hepatic glycogen levels (38). PP has been suggested for the diagnosis of PanNENs (NCCN guidelines) and ESMO 2012 consensus guidelines already considered PP diagnostic also for NF-PanNENs (138). PP is considered a specific neuroendocrine marker but displays variable to low sensitivity (139) (Table 2). Although elevated PP has been observed to predict metastatic disease with 80% sensitivity (2), <50% of PanNEN patients present elevated serum PP at diagnosis (132). Additionally, serum concentrations of PP can be affected by many factors, including physical exercise, hypoglycemia, and food intake, chronic renal disease and hyperglycemia, diarrhea, laxative usage, aging and inflammations (2) Increased PP/CHGA assessment is suggestive for PanNENs disease with higher sensitivity (139, 140). In contrast, decline of PP level during patients monitoring is considered a good prognostic marker (132).

Human chorionic gonadotropin (HCG) and **alpha fetoprotein (AFP)** can be also considered in biochemical assessment of NENs (2). HCG is a glycoprotein physiologically synthesized by syncytiotrophoblastic cells of the placenta during pregnancy and it is composed of α and β subunits. The β subunit (β-HCG) is specific, since tumor cells usually lack the mechanism to link α and β subunits. An increased secretion of the β subunit is reported in pancreatic tumors and PanNENs. AFP is a peptide hormone produced during development. In adults, an increase of circulating AFP has been described in NENs but AFP producing PanNENs are rare and often associated with other malignancies. For these reasons, the sensitivity and specificity of HCG and AFP are still debated, limiting their use in NENs (2).

Bioactive peptides retrieved in the blood of F-PanNET patients are useful prognostic and predictive biomarkers. However, hormones are not always secreted and retrievable from the blood. Several factors can preclude reliable measurements in the circulation, these limitations must be considered in the thoughtful application of biochemical testing.
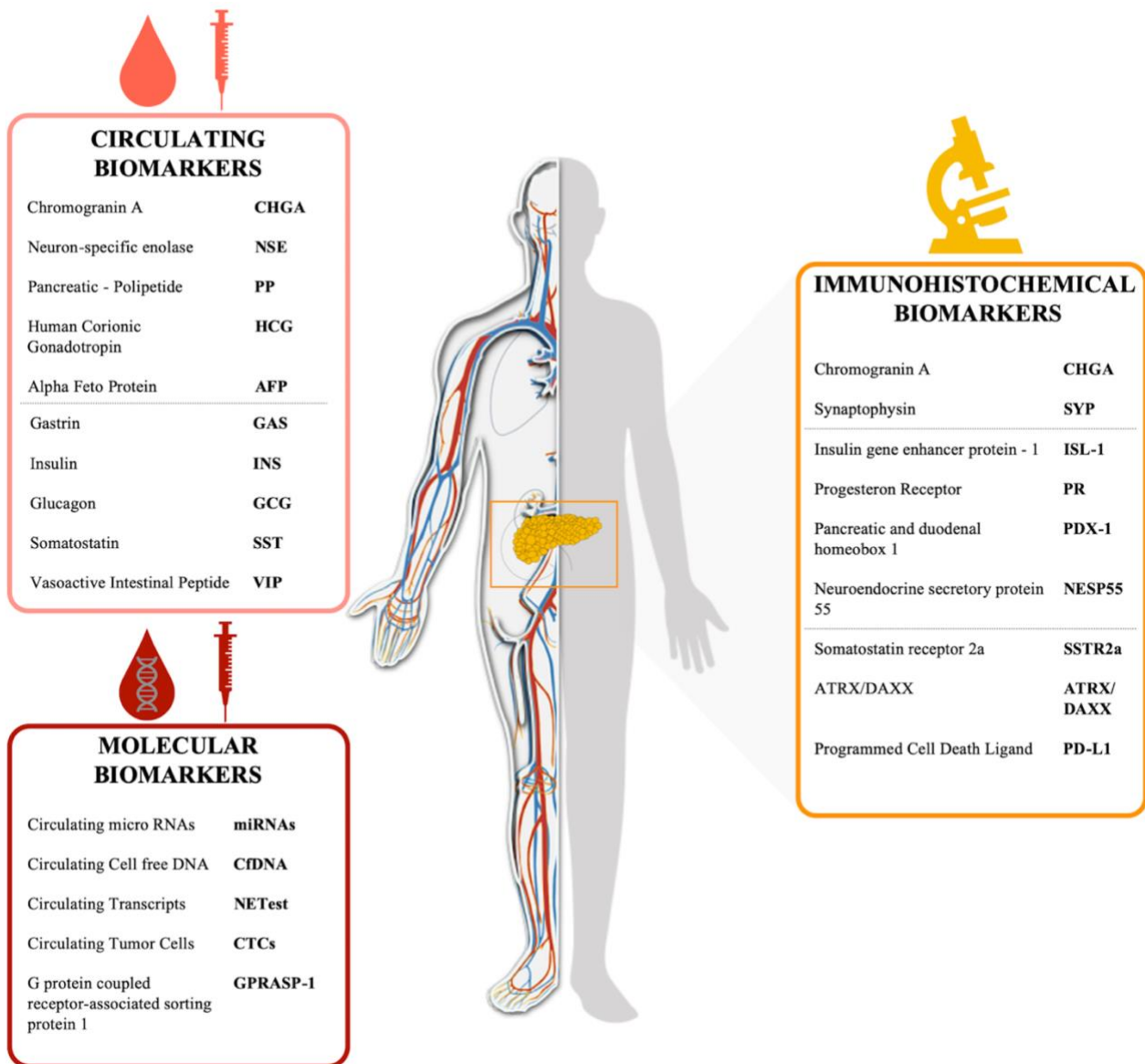
CIRCULATING BIOMARKERS

Chromogranin A	**CHGA**
Neuron-specific enolase	**NSE**
Pancreatic - Polipetide	**PP**
Human Corionic Gonadotropin	**HCG**
Alpha Feto Protein	**AFP**
Gastrin	**GAS**
Insulin	**INS**
Glucagon	**GCG**
Somatostatin	**SST**
Vasoactive Intestinal Peptide	**VIP**

MOLECULAR BIOMARKERS

Circulating micro RNAs	**miRNAs**
Circulating Cell free DNA	**CfDNA**
Circulating Transcripts	**NETest**
Circulating Tumor Cells	**CTCs**
G protein coupled receptor-associated sorting protein 1	**GPRASP-1**

IMMUNOHISTOCHEMICAL BIOMARKERS

Chromogranin A	**CHGA**
Synaptophysin	**SYP**
Insulin gene enhancer protein - 1	**ISL-1**
Progesteron Receptor	**PR**
Pancreatic and duodenal homeobox 1	**PDX-1**
Neuroendocrine secretory protein 55	**NESP55**
Somatostatin receptor 2a	**SSTR2a**
ATRX/DAXX	**ATRX/ DAXX**
Programmed Cell Death Ligand	**PD-L1**

Figure 2 Schematic representation of specific and non-specific biomarkers for PanNENs

Circulating peptides (i.e., CHGA, PP) are circled in light red; tissue markers (IHC) (i.e., CHGA, SSTR) are circled in yellow; circulating molecular biomarkers (i.e., RNA transcripts, cfDNA) are circled in red. Figure readapted from Bocchini M., et al. (2)

1.2.3 PanNEN specific biomarkers

1.2.3.1 *In situ* biomarkers

The diagnosis of NENs relies on morphology confirmation of neuroendocrine differentiation, accomplished by usage immunohistochemical assays for several antibodies (INSM1, synaptophysin, chromogranin A) displaying variable specificity and sensitivity. The most sensitive are INSM1 and synaptophysin, virtually identifying all NENs. INSM1 has been reported to be expressed in a small number of non-neuroendocrine thoracic carcinomas and in sarcomas (141); while SYP is an integral transmembrane glycoprotein expressed in neuroendocrine cells and neurons involved in synaptic transmission with a diffuse cytoplasmic immunostaining. SYP is normally expressed in PanNETs (142,143). Chromogranins and SSTRs are usually strongly positive in NETs, including PanNETs but focal and weak to absent in most NECs. CHGA and SYP combined assessment represents the first of a multi–step approach currently in use to confirm the neuroendocrine nature of the disease and then its pancreatic origin (**Figure 2, 3** and **Table 4**).
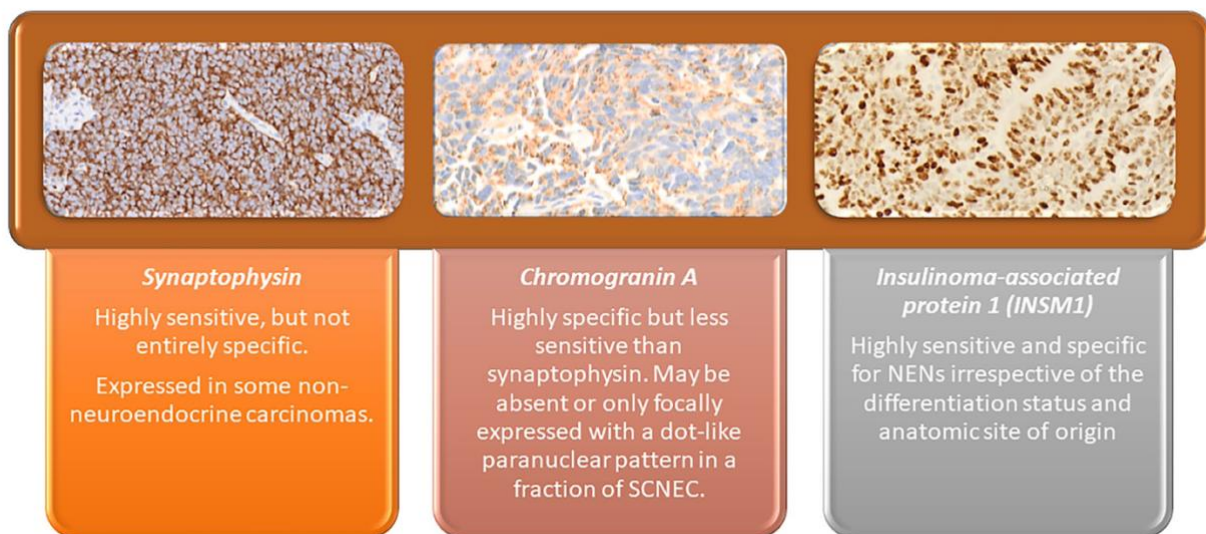

Figure 3 Markers of Neuroendocrine differentiation

From Prosperi D., et al. (96)

Histological diagnosis is performed on surgical or endoscopic biopsies, to assess specific marker distribution by IHC. Besides the validated diagnostic panels, other tissue biomarkers can improve PanNETs management providing information on the site of origin, grading, immune and genetic landscape of the disease. In addition, novel biomarkers could represent therapeutic targets. Up to now

several immunohistochemical panels have been proposed to identify primary tumor sites of origin, especially in PanNENs. Although many recent studies focused on these biomarkers they are not routinely used and validated for diagnosis and/or prognosis in PanNETs management (**Table 5**).

Immunohistochemical markers (IHC)			Source	Level	Combinations improving sens./spec.	Clinical use
Differentiation	Chromogranin A	CHGA	Surgical/endoscopic biopsy	Over-expressed	SYP	Diagnosis of NENs; Grading; Differentiation
	Synaptophysin	SYP	Surgical/endoscopic biopsy	Over-expressed	CHGA	Diagnosis of GEP-NENs; grading; differentiation
Site of Origin	Insulin gene neanche homeeobox - 1	ISL-2	Surgical/endoscopic biopsy	Over-expressed in endocrine pancreas	Low expression in case of Gastrinoma	Over-expressed in Pan NENs (especially in WD tumors)
	Progesteron Receptor	PGR	Surgical/endoscopic biopsy	Positive	CHGA + SYP	Indicative of pancreatic origin (40-75%) (negative in GI-NENs)
	Pancreatic and duodenal homeobox 1	PDX-1	Surgical/endoscopic biopsy	Positive	CHGA + SYP	Indicative of pancreatic origin
	Neuroendocrine secretory protein 55	NESP55	Surgical/endoscopic biopsy	Focally positive	CHGA + SYP	Indicative of pancreatic origin (40−50%)
Prognostic/ Predictive	Somatostatin receptors 2a	SSTR2a	Surgical/endoscopic biopsy	Over-expressed	CHGA + SYP	Indicative of pancreatic origin; Predictive for PRRT treatment; inverse correlation with grading.
	ATRX/DAXX	ATRX/ DAXX	Surgical/endoscopic biopsy	Loss of expression	CHGA + SYP	Prognostic for tumor aggressiveness; (associated with WD tumors)
	Programmed Cell Death Ligand	PD-L1	Surgical/endoscopic biopsy	Over-expressed	CHGA + SYP	Prognostic/Predictive for anti-PD-L1 therapeutic agents

Table 5 IHC most relevant biomarkers for PanNEN diagnosis, prognosis, and monitoring.

PanNENs, Pancreatic Neuroendocrine Neoplasia; GEP-NENs, Gastro-Entero-Pancreatic Neoplasia; WD NETs, well differentiated tumors. From Bocchini M, et al. (2)

Islet 1 (ISL-1) is a homeobox transcription factor expressed in all endocrine pancreatic cells. This pattern of expression suggests a general role in the development of multiple cell lineages of the endocrine pancreas. ISL-1 expression is detected in 70–82% of PanNETs. Gastrinomas of the pancreas show low expression of ISL-1 making its application less effective (2).

Progesteron Receptor (PR) has been reported in 40– 75% of PanNETs (56, 64). PR positivity has been demonstrated to be strictly localized to the endocrine compartment of normal and neoplastic human pancreatic islets and to be significantly associated with a favorable prognosis and a lower clinical stage. The relative expression of PR isoforms (PRA; PRB) have been reported to have a prognostic role in NENs from different site of origin. PRB activation promotes Cyclin D1 (CCND1)

overexpression and, because of c-Fos and c-Jun induction transcription factors supporting cell proliferation and tumorigenesis in PanNETs. In addition, PRA could inhibit tumorigenesis by PRB suppression signaling. Thus, PRA can be a suitable predictive factor in PanNETs and correlates with favorable prognosis (2).

Neuroendocrine secretory protein 55 (NESP55) belongs to the chromogranin family and can be considered a highly specific marker for PanNETs. Indeed, Focal and specific expression of NESP55 is reported in 40–74% of PanNETs in contrast with very rare expression in other GI-NENs and NENs of the lung and rectum (5 and 8%, respectively; 2).

Paired box 8 (PAX 8) represents a transcription factor able to regulate organogenesis in a variety of organs. Increased PAX8 reactivity has been observed in PanNETs and normal pancreatic islets, in contrast with GI or pulmonary NENs which show PAX8 very low or no expression. PAX8 has been demonstrated to be particularly useful in metastatic NENs with unknown primary tumor site: combination of PAX8 and ISL-1 overexpression could indicate pancreatic origin (2).

Pancreatic and duodenal homeobox 1 (PDX-1) is transcriptional activator of several genes, including insulin, somatostatin, glucokinase, islet amyloid polypeptide, and glucose transporter type 2. In addition, PDX-1 is involved in the early development of the pancreas and plays a key role in glucose-dependent regulation of insulin gene expression. PDX-1 immunoreactivity is reported in 54–100% of PanNETs in contrast with other GI-NENs. Combination of PDX-1, ISL-1, PAX8, and/or NESP55 can address pancreas as primary site of origin, when it is unclear.

Several peptides and growth factors have been explored as biomarkers for PanNETs to improve early diagnosis and follow- up, such as α-Internexin, Paraneoplastic antigen 2 (PNMA2) and X-linked inhibitor of apoptosis (XIAP) are emerging immunocytochemical markers. Currently, combinations of ISL-1, PR, NESP55, PAX8, and PDX1 suggest pancreatic origin (2; 40).

Glucose transporter 1 (GLUT-1) is a uniporter protein that mediates the transport of glucose molecules through the cell membrane. GLUT-1 is observed to be overexpressed in several tumors and it is supposed to be related with increased metabolism and cell growth. Several studies have shown association between GLUT-1 expression and tumor aggressiveness, poor prognosis and neuroendocrine differentiation in a number of carcinomas. GLUT-1 overexpression was observed to correlate with grading, Ki-67 mitotic index, vessel invasion, lymph node metastases and poor disease-free survival rate in G1/G2 PanNETs. In addition, HIF-1α and GLUT-1 co-expression suggests a

HIF-1α dependent induction of GLUT-1 in hypoxic conditions. Importantly, GLUT-1 overexpression in NENs correlates with an increased 18F-FDG uptake. High 18F-FDG uptake is a useful prognostic marker in PanNETs, thereby GLUT-1 expression may be a good surrogate prognostic marker for 18F-FDG uptake (2).

Programmed Cell Death Ligands (PD-L) are proteins involved in the immune checkpoints. PD-L1 is recently observed to be strongly upregulated in G3 tumor patients both on tumor and infiltrating immune cells, resulting in poor T-cell-mediated tumor surveillance. PD-L2 inversely correlates with presence of tumor necrosis and with PD-L1 expression levels and resulted to be significantly over-expressed in PanNETs compared to non-pancreatic NETs and to other NETs (2).

Delta-like protein 3 (DLL-3) is a member of the Notch ligand family that is aberrantly expressed on the cell surface of small cell lung cancer (SCLC), Merkel cell Carcinoma (MCC) and other neuroendocrine tumor cells making it an attractive therapeutic target in NECs (2). The Notch pathway is a cell–cell signaling involved in several and patho-physiological processes (144,145). It has been demonstrated that the Notch pathway plays a suppressor function in NEN diseases. Indeed, DLL-3 has been found highly upregulated and/or aberrantly expressed on the cell surface of aggressive NENs (146,147) unpairing of Notch-1 suppressor activity. DLL3 has been associated with aggressive neuroendocrine phenotype development, deletion of RB1 and shorter overall survival (OS) (148). The cell surface expression of DLL3 makes it an optimal target for directed therapies. DLL3 targeting holds great potential especially in SCLC and GEP-NEC, which are characterized by a very poor prognosis and by the lack of therapeutic options (149).

α-Internexin is a protein of the cytoskeleton, overexpressed by nervous system cells but also by insulinomas. α-Internexin *in situ* evaluation has been observed to be useful to predict treatment efficacy in insulinomas. Furthermore, the combination of α- Internexin and Ki-67 mitotic index, as a prognostic multianalyte assay, is observed to be prognostic in insulinomas. Loss or reduced expression of α-internexin protein represents a potential prognostic indicator for non-insulinomas PanNETs, as well in terms of overall survival (OS) (2).

Paraneoplastic antigen 2 (PNMA2) is a neuronal antigen identified in neurological paraneoplastic syndromes. PNMA2 over expression correlates with disease progression and recurrence free survival in PanNETs (2)

X-linked inhibitor of apoptosis (XIAP) suppresses apoptosis in cancer cells, representing a prognostic indicator for cancer patients. Although its role in PanNETs is not well established, it was found overexpressed in neuroendocrine GI tract, representing a potential target for therapies (2)

Novel DNA/RNA markers are also studied. DNA/RNA markers usefulness is mainly explored in the bloodstream via non-invasive liquid biopsy. Nevertheless, detection, analysis, and data interpretation of liquid and or genetic markers benefits from the correlation within *situ* marker detection. Molecular markers are not included in routine diagnostic workup of NENs but may be helpful in specific cases. For this reason, surrogate *in situ* markers for genetic alteration such as p53, Rb, ATRX, and DAXX, can be very helpful in distinguishing NET G3 from NEC (**Figure 4**).

ATRX or DAXX loss evaluated by means of IHC is a well-established independent prognostic factor in pancreatic NET, irrespective of size. Therefore, routine assessment of ATRX/DAXX loss (by IHC) and/or ALT is recommended in pancreatic NETs (40).

p53 and Rb represent the protein products of *TP53* and *RB1* can be surrogate indicators inactivating alterations of these genes that cause, respectively, overexpression or global loss of p53 and lack of Rb immunostaining. Such molecular abnormalities are frequent and unique for NECs, and their detection may be useful in the differential diagnosis between NEC and high-grade NET (40).
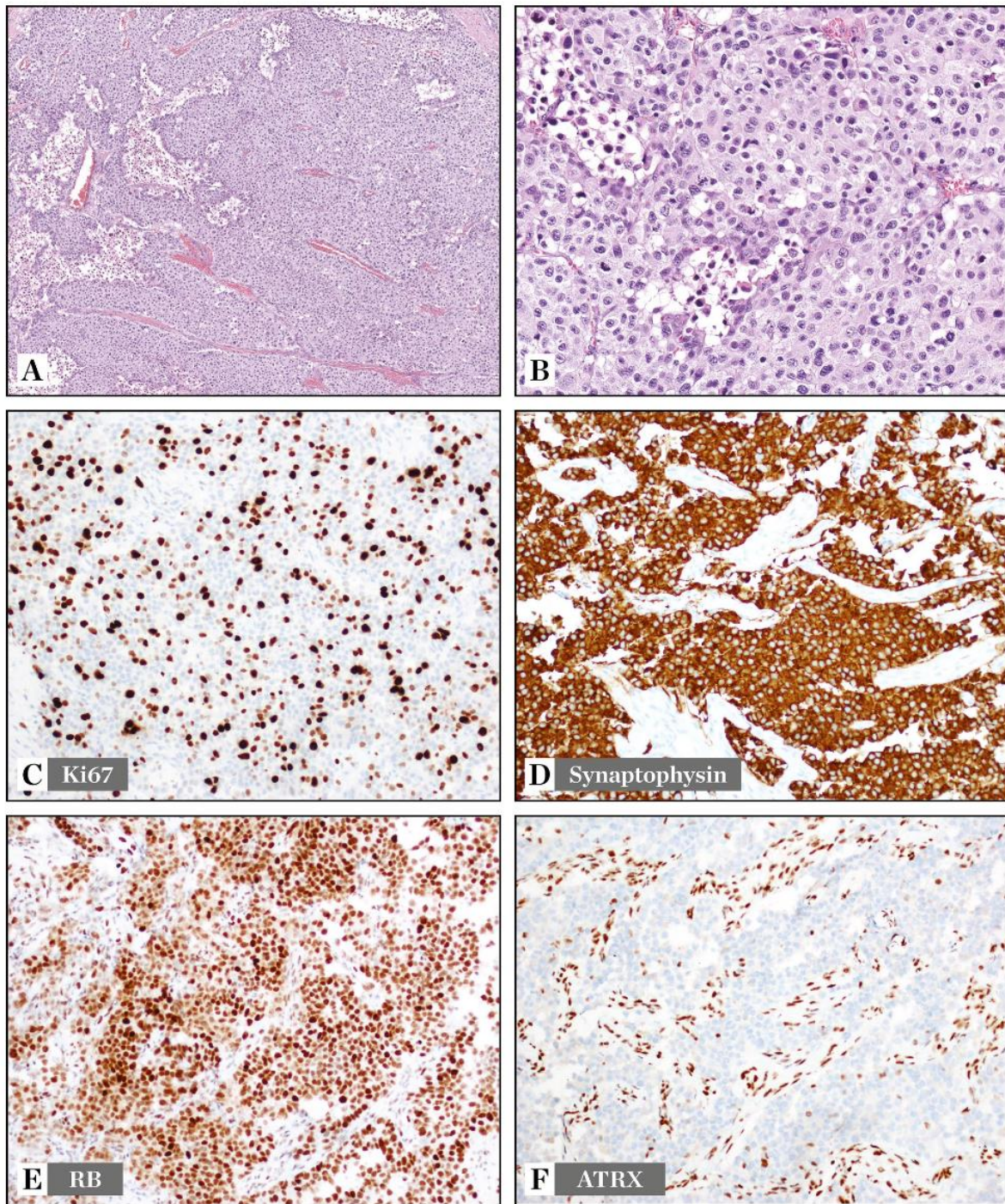
Figure 4 Well-differentiated PanNETs with high-grade features.

*(**A**, **B**) Well-differentiated panNET (G3) with irregular solid architecture, single-cell tumor necrosis; (**C**) high mitotic activity and a Ki67 >20%; (**D**) diffuse immunoreactivity for synaptophysin; (E) conserved Rb expression; (**F**) of ATRX expression while the endothelial cells and stromal cells (positive internal control) remain positive. From Prosperi D., et al. (96)*

In addition, expression patterns of DNA/RNA markers and/or molecular mechanisms, such as alternative lengthening of telomeres (ALT), non-coding RNAs, and mutational patterns have been investigated on tumor tissue specimens.

Alternative Lengthening of Telomeres (ALT) phenomenon is a tissue DNA prognostic marker for NENs. In PanNETs, ALT was shown to correlate with inactivating mutations in ATRX/DAXX genes (115, 116). The presence of ALT, shown by fluorescence in situ hybridization (FISH) is a well-established independent prognostic factor in PanNET, regardless of tumor size.

Tissue MicroRNAs (miRNAs) are 21-24 nucleotides non-coding RNAs (ncRNAs) that interfere with gene expression. A plethora of studies have been performed and propose specific tissue miRNA signatures to distinguish PanNETs patients from healthy individuals and the primary tumor from the metastatic disease with a prognostic and/or predictive role. For example, Roldo et al. described a tumor specific miRNA signature defined by miR-103 and miR-107 expression and by the absence of miR-155 expression distinguishing PanNET from normal pancreatic tissue. Furthermore miR-204 is primarily expressed in insulinomas and correlates with insulin expression on tissue (2).

Importantly, in the present study, we propose circulating hsa-miR-5096-5p as potential prognostic biomarkers for PanNENs (150) and as negative regulator of the well-known SSTR-2, which fulfill a primary role in PanNETs diagnosis and prognosis.

Somatostatin receptors (SSTRs) have been widely studied as prognostic and predictive biomarker in GEP-NENs since most of GEP-NENs shows diffuse SSTRs over-expression, especially G1 and G2 stage tumors (2). Indeed, an inverse correlation between SSTR2a expression and NENs differentiation has been observed (2). SSTR2a is particularly over-expressed in PanNETs compared to NENs of different origin (e.g., GI-NENs/NEC). SSTRs SSTR2 can be considered a theragnostic since it is the molecular target for 68Ga-DOTA-SSA-PET/CT. Moreover, an inverse correlation was observed between 68Ga-DOTA-SSA-PET/CT uptake and tumor differentiation in GEP-NENs at tissue level (2). Intriguingly, SSTR2 is more expressed in primary PanNETs than in metastases, suggesting a novel additional role of SSTR2a in monitoring the tumor progression (2). SSTR2 and SSTR5: SSTR2 and SSTR5 are the most frequent subtypes of SSTRs in NENs and are strongly expressed in NETs (151, 152) in contrast to NECs which are not targetable with somatostatin analogs for therapy (**Figure 5**).
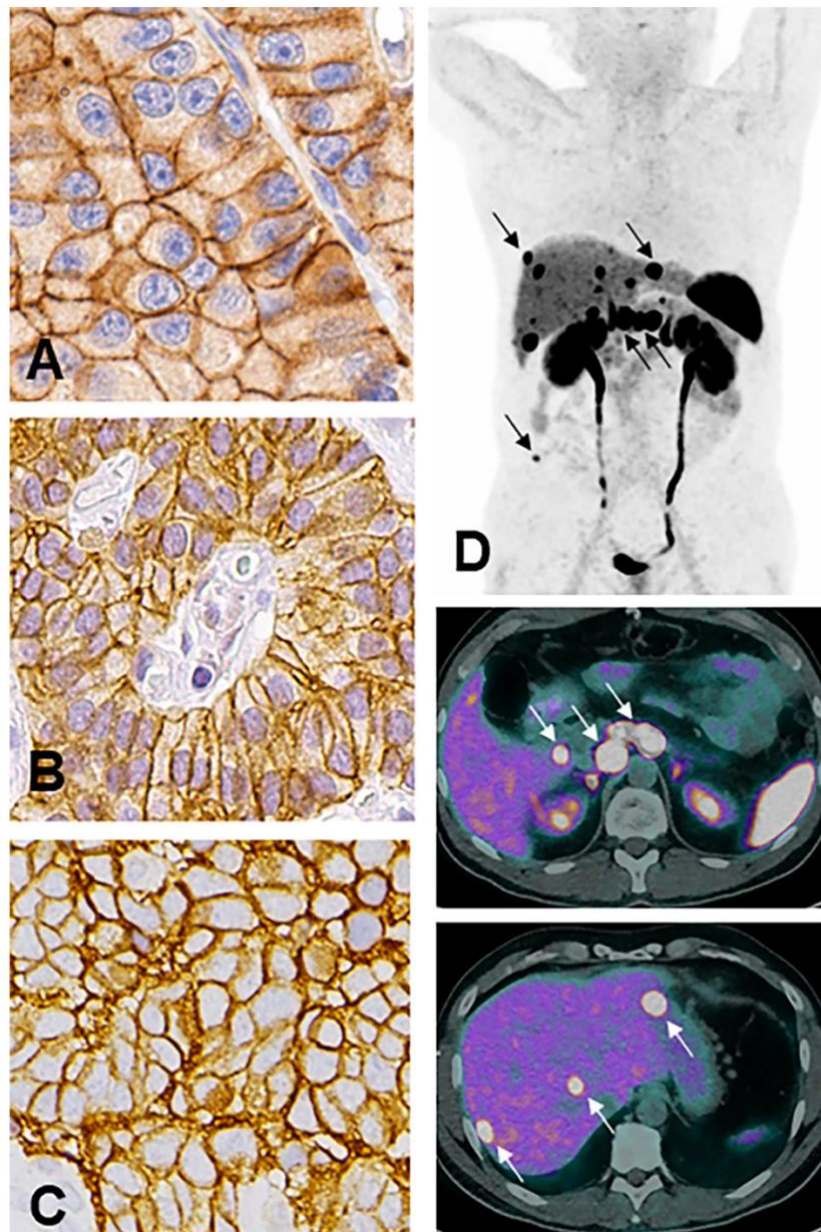
Figure 5 Somatostatin receptors (SSTRs) expression in PanNEN tissue and *in vivo*.

(A) Strong and diffuse membranous SSTR2 expression is identified in a well- differentiated functional B insulinoma B cell tumor (PanNET, G1) ; (B) SSTR5 expression in a well-differentiated, non-functioning (duodenum NET, G1); (C) This unusual poorly differentiated neuroendocrine carcinoma, small cell type, of the lung (NEC, SCLC) has diffuse membranous expression of SSTR2 ; (D) In vivo expression of SSTR2-5 in a pancreatic G2 NET with liver, peritoneal, and lymph node metastase the top figure shows the whole body scan multiple intensity projection (MIP); arrows indicate the pancreatic head lesion with adjacent positive lymph nodes, liver, and peritoneal deposits. The middle figure shows the upper trans-axial fused PET/CT scan with the pancreatic lesion, lymph nodes, and one liver deposit (arrows). The lower figure is the trans-axial fused PET/CT scan showing three liver deposits (arrows). From Prosperi D., et al. (96)

1.2.3.2 Liquid biomarkers

Three key methods allow an exhaustive assessment of the NEN disease: clinical evaluation, imaging, and biomarkers assessment (2,96). Blood biomarkers are easy to assess, minimally invasive, reproducible and can be used for real-time quantitative monitoring. Moreover, liquid markers overcome limitations of tissue specific information, providing a real-time snapshot of the disease and of tumor metabolism. Liquid biopsy allows the detection of specific nucleic acids in body fluids and it has particularly benefited from NGS and Real-Time quantitative PCR (RT/qPCR) approaches, partially overcoming the limit of tumor heterogeneity present in tissue biopsies (2). Liquid biomarkers include circulating cell-free DNA (cfDNA), circulating tumor cells (CTCs), microRNAs (miRNAs) or long non-coding RNAs (lncRNA), blood transcripts (mRNAs) and proteins (**Table 6**).

Molecular Markers			Source	Level	Clinical use	References
Potentially prognostic and/or predictive	Circulating Tumor Cells	CTCs	Serum/plasma	Increased	Related to the PFS and OS	(202)
	Circulating cell free DNA	cfDNA	Serum/plasma	Increased	Indicative of pancreatic tumor origin, correlates with primary tumors mutations (e.g., ATRX/DAXX)	(59)
	Circulating transcripts	NETest	Serum/plasma	Presence of NET "finger print" genes	Prognostic for tumor aggressiveness; predictive for treatment efficacy.	(203)
	MicroRNAs	miRNAs	Serum/plasma*	Up/down—regulated	Diagnostic for site of origin; prognostic and potentially predictive for treatment efficacy.	(58)

Table 6 Circulating molecular biomarkers for PanNENs diagnosis, prognosis and treatment monitoring.

Pancreatic Neuroendocrine Neoplasia (PanNENs); progression-free survival (PFS); (OS)overall survival (OS). Serum/plasma: also detected in tumor and healthy tissue. From Bocchini M, et al. (2)*

Cell-free DNA (cfDNA) was first reported in 1977 (153). CfDNA release in serum/plasma is associated with physiological phenomena such as cell apoptosis, active cellular release, autophagy, and necrosis. In the presence of malignancy, tumor tissues may release their DNA into peripheral blood. Tumor derived cfDNA exhibits a higher degree of fragmentation, methylation and it's about 20–50 base pairs shorter compared to normal cfDNA sequences (154). Next-generation sequencing (NGS) of ctDNA from PanNEN liquid biopsies identified genomic alterations in TP53, KRAS, EGFR, PIK3CA, BRAF, MYC, and CCNE1 genes (155), reflecting the presence of tumor-specific genetic alterations that could have a prognostic role. Nevertheless, official consensus on the role of

cfDNA in PanNEN disease has not been reached yet since they present a relative heterogeneity in recurrent mutations in comparison with other tumors (156; 157, 158).

Circulating Tumor Cells (CTCs) are defined as individual tumor cells shed passively or actively from the solid tumors into the vasculature. During the multistep metastasis process may locally infiltrate into the adjacent, intravasate and disseminate through the bloodstream becoming CTCs able to extravasate into distant sites, to proliferate in competent organs. CTCs, when found in clusters, are defined as circulating tumor microemboli (CTM; 158). Efficient CTC isolation is challenging since CTCs are extremely rare populations. The latest Delphic consensus on circulating biomarkers in NENs has defined CTCs as a non–reliable marker, due to technical issues for quantitation and characterization. Nevertheless, 36% CTC positivity was found to correlate with the presence of bone metastases ($p < 0.0001$) in a group of 119 PanNEN (158). More recently, a prognostic role of CTCs in predicting poor prognosis in PanNEN was described (159).

Blood Transcripts (mRNA) are considered for evaluating the diagnosis and prognosis of PanNENs. In this regard, the NETest has been recently introduced as a reliable tool. The NETest is a blood test panel of 51 genes derived from the transcriptional profiling of NET cells (2,158). Currently, this molecular signature shows prognostic and predictive utility for NENs since increased NETest levels at baseline (at least >33–40%) correlate with poor prognosis and/or treatment failure (160). NETest score represents a multivariate biomarker of circulating mRNA, with a diagnostic sensitivity of 80–100% combined with a specificity of 94% in PanNENs. In Vitro Diagnostic (IVD) tools, such as NETest aim to improve clinical practice, help patients' stratification and identify high risk of recurrence after radical surgery (160).

Long non-coding RNAs (lncRNAs) are a class of transcripts linked to different diseases and, in particular, to cancer. These are non-coding, 200-nucleotides long RNA molecules LncRNAs mainly act regulating gene expression of other RNAs, which may be coding or non-coding (2). LncRNAs can interact with miRNAs regulating their function, usually acting as miRNA sponges. LncRNAs can promote angiogenesis, metastasis, and tumor suppressors escape (210–213). The role of lncRNA in PanNETs remains poorly explored and most studies investigated their correlation with MEN1 gene-encoding "menin" protein in PanNETs. lncRNA *Meg3* can bind "menin" mRNA (maternally expressed gene) *was* described as tumor-suppressor in PanNET cells (161). See **Figure 6** for clinical relevance of liquid biomarkers.
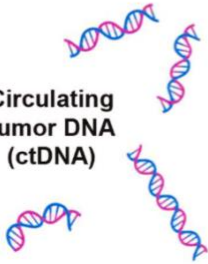
	PROS	CONS
Circulating tumor cells (CTC)	➢ Prognostic in PNENs ➢ Intact cells could be resistant clones thus providing valuable information for therapeutic decisions ➢ Can be used for functional assays (DNA, RNA, proteins) ➢ Can be cultured in vitro or in vivo ➢ Can be classified by intrinsic subtypes ➢ Can be used for response to treatment prediction	➢ Technically challenging ➢ Costly ➢ Sampling bias (affinity-based, size-based selection) ➢ Single-cell sequencing technically challenging (heterogeneity observed could be biological or technical bias)
Circulating tumor DNA (ctDNA)	➢ Technically easier to isolate than CTC ➢ DNA more stable than RNA ➢ Proportion of ctDNA related to tumor burden and overall survival ➢ High sensitivity and dynamic range ➢ More sensitive than CellSearch® CTC platform	➢ Can only be dissected at the genomic level ➢ Limitations of available material ➢ Blood cell death could spike cfDNA fraction ➢ Source not clear - lysis, apoptosis, CTC-derived ➢ Large background of normal cfDNA ➢ Unclear if ctDNA is released from cancer cells dying from therapy or resistant cells
Circulating non-coding RNAs	➢ High abundance and stability in body fluids ➢ Multiplexed ➢ Quantitative	➢ Wide variability of results and lack of reproducibility ➢ Influence of other factors ➢ Complexity in the comprehensive analysis ➢ Their source in the circulation is unclear ➢ Occurrence of similar non-coding RNAs in various diseases ➢ Lack of standardization
Exosomes	➢ Rich source of biomarkers ➢ Ability to cross the blood-brain barrier ➢ Higher stability, greater resistance to degradation ➢ Longer half-life ➢ Increased capacity to travel long distances in comparison with free proteins, lipids, and nucleic acids in the cytoplasm ➢ Permanence in the blood ➢ Low toxicity ➢ Non-immunogenic ➢ Therapeutic potential	➢ Few unique cell-specific proteins ➢ Challenging to determine their tissue of origin ➢ No state-of-the-art technology to isolate extracellular vesicles ➢ Lack of reproducibility

Figure 6 Clinical relevance of different liquid biomarkers for PanNENs.

From Smolkova B, et al. (158)

1.3 microRNAs (miRNAs) as biomarkers in PanNETs

1.3.1 miRNAs biology and role as biomarkers

miRNAs are short non-coding RNA molecules that target other RNAs (mRNA), mainly in their 3' untranslated region. miRNAs bind target RNA regulating expression, degradation, or impairing translation. MiRNAs biogenesis starts in the nucleus from long hairpin pri-miRNAs, which are then cleaved to become 70-nucleotides precursor miRNAs (pre-miRNAs). Pre-miRNAs are processed in the cytoplasm into a single-strand mature miRNA. Then, the RNA-induced silencing complex (RISC), functionalizes mature miRNAs to be addressed to bind specific mRNA transcripts for degradation or translational repression. Indeed, miRNAs are involved in several cell mechanisms and are frequently dysregulated under pathological conditions, including cancer (161,162). Over 2500 mature human miRNAs control approximately 30% of gene expression at post-transcriptional level (162). In addition to intracellular miRNAs, cells can actively or passively shed miRNAs through exosomes or after apoptosis or tissue injury, respectively. Circulating miRNAs can be retrieved in various biological fluids (162) have the advantage of being minimally invasive biomarkers that can be quantified through RT/qPCR assays, expression microarrays and next generation sequencing based approaches. Circulating miRNAs are well-established biomarkers for disease detection and monitoring. Exosome-encapsulated circulating miRNAs can be delivered to target cells promoting paracrine signaling and represent the source of choice for miRNAs in terms of quantity, quality, and stability. Circulating miRNAs are more stable than RNA transcripts in biofluids making them suitable as prognostic and/or predictive biomarkers for cancer patients (58, 202). Currently, several studies have produced signatures of circulating miRNAs associated with PanNET tissue expression with variable power in PanNETs (161). An updated list of miRNAs found deregulated in different NENs, including PanNEN is provided in Table 7 (161).

RNA type	RNA	Pathology
miRNA	miR-328	PanNENs
	miR-642	PanNENs
	miR-196a	PanNENs
	miR-10a, miR-106b	PanNENs
	miR-449a	PanNENs
	miR-210	PanNENs
	miR-3653	PanNENs
	miR-431	PanNENs
	miR-7-2-3p	PanNENs
	miR-24-1	PanNENs
	miR-144/451	PanNENs
	miR-137, miR-23b, miRNA-130/301	PanNENs
	miR-30a-3p	PanNENs
	miR-203a	PanNENs
	miR-224	PanNENs
	miR-214	PanNENs
	miR-193-b	PanNENs
	miR-93	PanNENs and SiNENs
	miR-375	PanNENs, SINENS TC, AC
	miR-21	PanNENs SCLC, LCNEC, TC, AC
	miR-96	SI-NENs
	miR-133a	SI-NENs
	miR-885-5p	SI-NENs
	miR183, miR-488, miR-19a, miR-19b, miR-145, miR-146, miR-222, miR-10b	SI-NENs
	miR-125b-5p, miR-362-5p, miR-425-5p, miR-500a-5p	SI-NENs
	miR-4516	SCLC
	miR-155	SCLC, LCNEC, TC, AC
	miR-29	SCLC, LCNEC, TC, AC
	miR-100	TC, AC
	miR-129-5p, miR-409-3p, miR-409-5p, miR-185, miR-497, miR-431-5p	TC, AC
	hsa-let-7f-5p	AC
	miR-518d-5p	SCLC
	miR-886-3p	SCLC
	miR-26b	SCLC
	miR-485-5p	SCLC
	miR-7-5p	SCLC
	miR-22-3p	SCLC
	miR-30a-5p	SCLC

Table 7 List of miRNAs expressed and associated with PanNENs and other neoplasms.

Adapted Blázquez-Encinas R et al. (161)

Despite the relatively limited clinical involvement of miRNAs in the diagnostic, prognostic, and treatment work-up of PanNET disease, current literature reports panels of miRNAs that resulted to be diagnostic and/or prognostic in the context of well-differentiated PanNETs (G1-G3). See **Figure 7** for an updated list of prognostic /diagnostic purposes for PanNETs.
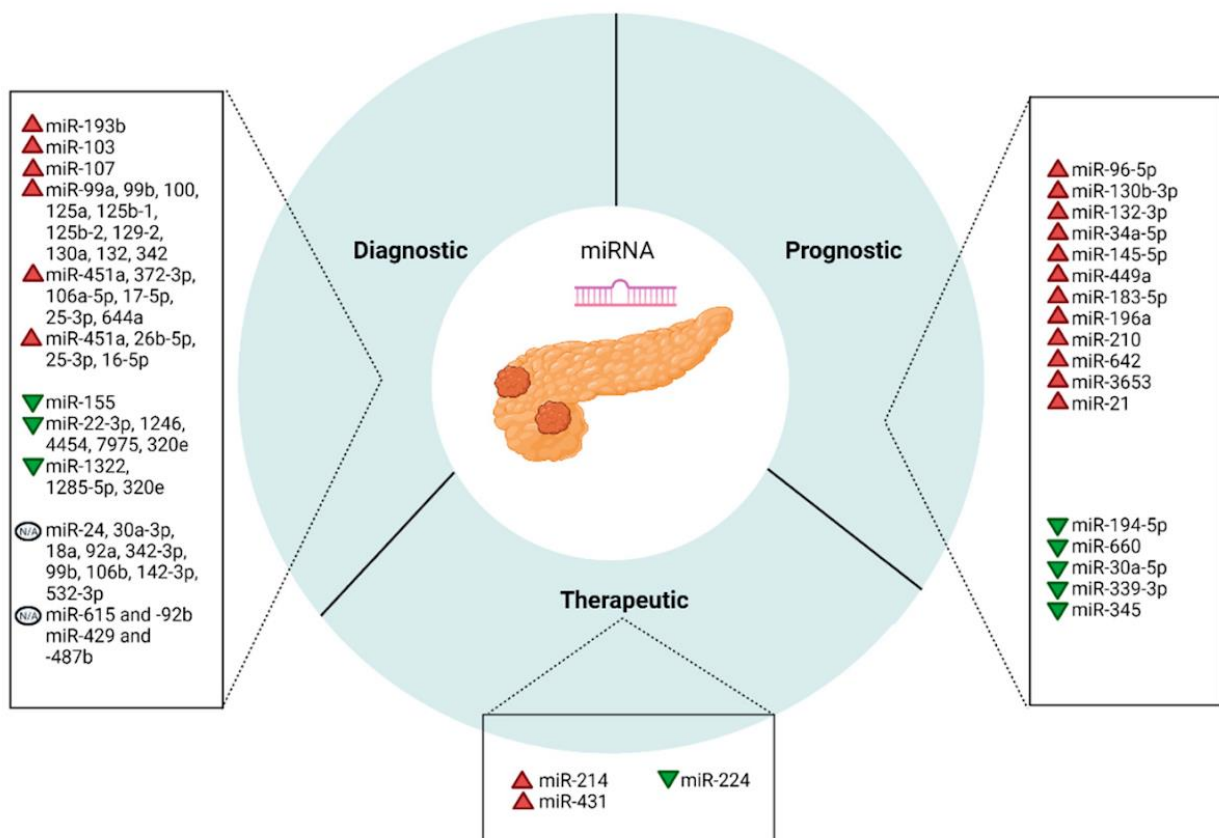

Figure 7 Schematic overview of prognostic, diagnostic and therapeutic miRNAs identified in PanNETs. *From Havasi, A. et al. (162)*

1.3.2 microRNAs (miRNAs) interference and as therapeutic agents

miRNAs control the expression of thousands of different genes, and they can also represent novel potential therapeutic targets or agents (163,165) providing novel therapeutic options for the management of PanNETs. There are currently two therapeutic strategies involving miRNAs and depending from its role in cancer biology: i) oncogenic miRNAs inhibition using anti-miR locked nucleic acids (LNA), target site blockers (TSB) that shield its binding site to target mRNA, thus preventing miRNAs oncogenic activity; ii) tumor-suppressor miRNA activity, can be enhanced using

miRNA mimics as therapeutics (161, 165) Recent studies report a panel of miRNAs candidates to be novel therapeutic molecules for PanNETs treatment (**Table 8**).

miRNA	Expression	Model	Treatment	Outcomes
miR-214	↑	Mouse	miR-214 inhibition	-Reduced tumor volume -Decreased volume of peripancreatic lymphatic metastases -Reduced tumor vascularization
miR-431	↑	Cell lines	miR-431-targeted locked nucleic acids	-Reduced invasiveness
miR-224	↓	Cell lines	miR-224 agomir	-Promotes apoptosis -Inhibits proliferation, invasion

Table 8 miRNAs with therapeutic role in PanNETs. *Adapted Havasi, A. et al. (162)*

2. Aims

The absence of early-stage diagnosis and companion circulating biomarkers delays therapeutic intervention and impacts on survival of patients with PanNENs. 68Ga-DOTA-SSA-PET/CT together 18F-FDG-PET/CT uptake, have shown predictive and prognostic power in PanNENs and are applied for the clinical management of patients treated with PRRT targeting SSTRs. SSTRs are expressed by 80% of GEP-NETs, and PanNETs display heterogeneous patterns of SSTRs expression from 50% to 100%, with isoform 2 being the most prevalent one (16). PRRT, targeting SSTR2, has shown cytoreductive potential and prolonged disease progression-free survival (PFS) in patients with unresectable metastatic disease (17,18). Although PRRT extends PFS, about 15–30% of patients with advanced well-differentiated GEP-NETs progress during treatment or six months to one year after PRRT (19–22). Future optimization of PRRT will depend on improved patient stratification (23,24). This study aimed to identify novel, liquid, miRNAs endowed with prognostic power and associated with 18F-FDG-PET/CT status, thus with aggressive tumor metabolism, evaluating their accuracy as prognostic biomarkers. The present PhD research program aimed to achieve the following goals:

◊   Identify a prognostic *miR-signature* that correlates with 18F-FDG-PET/CT uptake, thus with tumor metabolism;

◊   Assess the role of the *miR-signature* as independent prognostic biomarkers of 18F-FDG-PET/CT and other clinical and imaging parameters (site of origin; Ki-67; tumor burden; PFS and OS; and 68Ga-DOTA-SSA-PET/CT uptake);

◊   Assess the role of best candidate miRNA as SSTR2 modulator *in vitro*, thus as potential therapeutic target;

◊   Define the best *in vitro* miR interference strategy to increase SSTR-2 expression at the cell membrane in different PanNET preclinical models;

◊   Define future strategies for the therapeutic delivery of anti-miR/miR-regulator molecules to tumor cells to sensitize PanNETs to PRRT.

3. Methods

3.1 Study design

Plasma from well-differentiated G1, G2 and G3 GEP-NETs (n=24) were collected at baseline, prior to ^{177}Lu-DOTATATE, and whole miRNome Next Generation Sequencing (NGS) performed. miRNA differential expression analysis between 18F-FDG-PET/CT positive (n=12) and negative (n=12) patients of the screening set (n=24) was conducted. Since increased glucose uptake and higher prognostic power of 18F-FDG-PET/CT in PanNETs is described, in order to identify disease-specific metabolic signatures, bioinformatic analysis was applied to the screening set (n=24) considering PanNETs (n=6) and SINETs (n=18), separately. miRNA differential expression of 18F-FDG-PET/CT positive and negative PanNET and SINET separated subsets was performed. Differentially expressed miRNAs between 18F-FDG-PET/CT positive and negative patients were validated by RT/qPCR in plasma samples from two different validation cohorts of PanNETs (n=38) and SINETs (n=30). Additional comparison of miRNAs expression level was performed including healthy donors (n=17). Subsequently, we focused on the PanNET cohort only for further analyses. Assessment of validated miRNAs as potential independent Predictors of PFS and of OS, alone or together with other canonical clinical, pathological and imaging features in PanNETs was evaluated. On the basis of the results obtained in plasma from the significant correlations with clinical and pathological features of PanNETs, we lately focused on the best candidate miRNA, hsa-miR-5096-5p, to explore its relationship with 68Ga-DOTATOC-PET /CT SUV_{max} and SSTR2 expression. miRNA and SSTR2 relative expression were then detected and quantified on a pilot independent cohort of PanNET tissue specimens (n=8) in order to assess if the inverse correlation with 68Ga-DOTATOC-PET/CT SUV_{max} (mirroring SSTR2 expression), observed in plasma, could be retrieved also on the tumor tissue. The computational output analysis quantified the relative miRNA SSTR2 expression, at the single cell level providing the rationale to explore the mechanism behind this inverse correlation *in vitro* on PanNET preclinical models.

3.2 Clinical information on GEP-NET patients and healthy donors Plasma specimen's collection

From October 2016 to September 2019, patients with well-differentiated, advanced, metastatic, inoperable histologically or cytologically confirmed G1, G2 and G3 GEP-NET, were enrolled in the non-randomized LUX (NCT02736500) and LUNET (NCT02489604) clinical trials. Each patient enrolled in clinical trials was >= 18 years old, both genders and presented with a RECIST based progressive disease (PD). Patients displayed appropriate hematological, liver, and renal parameters (hemoglobin >= 10 g/dL; absolute neutrophil count (ANC) >= 1.5 x 109 /L; platelets >= 100 x 109 /L; bilirubin ≤1.5 X UNL (upper normal limit), ALT <2.5 X UNL (< 5 X UNL in presence of liver metastases), creatinine < 2 mg/dL) were enrolled. Eligible patients did not receive other treatments (e.g., chemo- or radiotherapy) from one month before to two months after the completion of 177Lu-DOTATATE cycles. Patients were naive from previous radionuclide treatments with radiopeptides (e.g., 111Inpentetreotide, 90Y-DOTATOC) or other radiopharmaceuticals (e.g., 131I-MIBG, 131I). All included patients expressed SSTR2 at time of diagnosis, presented measurable disease by means of conventional imaging (CT or MRI) and 68Ga-DOTATOC-PET/CT uptake (SUVmax) > 9 at PET-CT scan. Patients enrolled in LUX clinical trials displayed 18F-FDG-PET/CT SUVmax >2.5 at PET-CT scan, while patients in LUNET were negative.

For this biological retrospective study, the screening cohort of GEP-NETs (n=24) and validation cohorts of PanNETs (n=38) and SINETs (n=30) included patients with well-differentiated G1, G2 and G3 advanced metastatic disease prior to 177Lu-DOTATATE PRRT with a median follow up of 23.3 months (range: 6.5-60.9). Supplementary Table S1 for patients and healthy demographic, clinical and pathological features. All patients provided a signed informed consent for the blood withdrawal, prior to 177Lu-DOTATATE PRRT and downstream genomic analysis.

This study was approved by the local ethical committee (CEROM), approval no. 6711/5.1/2016, and performed according to Good Clinical Practice standards and the Declaration of Helsinki. The study protocol was amended to allow the collection of histologically confirmed G1, G2 and G3 PanNETs specimens to evaluate the hsa-miR-5096-5p and SSTR2 relative expression at the tissue level. Blood samples were collected by venipuncture at baseline, prior to 177Lu-DOTATATE PRRT. Blood was collected in a 3 mL K3-EDTA collection sterile vessel. Whole blood was centrifuged at 2500g for 10 minutes at room temperatures to obtain *platelet free* plasma. Plasma was carefully transferred into new 15 mL conical tubes (Falcon ™) for a second centrifugation at 2500× *g* for 10 min to remove further cellular debris. At least 1 ml of supernatant was collected and stored at -80°C until required. Samples from the healthy donor's cohort were and treated as well and collected at the same time to blood withdrawal to minimize differences in plasma composition.

3.3 Small - RNA exosome - enriched fraction precipitation

Thawed, frozen plasma samples were precipitated using Exoquick™, SCBI according to the manufacturer's protocol to obtain exosome-enriched fraction small-RNAs. Exoquick™, SCBI allows the precipitation of 20-100 nm vesicles and to extract their content. The pellet containing exosome-enriched fraction RNAs was resuspended in 200 ul of sterile PBS (1X). Qiazol™ was added to provide cryopreservation and lysis for exosome associated miRNA extraction.

Small RNAs, including miRNAs, were isolated with miRNeasy serum/plasma kit (Qiagen Cat No./ID: 217184) according to the manufacturer's protocol. One mL of plasma per sample was used as input for the small-RNAs extraction. Small-RNAs isolated from the exome-enriched fraction, were eluted in 56 µL of RNase-free water.

3.4 Whole miRNome NGS profiling and pipeline of analysis

Plasma specimens from the screening cohort of 24 GEP-NET patients were profiled for whole miRNome NGS. Small RNA transcripts were converted into barcoded cDNA libraries. Library preparation was created with the NEBNext Multiplex Small RNA Library Prep Set for Illumina (New England BioLabs Inc., USA). Libraries from each sample were pooled together and run-on Illumina NextSeq 550 platform, 75 cycles (Illumina, USA). The obtained BCL Files were converted to FASTQ Files and data quality was assessed by FastQC software (RRID:SCR_014583). Secondary analysis was performed using docker4seq package [docker4seq, RRID:SCR_017006] (30;31). Specifically, reads shorter than 14 nucleotides were discarded from the analysis; the remaining reads were trimmed from the adapter sequences using Cutadapt software(RRID:SCR_011841;https://journal.embnet.org/index.php/embnetjournal/article/view/200) . The trimmed reads were mapped against the precursor miRNA sequences downloaded from miRBase (Release 21) by the Shrimp algorithm (32). The counts matrix generated by the mapping was used as input for DESeq2 (RRID:SCR_000154) Bioconductor's package [RRID:SCR_006442; (33), to identify differentially expressed miRNAs between the 18F-FDG-PET/CT positive and negative groups. Endogenous controls for RT/qPCR were selected from the NGS data by considering the following criteria for each raw data: at least 5 reads for each sample and a $\log_2$ standard deviation value < 16. Bioinformatic pipeline of analysis encompassed principal components analysis (PCA) to exclude samples with poor number of reads. Only miRNA displaying at least one read in one of the

samples were considered. miRNAs differential expression analysis between 18F-FDG-PET/CT positive and negative GEP-NET patients was conducted considering $Log_2FC >=1$ and adj. p-value < 0.1. Second step correction was applied to exclude sample biases due to the tumor site of origin.

3.5 Real-Time quantitative (RT/qPCR)

Independent technical validation of candidate miRNAs was conducted by RT/qPCR in two distinct well-differentiated validation cohorts of 38 PanNETs and 30 SINETs. cDNAs from frozen and thawed RNA were obtained on C1000 Touch Thermal Cycler (Bio rad™, Hercules, CA, USA); using TaqMan™ MicroRNA Reverse Transcription Kit (Applied Biosystems™; Foster city, CA, USA. Cat No./ID: 4366596), cycling conditions were set according to the manufacturer's protocol. TaqMan™ MicroRNA Reverse Transcription protocol was optimized multiplexing the TaqMan® miRNA Assay's primers for the following targets: hsa-miR-3133, hsa-miR-4311, hsa-miR-5096-5p, hsa-let-7i-3p normalized with hsa-miR-30d as reference housekeeping miRNA (multiplexing group 1); hsa-miR-519c-3p, hsa-miR-582-3, hsa-miR-3614-5p, hsa-miR-1246 and hsa-miR-423-3p as reference housekeeping miRNA (multiplexing group 2).

Universal Master Mix without UNG and TaqMan™ miRNA Assay specific probes, for each target miRNA were used according to the manufacturer's protocol (Applied Biosystems™, Foster city, CA, USA. Cat No./ID: 4440040). RT/qPCR analysis was conducted using Applied Biosystems™ 7500 Real-Time PCR Systems (Applied Biosystems™; Cat No./ID: 4351104).

Expression level of single target miRNAs was normalized to hsa-miR-30d and the fold enrichment was obtained by means of the $2^{-\Delta CT}$ method, for the corresponding sample. In addition, "*Predictors*" (P1, P2, P3 and P) were created as the product of fold enrichments ($2^{-\Delta CT}$) of single miRNAs, to improve single targets and prognostic power (see Supplementary Table and Figure S2).

3.6 miR-Protein *in situ* detection

A novel semi-automated miR-protein *in situ* staining protocol was developed for the simultaneous detection of hsa-miR-5096-5p and SSTR2 protein expression.MiRCURY LNA miRNA Detection probe for hsa-miR-5096-5p, U6 small nuclear, *positive control* probe (Qiagen, Valencia, CA; Cat No./ID: 99002-15) and the scramble negative control probe (Qiagen, Valencia, CA Cat No./ID: 99004-15), were used. Each probe was labeled 5'3'DIG. Before starting, double-DIG-LNA probes

were denatured by heating (90°C for 4 min) and then diluted to 50 nM in the ISH buffer (miRCURY LNA miRNA ISH Buffer Set-FFPE).The first phase (tissue preparation, permeabilization and hybridization) has been performed in manual mode according to the miRCURY LNA miRNA detection probe protocol, while the second phase (signal detection) is automated using the Ventana BenchMark ULTRA platform (Ventana Medical Systems,Tucson, Arizona, USA). The automated protocol includes endogenous peroxidase blocking, casein blocking (16 min), incubation (37°C for 1 h) with primary prediluted mouse anti-DIG antibody (Ventana Medical Systems), to reveal the miR signal detected with OptiviewDAB Detection Kit (Ventana Medical Systems), consisting of HQ Universal Linker incubation (for 12 min), HRP Multimer incubation (for 12 min), and amplified with the Optiview DAB Amplification Kit (12 min). The revelation of SSTR2 protein expression was performed straight forward on Ventana BenchMark ULTRA, after cell conditioning with ULTRA CC1 (Ventana Medical Systems) for 24 min and casein blocking, using the antibody anti-SSTR2 (UMB1-C Terminal-ab134152-Abcam) in Ventana antibody diluent, incubated (37°C for 1 h), detected with Ultraview Universal Alkaline Phosphatase Red Detection Kit (Ventana Medical Systems). Finally, slides were counterstained for 8 minutes with Haematoxylin II (Ventana Medical Systems) and for 8 minutes with Bluing Reagent (Ventana Medical Systems), washed in tap water with soap to remove the liquid coverslip, dehydrated in the stove and mounted with xylene and EUKITT mounting medium (Sigma-Aldrich, Merck KGaA, Darmstadt, Germany). Specifically, this protocol reveals as first marker the miR in brown by using an anti-DIG antibody followed by the protein detection in red with the anti-SSTR2 antibody. Labeling with digoxigenin (DIG) allows miR-staining stability after double immunohistochemical rounds performed on the automated Ventana platforms. Additionally, our approach avoids antigen retrieval which typically occurs when IHCis performed prior to ISH. For this purpose, we compared the results obtained from the single IHC for SSTR2 expression with those obtained with the miR-protein protocol and we assessed that there were no differences in terms of protein expression (Source Data not shown, see Availability of data and materials section for data repository).

3.7 Microscopy, image processing and quantitative analyses

Whole slides images of IHC staining were acquired with the high-resolution slide scanner Aperio CS2 using the focus-ISH algorithm with a 40x magnification, which provides scanned images with the accuracy and resolution required for ISH.

To analyze the marker expression of the single nuclei in the histological samples, we designed a user-friendly open-source Graphical User Interface (GUI) requiring a minimal user interaction. The GUI has been named *Analysis Nuclei DAB (AND)-Tool* and it allows to automatically segment the nuclei and extract intensity/morphological features at the single-nuclei level. The AND-Tool was created using Matlab (The MathWorks, Inc., Massachusetts, USA). Source code, standalone executable version, documentation, and sample images are available for download from: https://sourceforge.net/p/andtool/. First, all the acquired RGB images were corrected for uneven illumination by subtracting the background estimated with the standard ImageJ/Fiji rolling ball algorithm. Then, the RGB images were unmixed using the Color Deconvolution ImageJ/Fiji plugin imposing the "FastRed-FastBlue-DAB" modality (34). The FastRed channel was used to subdivide the field of view into three distinguished types of regions of interest (ROIs, i.e., "dark-red", "light-pink" and "white" ROIs) according to the local intensity and two fixed thresholds (hereafter named Th1 and Th2, with Th1 lower than Th2), manually defined from the user just once for all the images to be analyzed. The "dark-red" ROIs are those regions with intensity values of the FastRed channel between 0 and Th1; the "light-pink" ROIs, with intensity values between Th1 and Th2; the "white" ROIs, with intensity values between Th2 and 255. Nuclei have been detected using the FastBlue and the DAB channels. To detect the nuclei, we used an intensity-based k-mean classifier automatically subdividing the single channels into three regions: white background, weak cytoplasmic signal, and nuclear signal. The standard watershed segmentation algorithm was then used to analyze the nuclear signal and split touching objects to proceed in a single-nuclei analysis. Objects with size not compliant with that of a nucleus were filtered out to compute the masks of the real nuclei.

Single-nuclei intensity/morphological features and region-based statistics were computed using the intensity maps created by subdividing the sample areas in dark-red, light-pink and white ROIs. Two types of nuclei have been considered: the ones positive for the DAB staining, and the ones positive for the FastBlue staining but not positive for DAB (see Supplementary File S2 for software analysis pipeline and manual). AND-Tool software analysis considered 10 fields per sample. The software was designed to identify three different levels of SSTR2 expressing nuclei: high as "dark-red" mask (identified by the software in the intensity range 0-Th1, with the threshold Th1: 100); intermediate as "light-pink" mask (identified by the software in the intensity range Th1-Th2, with the threshold Th2: 190) and the negative areas as "white" mask (identified by the software in the intensity range Th2-255, with 255 being the maximum value of intensity in the 8-bit gray-level conversion). AND-Tool was able to contemporary recognize areas with miR positive nuclei as DAB channel positivity. Correlation analysis has been conducted plotting the average percentage of hsa-miR-5096-5p positive

nuclei on overall analyzed cells in different SSTR2 expression areas. Spearman test was applied to determine r2 and p value.

3.8 Cell culture method and media

Hsa-miR-5096-5p and SSTR2 expression was assessed in NT-3, BON-1 and QGP-1 cell lines (RRID: CVCL_VG81; CVCL_3985; CVCL_3143). NT-3 cells were cultivated in culture dishes coated with collagen type IV from Human Placenta (Sigma-Aldrich, Homefield Road, Haverhill, UK; Cat No./ID: 27663) in RPMI medium supplemented with 10% FCS, 1% penicillin/streptomycin and L-glutammine, 15mM HEPES both with EGF (20 ng/mL; PreproTech, Rocky Hill, New Jersey), and FGF2 (10 ng/mL; PreproTech, Rocky Hill, New Jersey) and without growth factors (bFGF; EGF) (35). BON-1 and QGP-1 were cultivated in culture dishes in DMEM high glucose and RPMI medium respectively, supplemented with 10% FCS, 1% penicillin/streptomycin and L-glutammine, 15mMHEPES.

3.9 Mimic and inhibitor treatment *in vitro*

To evaluate SSTR2 downmodulation in NT-3 cell lines, 3×10^5 cells were plated into 6-well dishes coated with collagen type IV from Human Placenta. After 24 hours, 15 and 30 pmol of hsa-miR-5096-5p miRCURY LNA miRNA Mimic and Scramble (Qiagen, Valencia, CA) were transfected using RNAiMAX transfection reagent (Invitrogen®, Carlsbad, CA, USA) according to the manufacturer's instructions. Conversely, to evaluate SSTR2 up-modulation in NT-3 cell lines, 5×10^5 cells were plated into 12-well dishes coated with collagen type IV from Human Placenta; while 1.75 and 2.5 $\times 10^5$ of BON-1 and QGP-1 were plated into standard 12-well dishes, respectively. Then, 100 nM pmol of hsa-miR-5096-5p miRCURY LNA miRNA Inhibitor and Scramble (Qiagen, Valencia, CA) were transfected using RNAiMAX transfection reagent (Invitrogen®, Carlsbad, CA, USA) according to the manufacturer's instructions. Cells and culture medium were collected after 48 and 72h transfection. A Fixed volume of 350 ul of Trizol® reagent has been added to dried pellets and miRNeasy Mini Kit 50 (Qiagen, Valencia, CA Cat No./ID: 217004) was used for RNA extraction to quantify hsa-miR-5096-5p and SSTR2 RNA levels. *SSTR2* expression in NT-3 cell lines was assessed by RT/qPCR, after 48h and 72h mimic and inhibitor transfection. Expression values were

expressed as (Ct) values normalized to the housekeeping gene HPRT ($2^{-\Delta Ct}$ method), and then represented in terms of percentage of expression.

3.10 Immunofluorescence

To evaluate SSTR-2 protein expression after the inhibition of hsa-miR-5096 via miRCURY LNA, we performed immunofluorescence staining on QGP-1 cells grown and transfected on coverslip slides. QGP-1 cells were fixed for 10 minutes at 4° C with 10% Formalin, permeabilized with Tween-Triton 0.3% in PBS and blocked with 1% Bovine Serum (BSA) before incubation with the Human Somatostatin R2/SSTR2 PE- conjugated Mouse IgG2A Antibody (Clone # 402038) for 2h at room temperature. DAPI staining was used to counterstain the nucleus.

3.11 Statistical analyses check Predictors.

Sample size (n=24) of the screening cohort GEP-NET was established on the basis of a desired 2-fold change, a sigma=0.5 from a previous knowledge, a power of 80%, an FDR (false discovery rate) of 0.05 and a proportions of non-differentially expressed genes of 98%, using ssize.twoSamp R package. In addition, balancing of patients bearing 18F-FDG-PET/CT (n=12) and negative (n=12) was considered to avoid biases of the differential expression analysis. Sample size of the validation cohorts of PanNETs (n=38) and SINETs (n=30) was determined considering enrollment rate of LUX and LUNET clinical trials, the low prevalence and incidence of GEP-NET disease, NGS technical or stratification requirements, mutual subgrouping (FDG+; FDG-), presence of hemolytic samples and economic feasibility. Considering a drop-out rate of 10%, it was feasible to enroll at least 66 patients in the study. An additional cohort of 17 healthy donors balanced in terms of age, sex and time to blood withdrawal was considered for blood withdrawal and subsequent molecular comparison with PanNETs. The sample size of the healthy volunteer cohort was designed to be consistent with the patient's population, considering that comparison with healthy volunteers was not the goal of the present study. Of note, as reported in the Supplementary File S1 and Supplementary Figure S1, we ruled out age as a confounding factor for hsa-miR-5096-5p levels in both PanNETs and healthy donors. Categorical data were expressed as absolute numbers and percentage, while continuous variables were shown as median and range. Normality of distribution of continuous data was assessed through the Shapiro-Wilk test. MiRNAs normalized median expression level ($2^{-\Delta Ct}$) were compared between 18F-FDG-PET/CT positive and negative groups. Wilcoxon and Mann-Whitney test, chi-

square tests were applied respectively for continuous data and categorical data. For comparison between three groups Kruskal-Wallis test was used and Dunn test was used for post-hoc comparisons. The Receiver Operating Characteristic (ROC) curve, defined as a plot of sensitivity vs 1-specificity, was performed as evaluation of the performance of candidate miRNAs and their combination to predict PET positivity, 6-month (-mo) PFS and 12-mo OS. AUC (with 95% confidence - CI) was calculated as a common measure of accuracy and values range from 0.5 to 1.0: higher values are corresponding to a better performance of tested values. AUC values higher than 0.7 were considered as acceptable values. Roccomp STATA command was used to compare the ROC curves. For each curve, roccomp reports summary statistics and provides a test for the equality of the area under the curves, using an algorithm suggested by DeLong and Clarke-Pearson (36).

Cut-off with higher value of sensitivity and specificity was evaluated. OS was calculated as the time from date of start PRRT therapy to date of death or last follow-up visit, while PFS was calculated as the time from date of start PRRT therapy to date of progressive disease, death, or last follow-up visit. Alive patients were censored at last visit while patients without disease progression were censored at last tumor evaluation. Kaplan-Meier (KM) curves were used to estimate the survival function and the log-rank test was used to compare different subgroups in terms of OS or PFS. Median OS and median PFS were calculated, and 95% confidence intervals (95%CI) were reported. Univariable and multivariable Cox regression models were carried out with the explorative intent of evaluating the potentially independent clinical parameters associated with PFS and OS, including miRNAs of interest (data not shown). These models have been evaluated for exploratory intent and should be validated on an enlarged cohort. Threshold for including variables in multivariable models for PFS was a p-value of 0.10. Further evaluation will be done regarding collinearity among potential independent factors. Analysis to explore imaging parameters didn't consider any threshold. Outcome evaluation was performed using a complete case analysis, without any type of imputation. Transfection efficacy and statistical significance for in vitro experiments were assessed by parametric t-test, comparing expression median value (+/-SD). For comparison between three groups Kruskal-Wallis's test was used and Dunn test was used for post-hoc comparisons.

All statistical analyses were performed using Stata/SE version 15.1 for Windows (StataCorpLP, College Station, TX, USA). Time ROC R package was used to plot time-dependent AUC curve and 95% confidence interval.

4. Results

4.1 Patients' clinical features

Demographic (year of birth, age to diagnosis and gender) and clinical pathological features of the disease (site of origin, ki-67%, grading, tumor burden, presence and number of bone and/or liver metastases, 68Ga-DOTA-SSA-PET/CTand 18F-FDG-PET/CT SUVmax) were collected. Chi-square test or Fisher exact test for categorical data were applied on PanNEN subset, while Wilcoxon Mann-Whitney test was used for continuous data. Normality of distribution was assessed through Shapiro-Wilk test. Kruskall Wallis test was performed, according to age, to assess discrepancies between the PanNEN subset according to 18F-FDG-PET/CT status and healthy donors' cohort. Dunn's test was performed as a post-hoc comparison. Progression free survival (PFS) and overall Survival (OS) were calculated according to the Kaplan-Meier method and 95% confidence interval was provided (95%CI). Statistical analysis was performed to evaluate the presence of potential confounding factors on 38 PanNEN patients' subset according to 18F-FDG-PET/CT outcome (see **Table 9** for PanNET for clinico-pathological features).

Variable	¹⁸FDG/PET Positive (%) N = 25	¹⁸FDG/PET Negative (%) N = 13	Healthy donors (%) N = 17	Overall	p-value
Age at ¹⁸PET-FDG					
Median (range)	52 (24-78)	61 (44-79)	42 (30-79)	54 (30-79)	0.046
Gender					
Male	16 (64.0)	11 (84.6)	11 (64.7)	38 (69.1)	0.038
Female	9 (36.0)	2 (15.4)	6 (35.3)	17 (30.9)	
Ki67					
Median (range)	12 (1-50)	2 (1-15)		8 (1-50)	0.003
Grading (WHO 2017)					
1	4 (16.0)	8 (61.5)		12 (31.6)	
2	17 (68.0)	5 (38.5)		22 (57.9)	0.015
3	4 (16.0)	0 (0.0)		4 (10.5)	
Tumor burden					
Limited	6 (24.0)	5 (38.5)		11 (28.0)	
Moderate	12 (48.0)	5 (38.5)		17 (44.7)	0.680
Extensive	7 (28.0)	3 (23.0)		10 (26.3)	
Number of metastatic sites					
None	4 (16.0)	1 (7.7)		5 (13.2)	
One	9 (36.0)	4 (30.8)		13 (34.2)	0.282
Two	8 (32.0)	8 (61.5)		16 (42.1)	
Three	4 (16.0)	0 (0.0)		4 (10.5)	
Liver lesions					0.817
None	5 (20.8)	2 (15.4)		7 (18.9)	
<6	7 (29.2)	5 (38.5)		12 (32.4)	
>=6	12 (50.0)	6 (46.1)		18 (48.7)	
Unknown	1	0		1	
Presence of bone metastasis	6 (24.0)	3 (23.1)		9 (23.7)	1.000
Rotterdam Index					
3	4 (16.0)	6 (60.0)		10 (28.6)	0.016
4	21 (84.0)	4 (40.0)		25 (71.4)	
SUV PET GA					
Median (range)	33 (5.8-93)	62.5 (15.0-257)		36.9 (5.8-257)	0.077
Unknown	9	12		12	

Table 9 Demographic and clinical pathological features according to 18F-FDG-PET/CT outcome: PAN-NEN case series

p-value from Fisher exact test for categorical variables and Wilcoxon Mann-Whitney for continuous variable

3.2 NGS profiling identifies a circulating *miRNA-signature* associated with 18F-FDG-PET/CT in PanNET patients

To identify circulating prognostic and measurable miRNAs associated with ^{18}F-FDG PET/CT positivity in GEP-NET patients, we evaluated plasma specimens from advanced metastatic GEP-NETs, comparing ^{18}F-FDG PET/CT positive and negative patients. In the screening step, plasma from well-differentiated G1, G2 and G3 GEP-NETs (n=24) was collected at baseline, prior to 177Lu-DOTATATE PRRT and whole miRNome using Next Generation Sequencing (NGS) was performed (See **Figure 8** for the study design flowchart).
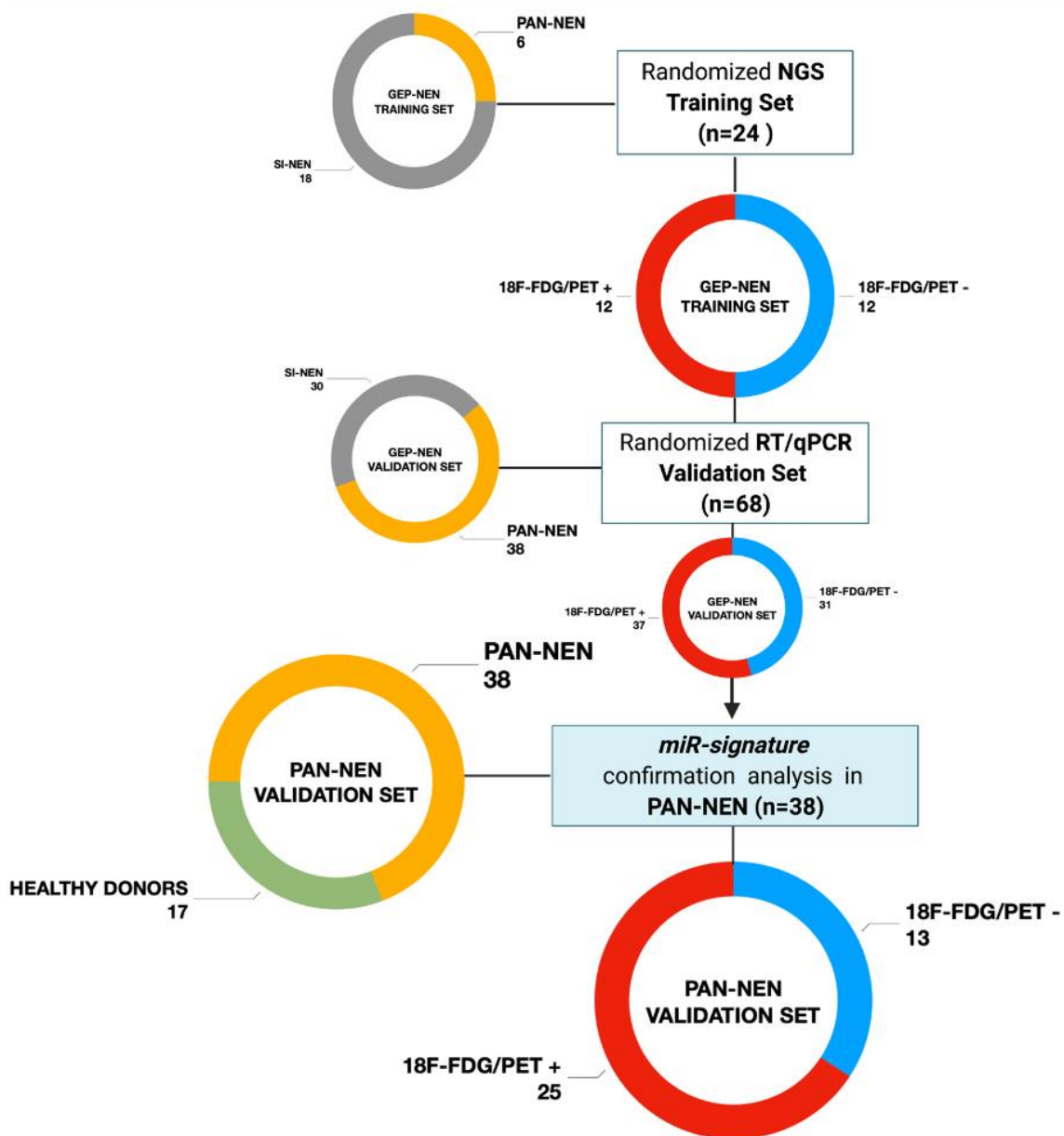
Figure 8 NGS and RT/qPCR validation flowchart

52

Patients' population schematic view summarizing the study design flow-chart. GEP-NET (n=68): Gastro-Entero-Pancreatic Neuroendocrine Tumor; PanNET (n=38): Pancreatic Neuroendocrine Tumor; SI-NET (n=30): Ileal Neuroendocrine Neoplasm; ^{18}F-FDG/PET + (n=25): positive (SUV$_{max}$ > 2.5) ; ^{18}F-FDG/PET - (n=13): negative (SUV$_{max}$ < 2.5). Created with BioRender.com.

NGS Profiling was conducted on a screening set of well-differentiated (G1, G2 and G3) GEP-NETs comparing ^{18}F-FDG-PET/CT positive (n=12) and negative (n=12) tumors. Principal component analysis (PCA) excluded one out of 24 samples due to poor number of reads. NGS analysis identified 2588 miRNAs. Of those, 2474 miRNAs displayed at least one read in one of the samples analyzed. The bioinformatic analysis revealed hsa-miR-1246, hsa-miR-4311 and hsa-miR-485-5p as differentially expressed miRNAs (Log$_2$FC>=1; adj. p-value:<0.1) between ^{18}F-FDG PET/CT positive and negative GEP-NET patients (**Figure 9**).
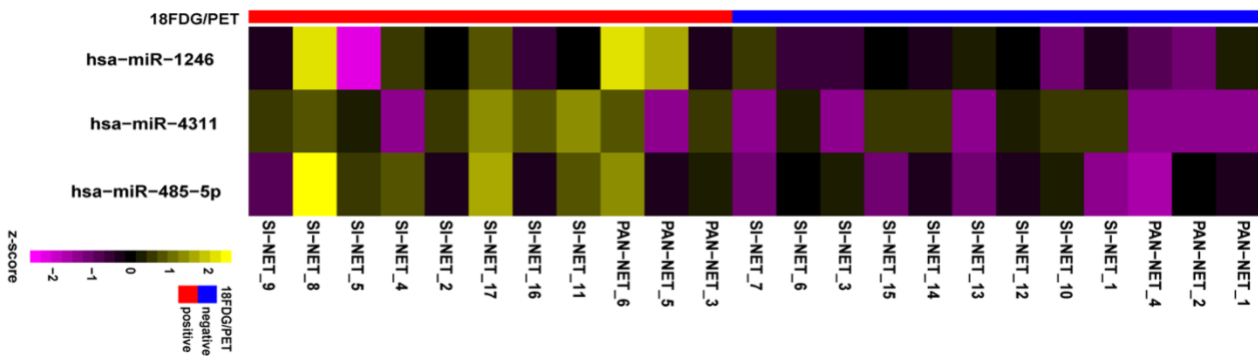
Figure 9 NGS analysis of circulating exosomal miRNAs in GEP-NETs revealed a potential metabolic signature in GEP-NET patients.

The heat-map shows the expression pattern of three differentially expressed miRNAs between ^{18}F-FDG/PET positive (n=12) and negative (n=12) GEP-NET training set (n=24). Each column represents a single miRNA while each row represents a single sample. The heat-map was obtained with the DeSeq2 package on regularized logarithm transformed counts. Color code is reported above the heat-map.

Second step analysis considered SINETs and PanNETs separately, to assess if disease specific signatures exist, and 8 miRNAs (hsa-miR-1246; hsa-miR-5096-5p; hsa-let-7i-3p; hsa-miR-3133; hsa-miR-3614-5p; hsa-miR-483-5p; hsa-miR-519c-3p; hsa-miR-582-3p) were found differentially expressed between 18F-FDG-PET/CT positive and negative PanNETs patients (**Figure 10**). Conversely, no miRNA correlated with 18F-FDG-PET/CT status in the SINET subset (data not shown). Finally, hsa-miR-30d emerged to be the target with the lowest standard deviation in the number of normalized reads among all case series, thus in light of its stability it was selected as the endogenous reference for all comparisons.
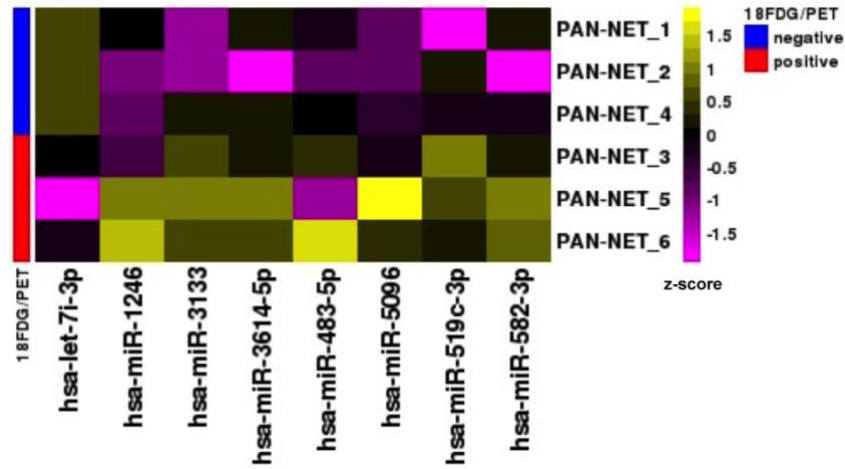
Figure 10 NGS analysis revealed 8 miRNAs associated with 18F-FDG-PET/CT in PanNETs patients subset.

The heat-map shows log2 normalized counts for all significant DEGs selected from comparison between ^{18}F-FDG/PET positive (n=3) and negative (n=3) PAN-NET training subset. Yellow colors indicate over-represented and purple colors under-represented genes in comparison to the corresponding PAN-NET ^{18}F-FDG/PET negative.

4.3 RT/qPCR validation of the *miRNA-signature* confirms hsa-miR-5096-5p, hsa-miR-4311 and Let-7i-3p or combinations, to correlate with 18F-FDG-PET/CT.

Independent assessment of NGS data emerged from PanNETs profiling using RT/qPCR technique confirmed three out of eight circulating miRNAs (hsa-miR-4311, p-value:<0.001; hsa-miR-5096-5p, p-value:<0.0001; hsa-let-7i-3p, p-value:<0.00001) significantly correlated with 18F-FDG-PET/CT status in the PanNET subgroup (**Figure 11**).
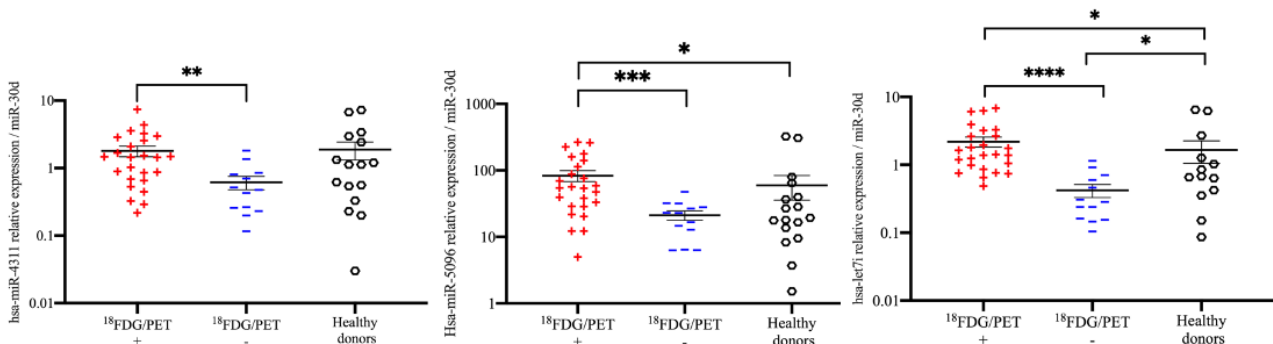

Figure 11 RT/qPCR validation confirmed the three miRNAs metabolic signature of PanNETs patients

*Deregulated miRNAs between ^{18}F-FDG/PET positive (n=25) and negative (n=13) PanNETs validation sets: (c) hsa-miR-4311 (d) hsa-miR-5096-5p and (e) hsa-let-7i-3p. Hsa-miR-30d was selected from NGS profiling as an endogenous control. Results are presented as mean ± SD (*p-value<0.05; ****p-value<0.00005). Wilcoxon and Mann-Whitney*

test, chi-square tests were applied respectively for continuous data and categorical data. For comparison between three groups Kruskall-Wallis test was used and Dunn test was used for post-hoc comparisons.

Fold change expression values for the three single miRNAs were then combined into *"Predictors"* to achieve higher prognostic power. *"Predictors"* were mathematically built multiplying the fold enrichment value obtained for the single miRNAs in different combinations (**Figure 12**). In order to obtain the fold enrichment for the single miRNAs, each miRNA expression level was normalized on the level of the reference hsa-miR-30d through a standard 2-ΔCT method. We calculated 3 binary *"Predictors"* by combining, hsa-miR-4311*hsa-let-7i-3p (P1), hsa-miR-5096-5p*hsa-let-7i-3p (P2), hsa-miR-4311*hsa-miR-5096-5p (P3), and 1 triple predictor which combines all 3-fold changes, hsa-miR-4311*hsa-miR-5096-5p*hsa-let-7i-3p (P). All *"Predictors"* significantly correlated with 18F-FDG-PET/CT. Fold change expression values for the three single miRNAs and combined *"Predictors"* are provided in **Table 10**.
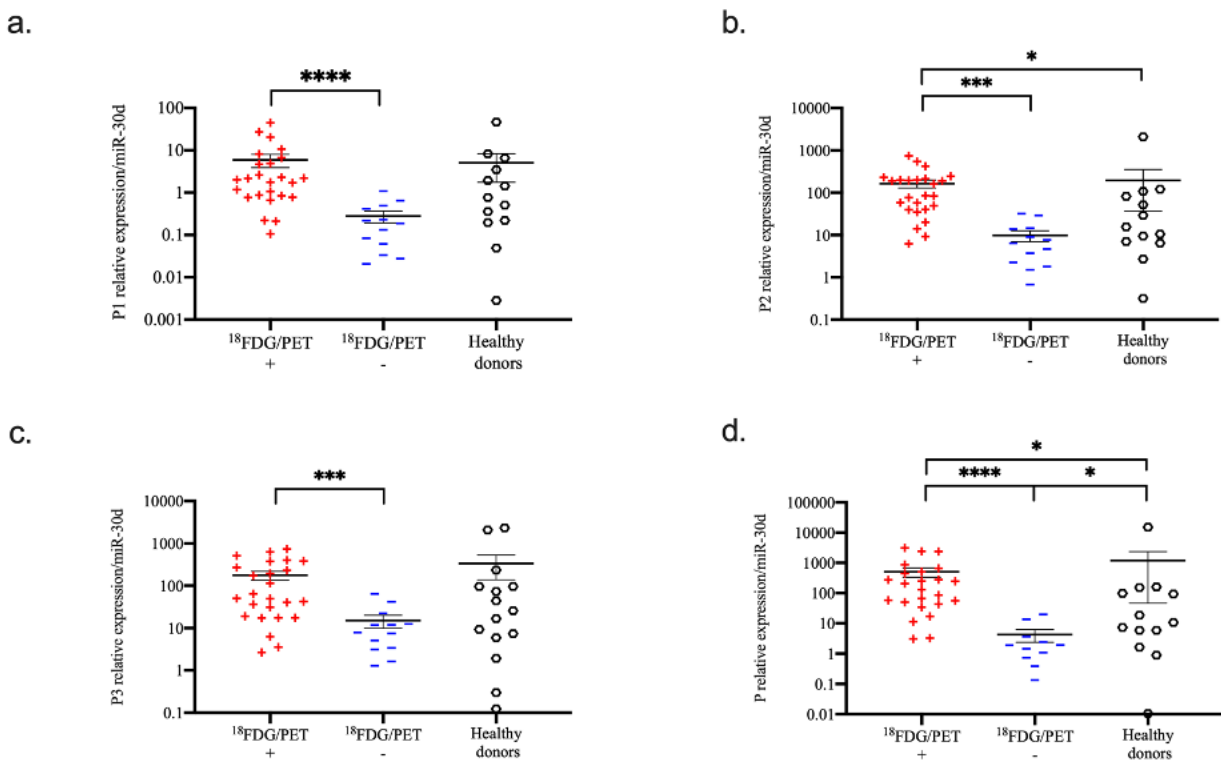

Figure 12 RT/qPCR validation of combined *"Predictors"* (P1, P2, P3 and P) correlates with 18F-FDG-PET/CT as multi-analyte biomarker

(a-d) Deregulated predictor between 18F-FDG/PET positive and negative PanNETs: (a) P1 (hsa-miR-4311 hsa-let-7i-3p), (b) P2 (hsa-miR-5096-5p*hsa-let-7i-3p), (c) P3 (hsa-miR-4311* hsa-miR-5096-5p), (d) P (hsa-miR-4311*hsa-miR-5096-5p*hsa-let-7i-3p). Hsa-miR-30d was selected from NGS profiling as an endogenous control. Results are presented as mean ± SD (*p-value<0.05; ****p-value<0.00005). Each graph was represented in Log10 scale and Wilcoxon and Mann-Whitney test, chi-square tests were applied respectively for continuous data and categorical data. For comparison between three groups Kruskal-Wallis test was used and Dunn test was used for post-hoc comparisons.*

miR-	^{18}FDG/PET Positive N = 25	^{18}FDG/PET Negative N = 13	Healthy donors N = 17	Overall N = 55	p-value	p-value (neg. *vs* HDs)	p-value (pos. *vs* HDs)	p-value (pos. *vs* neg)
Has-miR-4311								
Median (range)	1.44 (0.21-7.38)	0.47 (0.11-1.81)	1.13 (0.03-7.21)	0.88 (0.03-7.38)	0.013	0.086	0.545	0.005
Hsa-miR-5096								
Median (range)	54.31 (4.98-264.79)	22.94 (6.30-47.44)	19.38 (1.51-323.08)	28.76 (1.51-323.08)	0.003	0.532	0.0312	0.002
Has-Let-7i-3p								
Median (range)	1.42 (0.48-6.83)	0.28 (0.10-1.14)	0.67 (0.08-6.47)	0.91 (0.08-6.83)	<0.001	0.065	0.046	<0.001
P1								
Median (range)	50.5 (2.65-736.43)	7.89 (1.27-64.39)	21.23 (0.12-2332.32)	28.42 (0.12-2332.32)	0.003	0.151	0.144	0.001
P2								
Median (range)	85.16 (6.19-741.88)	6.39 (0.67-32.05)	15.55 (0.31-2091.76)	35.06 (0.31-2091.76)	<0.001	0.086	0.024	<0.001
P3								
Median (range)	50.53 (2.65-736.43)	7.89 (1.27-64.39)	21.23 (0.12-2332.33)	28.42 (0.12-2332.33)	0.003	0.151	0.144	0.001
P								
Median (range)	130.11 (2.69-3111.11)	1.93 (0.13-25.06)	18.63 (0.01-15100.2)	34.28 (0.01-15100.2)	<0.001	0.052	0.097	<0.001

Table 10 Single miRNAs and combined *"Predictors"* (P1, P2, P3 and, P) expression values in PANNET 18F-FDG-PET/CT positive and negative patients and Healthy Donors (HDs)

Kruskal-Wallis test was used to compare the three groups. Dunn test was used for post-hoc comparisons.

NB: ID Patient=13 in ctrl group was always not evaluable for MIRNA and was excluded.

To confirm these results, we evaluated the contribution of age as a potential confounder of the analyses. Indeed, we evaluated the *miR-signature* expression value in PanNETs and healthy donors according to PanNET population median age (cut-off: 54·5 years) (see Fig.8 for age contribution to *miR-signature* and *"Predictors"* expression level in plasma of PanNETs and Healthy Donors, according to 18F-FDG-PET/CT). Median age of 38 PanNETs subset was 54·5 years (range: 24-79 years): among PanNET cohort, 18F-FDG-PET/CT positive patients (n.25) displayed 52 years (range: 24-78 years) as median age while 18F-FDG-PET/CT negative patients showed 61 years (range: 44-79 years) as median age, with a statistical difference among the two groups (0.011). In addition, a significant difference in terms of age between PanNET patients and healthy donors ($p<0.05$), further addressing the issue of age as a confounder. To exclude the potential role of age as confounder we evaluated the *miR-signature* expression value in PanNETs and healthy donors according to PanNET population median age (cut-off: 54·5 years). Of primary relevance, no significant differences were highlighted in *miR-signature* expression level between younger (<54·5) and elder (>54·5), excluding the possible contribute of age in determining miRNAs associated with the 18F-FDG-PET/CT outcome (see Figure 13 for age contribution to *miR-signature* and *"Predictors"* expression level in plasma of PanNENs and Healthy Donors, according to 18F-FDG-PET/CT). Finally, no significant differences in gender of patients and donor populations emerged. Median PFS was 41.1(95%CI:18.5%-45.2) while median OS was not reached at the time of the analysis and 12 months OS was 94.1 (95%CI:78.5-98.5). Statistical analysis, according to 18F-FDG PET/CT excluded age contribution to *miR-signature* predictivity (**Figure 13).**
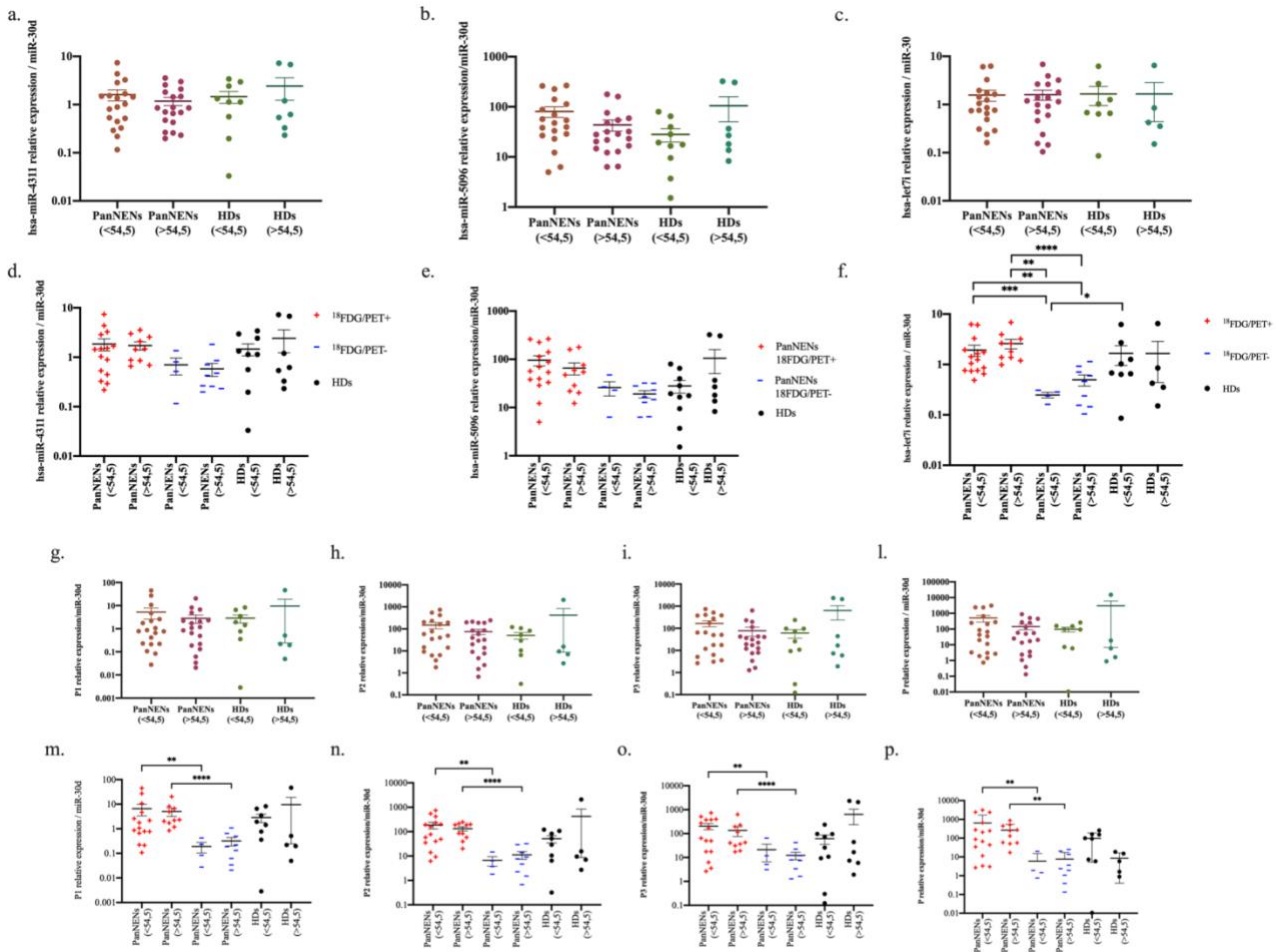
Figure 13 Demographic and clinical pathological al features according to 18F-FDG-PET/CT outcome: PAN-NEN case series

Age contribution to single miR expression level in plasma of PAN-NENs and Healthy Donors (a-c): (a) hsa-miR-4311; (b) hsa-miR-5096-5p; (c) hsa-let-7i-3p. Age contribution to single miR expression level in plasma of PAN-NENs and Healthy Donors, according to ^{18}F-FDG/PET (e-g): (e) hsa-miR-4311, in ^{18}F-FDG/PET positive and negative patients; (f) hsa-miR-5096-5p, in ^{18}F-FDG/PET positive and negative patients; (g) hsa-let-7i-3p,in ^{18}F-FDG/PET positive and negative patients. Age contribution to "Predictors" expression level in plasma of PAN-NENs and Healthy Donors, according to ^{18}F-FDG/PET (m-p): (m) P1 (hsa-miR-4311* hsa-let-7i-3p), in ^{18}F-FDG/PET positive and negative patients;.; (h) P2 (hsa-miR-5096-5p*hsa-let-7i-3p), in ^{18}F-FDG/PET positive and negative patients;.; (i) P3 (hsa-miR-4311* hsa-miR-5096-5p), in ^{18}F-FDG/PET positive and negative patients; (l) P (hsa-miR-4311*hsa-miR-5096-5p*hsa-let-7i-3p), in ^{18}F-FDG/PET positive and negative patients. Healthy Donors = HDs

4.4 Hsa-miR-5096-5p expression level can distinguish PanNET from SINET

Due to GEP-NETs intrinsic heterogeneity, differential diagnosis and primary site of origin identification could be challenging. For this reason, hsa-miR-5096-5p, hsa-let-7i-3p and/or hsa-miR-4311 were tested as potential biomarkers for differential diagnosis of PanNETs from SI-NETs. Thus, we compared the expression levels of the three miRNA signatures and combined *"Predictors"*

retrieved in PanNET with SI-NETs expression levels. Intriguingly, hsa-miR-5096-5p alone or in combination with hsa-let-7i-3p (P2) resulted to be expressed both in PanNETs and SI-NETs subsets at relatively high levels. Nevertheless, hsa-miR-5096-5p and P2 appeared be significantly upregulated in SI-NETs when compared to PanNETs (p<0,00005 and p<0,05, respectively), representing useful markers for GEP-NETs management, for differential diagnosis or when primary site of origin is unknown or doubtful. (**Figure 14**)
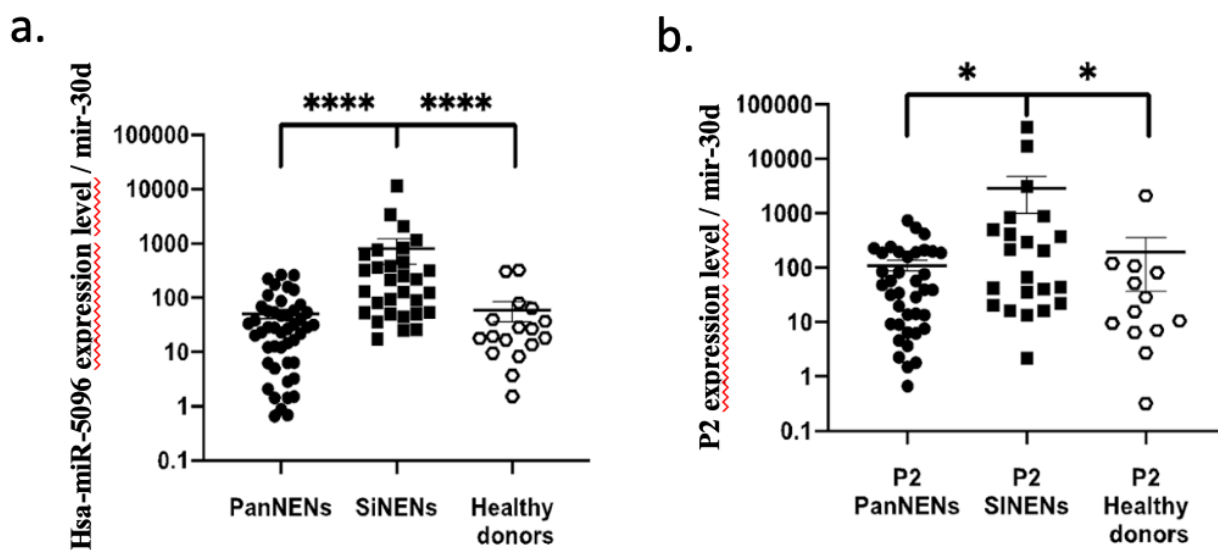
Figure 14 hsa-miR-5096-5p and P2 are significantly upregulated in SI-NETs then PanNETs

(a) hsa-miR-5096-5p expression level in PanNETs, SI-NETs and Healthy Donors; (b) P2 (hsa-miR-5096-5p*hsa-let-7i-3p expression level in PanNETs, SI-NETs and Healthy Donors.Hsa-miR-30d was selected from NGS profiling as an endogenous control. Results are presented as mean ± SD (*p-value<0.05; ****p-value<0.00005). Each graph was represented in Log10 scale and Wilcoxon and Mann-Whitney test, chi-square tests were applied respectively for continuous data and categorical data. For comparison between three groups Kruskal-Wallis test was used and Dunn test was used for post-hoc comparisons.

4.5 Circulating *miRNA-signature* and combined *"Predictors"* correlate with clinical parameters

Considering overall PanNET patients, correlation between single miRNAs and combined *"Predictors"* and clinical parameters, such as grading, ki-67% and tumor burden were explored according to calculated cut-off. The analysis revealed significant correlation between hsa-miRNA-4311 alone (cut-off: 1,44) or in combination with hsa-let-7i-3p (P1; cut-off <0,98) and ki-67% (**Figure 15** a,b), and tumor burden (**Figure 15** c,d), suggesting a prognostic role in stratifying PanNETs patients according to differentiation and proliferation status.
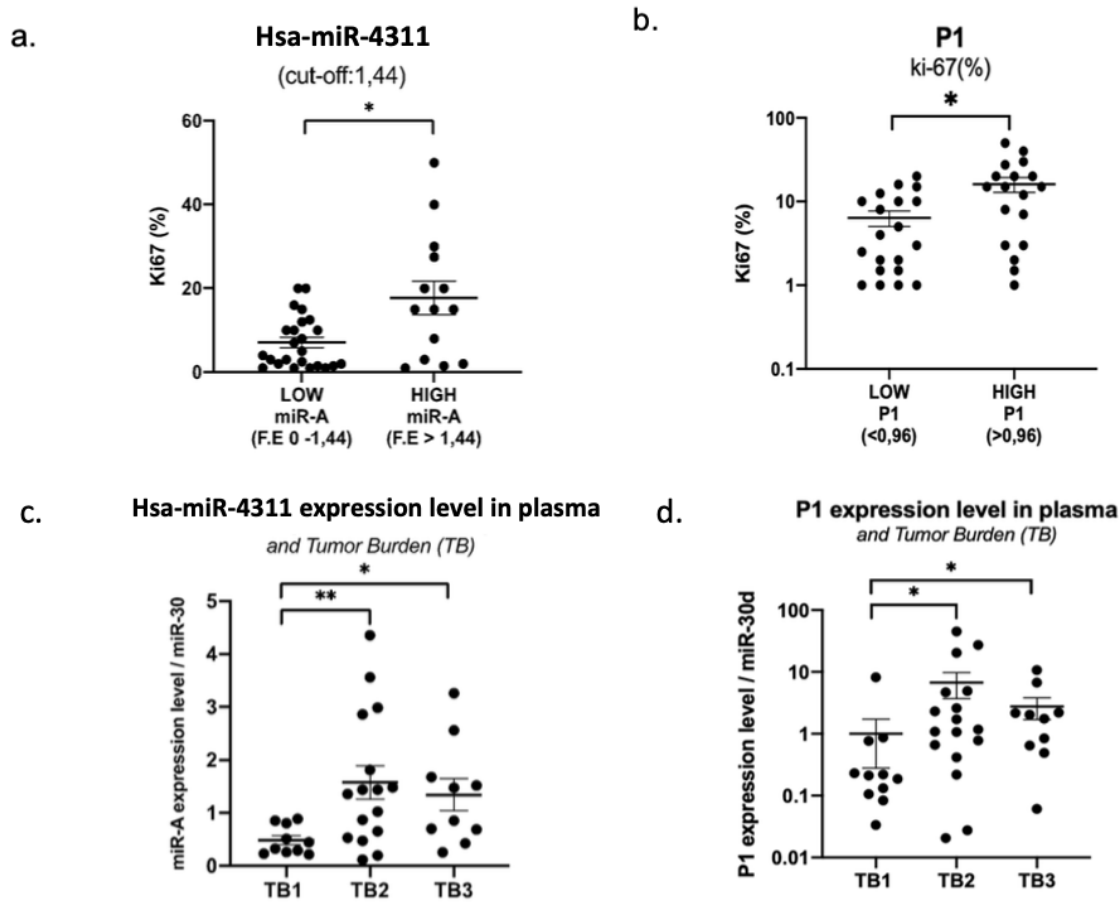
Figure 15 Significant correlations between single miRNAs and combined *"Predictors"* and clinical parameters

In addition, correlation with grading showed that combination of three miRNAs signature (P) can significantly stratify G1, G2 and G3 patients (**Figure 16**). Intriguingly a proposed cut-off of 57,1 for P can significantly distinguish between two different G2 categories (**Figure 16** c). Indeed, PanNET G2 patients with P>57,1 showed a significantly shorter PFS in respect to patients with lower circulating level of P < 57,1 (**Figure 16** d). Therefore the detection of those miRNAs can be useful in PanNET patients management, addressing G2 patients' therapeutic schedules.
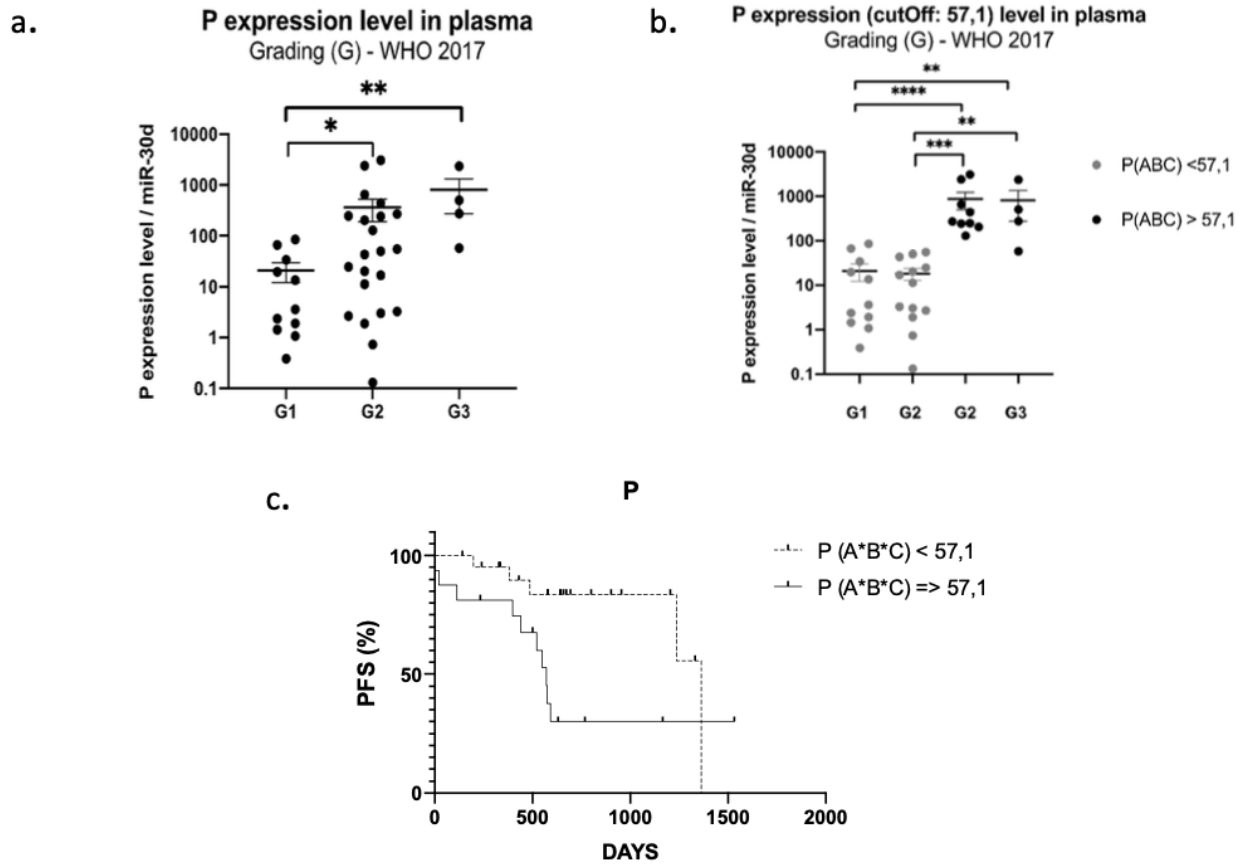
Figure 16 P correlation with grading and PFS

4.6 Circulating hsa-miR-5096-5p and *"Predictors"* are independent biomarkers of 18F-FDG-PET/CT status

The predictive power of single miRNAs and combined *"Predictors"* in relation to 18F-FDG-PET/CT positivity was evaluated. ROC analysis revealed that higher circulating expression levels of hsa-miR-4311, hsa-miR-5096-5p and hsa-let-7i-3p alone or combined can predict 18F-FDG-PET/CT positive outcome with significant AUCs between 0.81 and 0.95 (**Figure 16** and Table 1).
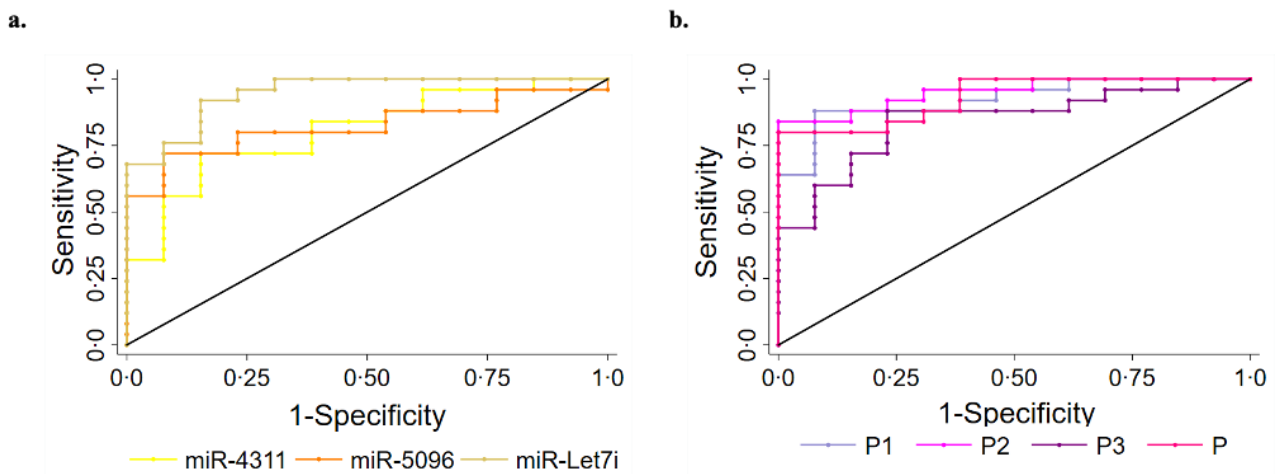

Figure 16 Performance of the circulating signature in predicting ^{18}F-FDG/PET outcome in PanNET validation set (n=38).

(a) ROC curve of the single miRNAs: hsa-miR-4311; hsa-miR-5096-5p: hsa-miR-5096-5p; miR-let7i: hsa-let-7i-3p. Roccomp plots the ROC curves on the same graph. DeLong, and Clarke-Pearson (1988) algorithm was applied to provide a test for the equality of the area under the curves ROC curve of combined (b)"Predictors": P1 (hsa-miR-4311* hsa-let-7i-3p); P2 (hsa- mir-5096*hsa-let-7i-3p); P3 (hsa-miR-4311* hsa-miR-5096-5p); P (hsa-miR-4311*hsa-miR-5096-5p*hsa- let-7i-3p), with comparable significant AUCs. The combination of hsa-miR-5096-5p and hsa-let-7i-3p into predictor P2 (cut-off: 33.55) showed the highest predictivity (AUC: 0.95; 95% CI: 0.89-1.00) for 18F-FDG PET/CT positive status.

The statistical comparison confirmed that AUCs of single mirRNAs and combined "*Predictors*" are significative and comparable (**Table 11**). Notably, hsa-miR-5096-5p and hsa-let-7i-3p alone or in combination into P2 displays the best metrics as prognostic biomarkers for 18F-FDG PET/CT positive status (AUC: 0.95; 95% CI: 0.89-1.00).

Clinical Endpoint	Predictor	AUC (95%CI)	Compared predictor	AUC (95%CI)	p-value
[18]FDG/PET positivity	miR-4311	0.8062 (0.66-0.94)	miR-5096	0.8246 (0.69-0.95)	0.8257
			let-7i-3p	0.9477 (0.88-1.99)	0.0541
			P1	0.9231 (0.83-1.00)	0.0068
			P2	0.9508 (0.89-1.00)	0.0285
			P3	0.8462 (0.71-0.97)	0.3794
			P	0.9323 (0.85-1.00)	0.0188
	miR-5096	0.8246 (0.69-0.95)	let-7i-3p	0.9477 (0.88-1.99)	0.0913
			P1	0.9231 (0.83-1.00)	0.1731
			P2	0.9508 (0.89-1.00)	0.0310
			P3	0.8462 (0.71-0.97)	0.0642
			P	0.9323 (0.85-1.00)	0.0505
	let-7i-3p	0.9477 (0.88-1.99)	P1	0.9231 (0.83-1.00)	0.534
			P2	0.9508 (0.89-1.00)	0.9260
			P3	0.8462 (0.71-0.97)	0.1313
			P	0.9323 (0.85-1.00)	0.6598
	P1	0.9231 (0.83-1.00)	P2	0.9508 (0.89-1.00)	0.4841
			P3	0.8462 (0.71-0.97)	0.1240
			P	0.9323 (0.85-1.00)	0.7333
	P2	0.9508 (0.89-1.00)	P3	0.8462 (0.71-0.97)	0.0217
			P	0.9323 (0.85-1.00)	0.3671
	P3	0.8462 (0.71-0.97)	P	0.9323 (0.85-1.00)	0.0259

Table 11 Combined "*Predictors*" (P1, P2, P3 and P) show significant comparable AUCs for 18FDG/PET positivity predictions.

"Predictors": P1 (hsa-miR-4311 hsa-let-7i-3p); P2 (hsa- mir-5096*hsa-let-7i-3p); P3 (hsa-miR-4311* hsa-miR-5096-5p); P (hsa-miR-4311*hsa-miR-5096-5p*hsa- let-7i-3p), with comparable significant AUCs. The combination of hsa-miR-5096-5p and hsa-let-7i-3p into predictor P2 (cut-off: 33.55) showed the highest predictivity (AUC: 0.95; 95% CI: 0.89-1.00) for 18F-FDG PET/CT positive status.*

4.7 Circulating hsa-miR-5096-5p and *"Predictors"* are independent biomarkers of survival and identify PanNET patients not benefitting from PRRT

In addition, ROC and Kaplan–Meier (KM) analysis of single miRNAs and combined "*Predictors*" was conducted for PanNET subset (n=38) treated with ^{177}Lu-DOTATATE based PRRT towards Survival Endpoints (PFS and OS; **Figure 17**). The analyses showed that hsa-miR-5096-5p best predicts 6-mo PFS (AUC: 0.8966; 95% CI: 0.76 - 1.00; Figure 17a) and 12-month OS (AUC: 0.8929; 95% CI: 0.72-1.00; Figure 17b). Time dependent (range: 3 - 24 months) ROC curve analysis for PFS showed that hsa-miR-5096-5p maintains prognostic AUC values up to 24 months (Figure 17c; TimeROC package in R software was used to provide an estimation of time-dependent ROC curve and the associated time dependent AUC in the presence of censored data). Furthermore, circulating hsa-miR-5096-5p expression level (cut-off: 70) distinguished PanNET patients with poor prognosis from responders to PRRT for both PFS (p-value:<0.001; Figure 17d) and OS (p-value:< 0.05; Figure 17d).
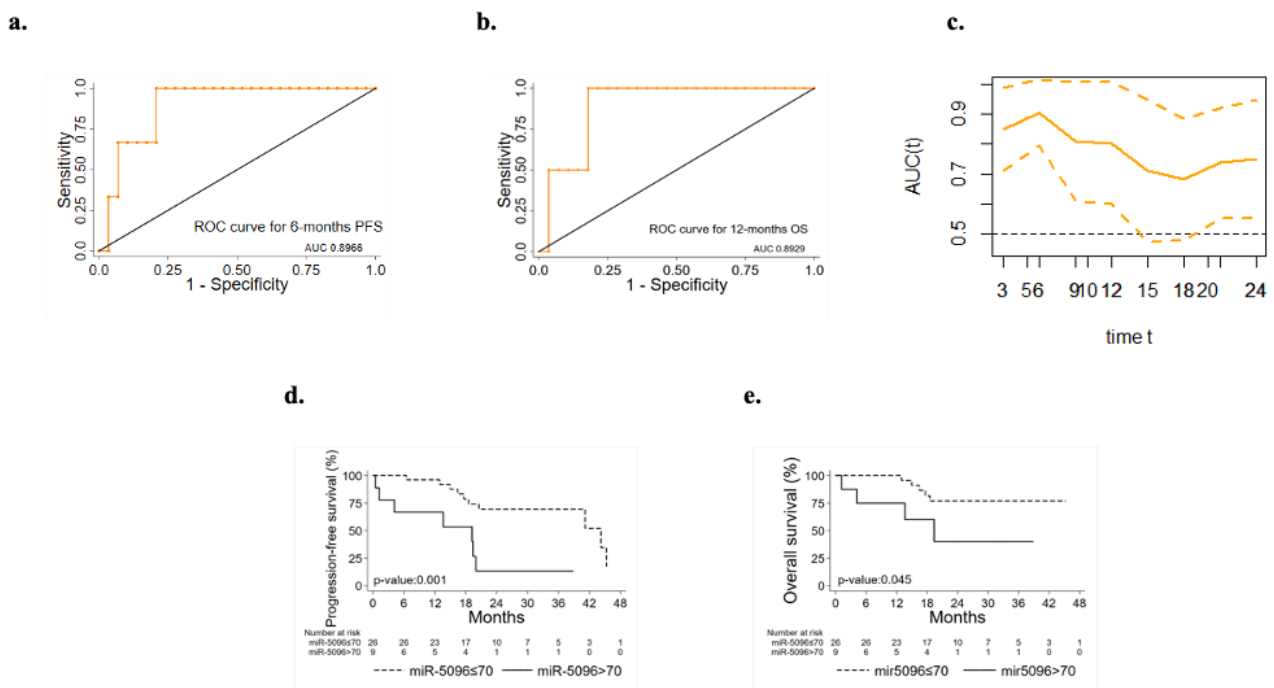

Figure 17 Hsa-miR-5096-5p can predict PFS and 12-mo OS in PanNET patients.

Performance of circulating hsa-miR-5096-5p in predicting 6-mo PFS and 12-mo OS in PanNET patients treated with ^{177}Lu-DOTATATE (n=38). ROC curve analysis (a;b) of: (a) hsa-miR-5096-5p for 6-mo PFS; (b) hsa-miR-5096-5p for 12-month OS. (c) Time dependent AUC curve (95% C.I) for hsa-miR-5096-5p prediction of 3–24-month PFS; TimeROC package in R software was used to provide an estimation of time-dependent ROC curve and time dependent AUC in the presence of censored data. Kaplan–Meier analysis (d-e) of: (d) PFS by hsa-miR-5096-5p in PanNET

Importantly, hsa-miR-5096-5p emerged to be an accurate predictor of 6-mo PFS (AUC: 0.8636; 95% CI: 0.68-1.00; Figure 18a) in the subgroup of ^{18}F-FDG PET/CT positive patients, characterized by more aggressive disease. Specifically, a cut-off of 70 resulted in 100% sensitivity and 68% specificity identifying a subset of patients that progress earlier and do not benefit from ^{177}Lu-PRRT treatment (p-value:< 0.01; Figure 18c). It is worth noting that the LIU/Yuden *standard computed* cut-off shows equal performances to our *in-house* defined cut-off (70) for all investigated clinical endpoints, thus substantiating its robustness (data not shown). Finally, although hsa-miR-5096-5p represents an accurate predictor also for 12-mo OS in the ^{18}F-FDG PET/CT positive subset (AUC: 0.8571; 95% CI: 0.63-1.00; Figure 18b), a cut-off of 70 could not significantly stratify ^{18}F-FDG PET/CT positive patients for 12-mo OS predictions (p-value:0.22; Figure 18d).
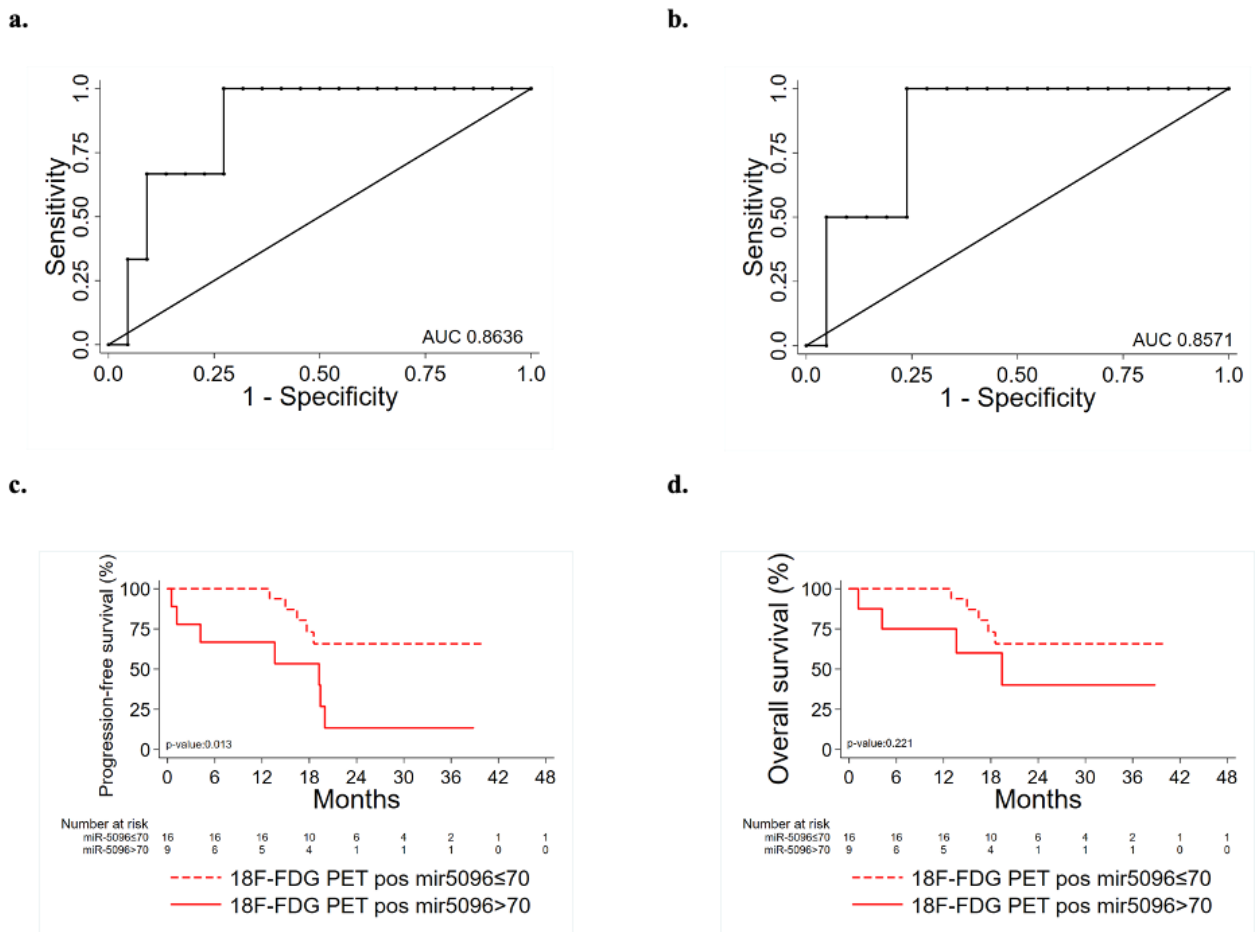

Figure 18 Hsa-miR-5096-5p can predict PFS and 12-mo OS in ^{18}F-FDG/PET positive PanNET patients.

Performance of circulating hsa-miR-5096-5p in predicting 6-mo PFS and 12-mo OS in ^{18}F-FDG PET/CT positive (+) PanNET patients treated with ^{177}Lu-DOTATATE (n=25). ROC curve analysis (a;b): (a) hsa-miR-5096-5p for 6-mo PFS in ^{18}F-FDG PET/CT positive (+) patients; (b) hsa-miR-5096-5p for 12-month OS in ^{18}F-FDG PET/CT positive (+) patients. Kaplan–Meier analysis (d-e) of: (d) PFS by hsa-miR-5096-5p, including at risk patients for each stratum; in

^{18}F-FDG PET/CT positive subgroup; (e) OS by hsa-miR-5096-5p including at risk patients for each stratum in ^{18}F-FDG PET/CT positive subgroup.

Moreover, ROC of combined *"Predictors"* was conducted, reporting comparable significant AUCs (> 0.8; 95%) for P2, P3 and P in predicting Survival Endpoints (6-mo PFS; Figure 19a). KM for PFS showed significant p-values for P3 (cut-off: 142·9) and P (cut-off: 108·3) in predicting PFS (figure 19e; h). Intriguingly, KM for PFS, according to ^{18}F-FDG/PET-CT outcome revealed that P3>142·9 can stratify PanNENs with poorer prognosis. Finally, the analyses conducted on PanNETs positive subgroup alone identify P>108·3 as best candidate among *"Predictors"* to identify patients who progress earlier and may benefit to different therapeutic schedule (figure 19i). **Figure 19** highlights the performance of circulating P2, P3 and P in predicting Progression Free Survival (PFS) outcome in PanNET patients overall case series and in PanNET 18F-FDG/PET-CT positive subgroups.
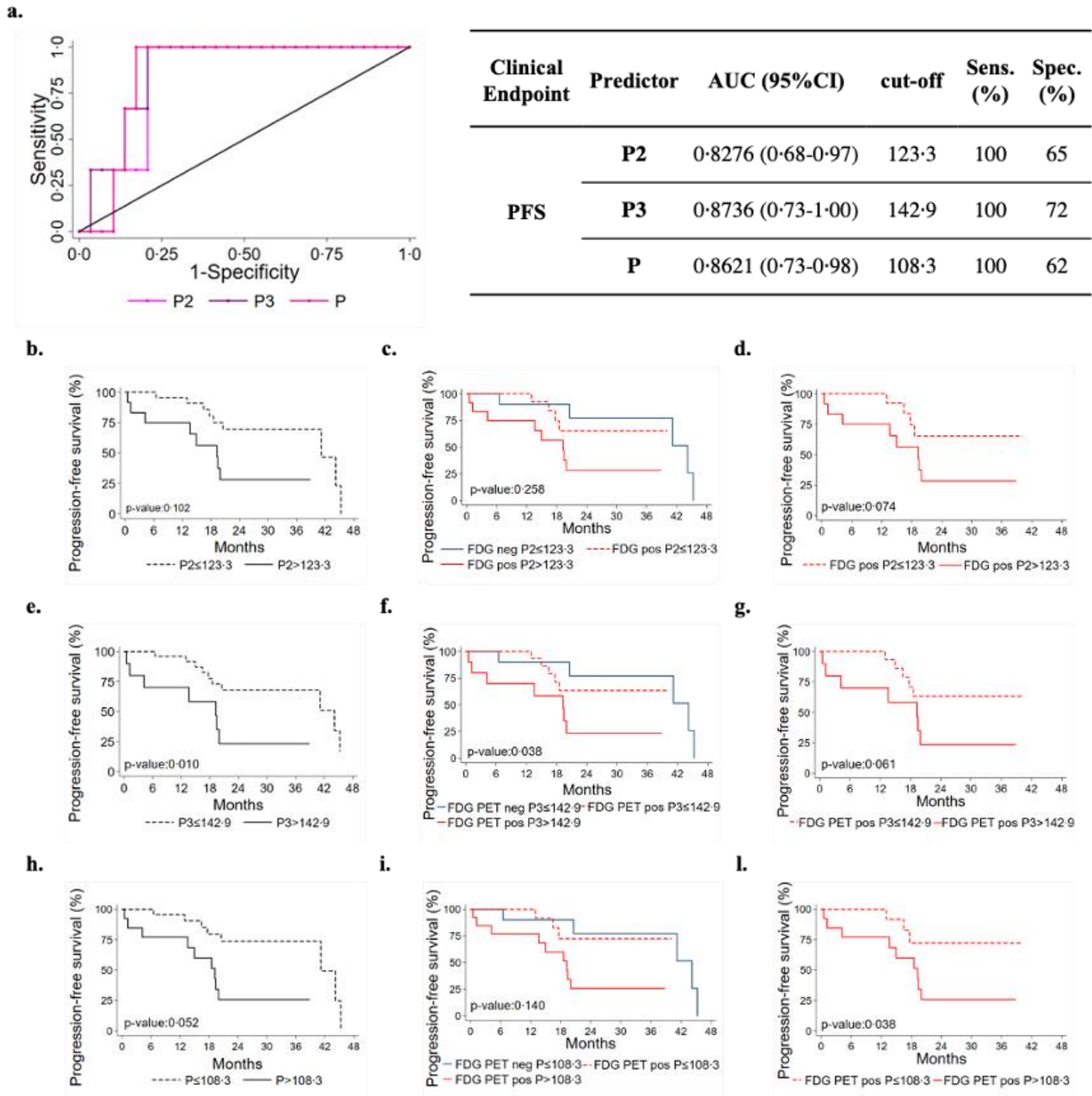
Figure 19: The performance of circulating P2, P3 and P in predicting Progression Free Survival (PFS) outcome in PanNEN patients treated with ^{177}Lu-DOTATATE

(a-l). (a) Combined ROC curve of P2, P3 and P, with significantly high AUCs. Associated table reports AUCs values, the identified cut-off and sensitivity and specificity percentages of proposed biomarkers. (b-l) Kaplan–Meier analysis (KM) for Progression Free Survival (PFS) of: (b) P2 (cut-off: 123·3); (c) P2 (cut-off: 123·3), according to ^{18}F-FDG/PET-CT outcome; (d) P2 (cut-off: 123·3), in ^{18}F-FDG/PET-CT positive patients. (e) P3 (cut-off: 142·9) (f) KM analysis of P3 (cut-off: 142·9), according to ^{18}F-FDG/PET-CT outcome; (g) P3 (cut-off: 142·9), in ^{18}F-FDG/PET-CT positive subgroup; (h) P (cut-off: 108·3); (I) P (cut-off: 108·3), according to ^{18}F-FDG/PET-CT outcome; (l) P (cut-off: 108·3), in ^{18}F-FDG/PET-CT positive subgroup.

4.8 Hsa-miR-5096-5p inversely correlates with SSTR2 expression in PanNETs

To further assess its clinical impact in PanNET management, the correlation analyses of miRNA signature with ^{68}Ga-DOTATOC PET/CT SUV$_{max}$ and SSTR-2 expression was conducted (**Figure 20**). Interestingly, increased expression levels of circulating hsa-miR-5096-5p (cut-off: 70) correlated with lower ^{68}Ga-DOTATOC PET/CT SUV$_{max}$ (Mann Whitney test, p-value < 0.05) in PanNET patients (Figure 20a). According with previous observation, a negative association of 68Ga-DOTATOC PET/CT SUVmax and ^{18}F-FDG-PET/CT positivity in patients displaying low and high levels of hsa-miR-5096-5p (cut-off:70; Spearman: p< 0,0169; r2: -0,4928) was observed (Figure 20b). Since ^{68}Ga-DOTATOC PET/CT SUV$_{max}$ mirrors SSTR2 expression level in PanNET patients, the observed inverse correlation suggested that hsa-miR-5096-5p may be involved in SSTR2 regulation also at the tissue level. To confirm this hypothesis, a semi-automated immune-miRNA-ISH approach coupled with a dedicated pipeline of analysis (AND-Tool software) was set up and applied to detect and quantify hsa-miR-5096-5p and SSTR2 expression simultaneously on FFPE tumor tissue samples. Eight independent G1, G2 (n.5) and G3 (n.3) PanNET FFPE tumor tissue specimens were first reviewed by an expert pathologist for SSTR2 expression level. Two were negative, four were frankly positive (100%; 3+) and two displayed SSTR2 heterogeneous expression (Figure 20c-d). AND-Tool software analysis of n=8 PanNET FFPE samples, considering 10 ROIs (Regions Of Interest) per patient, 76 total ROIs (four ROIs drop-out due to presence of a tissue folding in one case sample), resulted in the extraction of 197847672 pixels, corresponding to an average value of 15186±7547 analyzed cells per sample. Using AND-Tool software we extracted Dark-red, Light-pink, and White masks for each ROIs separately. Subsequently, we applied a pixel-based analyses of Dark-Red (SSTR2 positive), Light-Pink (SSTR2 low) and White (SSTR2 negative) masks showing 27% Dark-Red pixels, corresponding to the amount of frankly positive cells; 22% of Light-Pink pixels, corresponding to the amount of low expressing cells; and 51% White pixels of negative expression areas (Figure 20e). Correlation analysis confirmed a significant inverse association between the number of hsa-miR-5096-5p positive cells and SSTR2 expression level on PanNET tissue (Spearman; r=-0,4676; p<0,0001; Figure 20f). Importantly, areas with low/moderate SSTR2 expression, which also define patients eligible for PRRT, showed an intermediate frequency of hsa-miR-5096-5p positive nuclei. These observations agree with a mechanistic model where hsa-miR-5096-5p expressing cells can contribute to tumor heterogeneity and mosaicism through a paracrine SSTR2 interference which could hinder PanNET targeting and ineffective responses to PRRT. Those results show that hsa-miR-5096-5p is expressed by PanNET tumor cells and that, the inverse

correlation between circulating hsa-miR-5096-5p levels and ^{68}Ga-DOTATOC PET/CT SUV$_{max}$ values, mirrors an interplay occurring also at the tissue level.
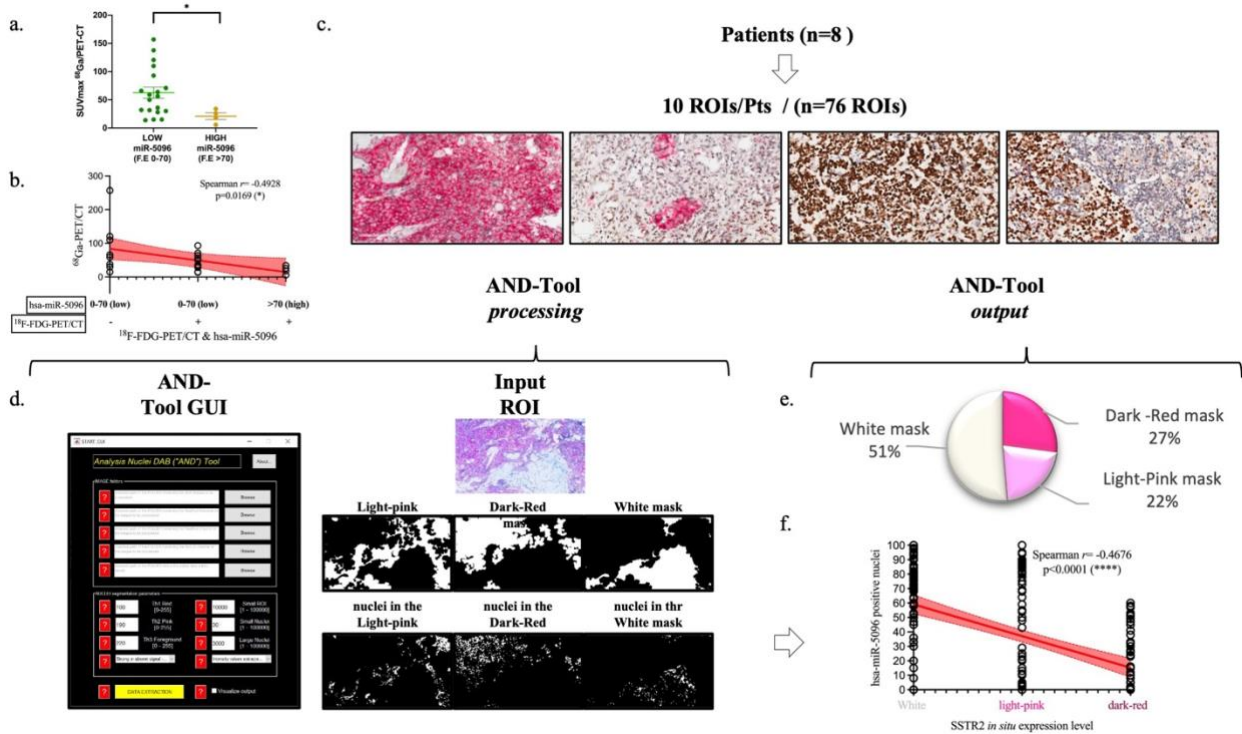

Figure 20 Hsa-miR-5096-5p expression inversely correlates with SSTR2 expression levels in PanNET patients.

(a) Correlation analysis of expression of circulating hsa-miR-5096-5p and 68Ga-PET SUVmax in plasma of PanNET patients (n=38 excluding 15 patients due to missing data on 68Ga-PET SUVmax value). Data comparison was conducted by means of Mann Whitney test (p: 0,04). (b) Correlation analysis (Spearman; p< 0,0169; r2: -0,4928) of 68Ga-PET/CT SUVmax and 18F-FDG-PET/CT positivity in patients displaying low and high levels of hsa-miR-5096-5p (cut-off:70) in plasma of PanNET patients. (c) Representative images of PanNET tumor heterogeneity: simultaneous detection of hsa-miR-5096-5p (DAB-BROWN) and SSTR2 protein (RED) in FFPE tumor tissue through our miR-protein protocol. (d) AND-Tool automated analysis on PanNET FFPE samples (n=8). On the left, a screenshot of the AND-Tool graphical user interface (GUI). On the right, an example of analysis with at the top part an input ROI. In the central part, light-pink, dark-red, and white masks, respectively. In the bottom part, segmented nuclei are subdivided for the different masks. (e) Illustrative diagram of overall analyzed pixels in terms of SSTR2 expression: frankly positive (27%), heterogeneous (22%) and negative (51%) expression areas; (f) Correlation analysis (Spearman; r=-0,4676; p<0,0001) of hsa-miR-5096-5p positive nuclei (%) in and SSTR2 expression level in FFPE PanNET specimens

4.9 Hsa-miR-5096-5p modulates SSTR2 expression *in vitro*

In order to investigate the mechanism of action of hsa-miR-5096-5p on SSTR2 expression, we performed bioinformatic analysis with the following web-based softwares, TargetMiner, TargetScanVert and miRDB. This analysis revealed that the 3'-UTR of SSTR2 (NCBI Gene ID: 6752; GenBank Accession:NM_001050.03) harbors 4 potential binding sites for hsa-miR-5096-5p

(miRbase Accession: MIMAT0020603; Sequence: GUUUCACCAUGUUGGUCAGGC). In particular, two different sequences (GUGAAAA; GGUGAAA) are distributed on 4 sites at the 3'-UTR of the gene (723-729; 3001-3007 and 1008-1015; 2290-2260, respectively) and are predicted to be recognized by the CACUUU and CCACUUU sequences of hsa-miR-5096-5p. The presence of the binding sites supported a possible regulation of expression via direct RNA interference in PanNET tumor cells.

In order to test this hypothesis, we performed *in vitro* experiments on the insulinoma NT-3 cell line, a newly established preclinical model of well differentiated low-grade PanNET (35). Importantly, the neuroendocrine phenotype and morphology as well as the proliferative rate and the expression of different SSTR isoforms in NT-3 cells can be modulated by the presence of growth factors (bFGF/EGF) in culture (35). SSTR2 and hsa-miR-5096-5p basal expression levels are inversely correlated in NT-3 cells, cultivated both with and without (w/o) growth-factors (GFs) (Figure 21b). In particular, SSTR2 expression was significantly enhanced (p-value<0.005) in NT-3 cells cultivated in standard RPMI (w/o GFs), characterized by low proliferation rate (10.9 +/- 0.7 days) and low ki-67 percentage (20%) (35). Conversely, hsa-miR-5096-5p resulted to be significantly downregulated (p-value< 0.005) in these conditions confirming its negative correlation with SSTR2 expression and in agreement with the mechanism of action we have envisioned. Furthermore, NT-3 cells were ectopically treated with hsa-miR-5096-5p-mimic while cultivated without bFGF and EGF (SSTR2^{high}/hsa-miR-5096-5p^{low}endogenous expression). As expected, the ectopic delivery of hsa-miR-5096-5p via miRCURY LNA transfection resulted in a significant intracellular increase of hsa-miR-5096-5p/mimic, compared to not-transfected and scramble controls, confirming transfection effectiveness (p-value<0.0001; Figure 21c). Treatment of NT-3 cells with hsa-miR-5096-5p mimic for 72hr decreased SSTR2 mRNA level of 51% as compared to scramble-treated cells (p-value<0.005; Figure 21c). Conversely, NT-3 cells treated with hsa-miR-5096-5p-inhibitor while cultivated with growth-factors (SSTR2^{low}/hsa-miR-5096-5p^{high} endogenous expression) showed a significant increase in SSTR2 transcript quantity (+42%, p<0.005; Figure 21d). The magnitude of these modulations is in line with literature, indeed the high amount of intracellular hsa-miR-5096-5p mimic detected by RT/qPCR, corresponds to a modest modulation of the targets, due to the non functional/activated portion of spiked mimic (37). To further substantiate the function of hsa-miR-5096-5p as putative post-transcriptional modulator of SSTR2 expression, its basal expression level was investigated also in preclinical models of high-grade PanNEN: QGP-1 and BON-1 cells, characterized by high proliferation rate and high ki-67 percentage (about 80%). QGP-1 and BON-1 displayed significantly different amounts of SSTR2, inversely associated with significantly different

hsa-miR-5096-5p amounts ($p<0.001$ and $p<0.01$, respectively; Figure 21e). Importantly, QGP-1 treated cells showed a 39% significant increase of SSTR2 transcripts ($p<0,01$; Figure 21f). Altogether these results suggest that the delivery of specific small non-coding molecules hindering hsa-miR-5096-5p activity into PanNET cells can translate into *SSTR2* transcripts increased stability and higher SSTR2 amount at the cell membrane. Given their high amount of hsa-miR-5096-5p, associated with low SSTR2 expression, QGP-1 cells were chosen as a model to revert SSTR2 expression in high grade PanNET cells by hsa-miR-5096-5p-inhibitor treatment.
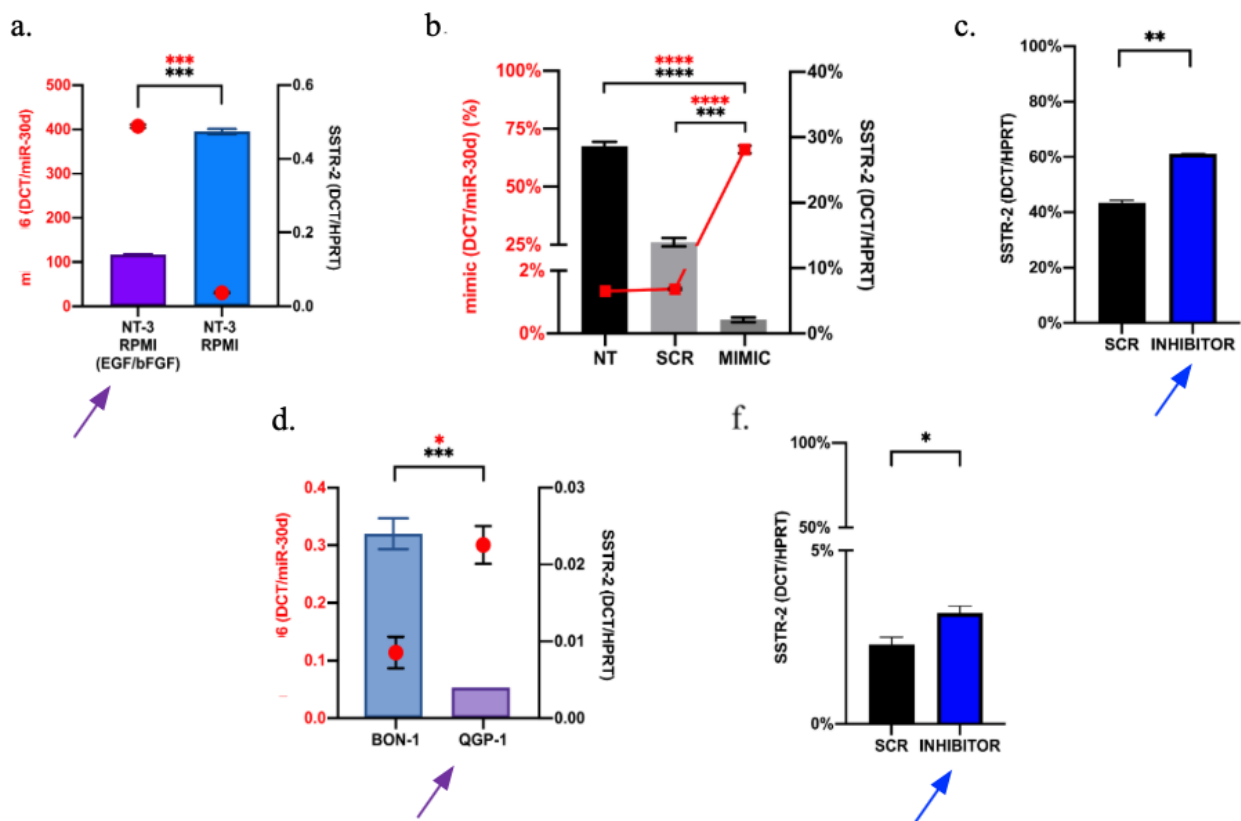

Figure 21 Hsa-miR-5096-5p modulates SSTR2 expression in PanNET preclinical model

(a) hsa-miR-5096-5p (red dot) and SSTR2 (Bars) basal expression level in low-grade NT-3 cell lines cultivated with(arrow) or w/o growth factors (EGF; bFGF); (b) hsa-miR-5096-5p (red dot) and SSTR2 (Bars) after treating with mimic and scr control (c) hsa-miR-5096-5p and SSTR2 expression in NT-3 cell lines 72h post transfection with inhibitor miR-5096 mimic and scramble control; (d) SSTR2 expression in NT-3 cell lines, cultivated with growth factors, 72h post transfection with miRCURY LNA miR-5096 inhibitor and scramble control; (e) hsa-miR-5096-5p and SSTR2 basal expression level in high-grade BON-1 and QGP-1 cell line; (f) SSTR2 expression in QGP-1 cell lines, 72h post transfection with miRCURY LNA miR-5096 inhibitor and scramble

Given this, the effect of the interference of has-miR-5096 inhibitors on SSTR-2 was assessed also at the protein level in QGP-1. Immunofluorescence analysis confirmed a significant increase in the expression of SSTR-2 in QGP-1 cells treated with hsa-miR-5096 inhibitor (Figure 22 lower panels)

when compared to cells not treated or treated with scramble control (Figure 22 upper panels). Potentially this finding represents an important addition in the context of PRRT treatment targeting SSTR2 protein at the cell membrane. Indeed upregulation of SSTR2 at the tumor level induced by those molecules could improve radionuclide treatment efficacy thereby addressing better tumor heterogeneity.
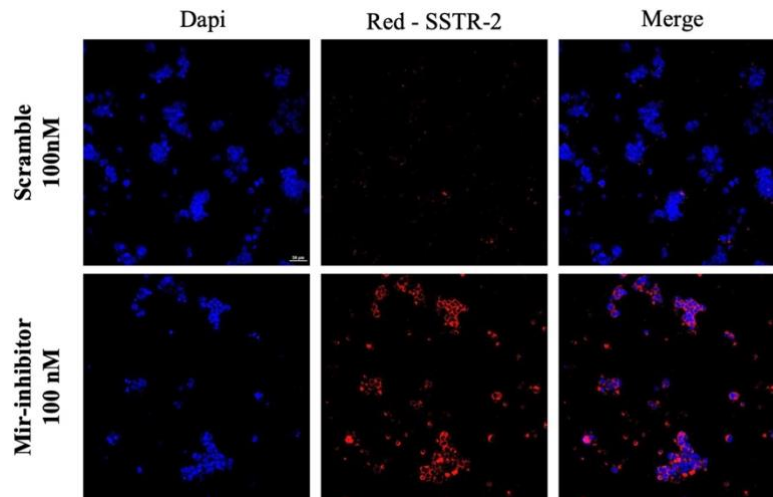

Figure 22 Hsa-miR-5096 inhibition results in SSTR2 upregulation at the protein level in QGP-1 cell lines.

Representative immunofluorescence staining of SSTR2 (red) in QGP-1 cells treated with miRCURY LNA miR-5096 inhibitor and scramble control.DNA stained with DAPI (blue)
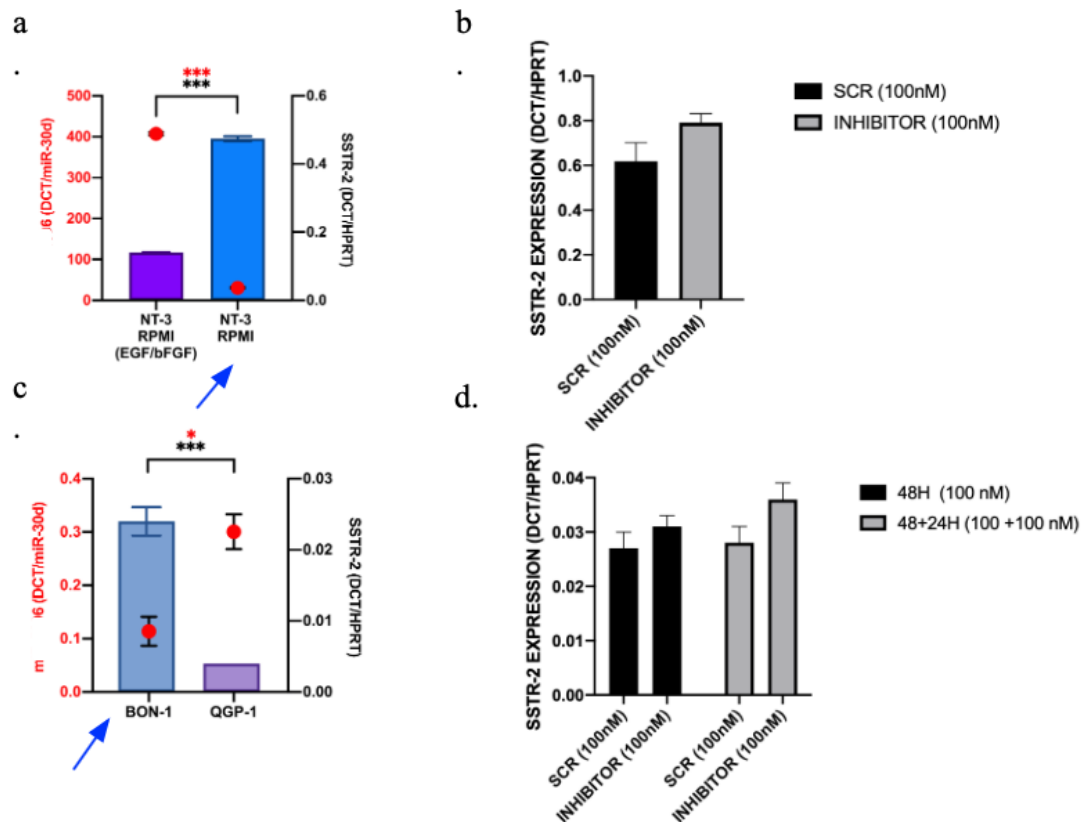
Figure 23 NT-3 and BON-1 showed lower level of has-mir-5096 and do not significantly respond to treatment with mir-inhibitor.

(a) Has-miR-5096 (red dot) and SSTR2 basal expression (bars) in NT-3 with w/o GF (arrow) cell lines (c) Has-miR-5096 (red dot) and SSTR2 basal expression (bars) in high-grade BON-1 1 (arrow) and QGP-1 (arrow) cell line. SSTR2 expression 72h post transfection with miR-5096 inhibitor and scramble control in NT3 w/o GF(b) and BON-1 (d)

Indeed, BON-1 and NT-3 (w/o GFs) showing lower basal levels of has-miR-5096 (Figure 23a, c) do not significantly upregulate SSTR-2 (Figure 23 b, d).

For this reason, BON-1 and NT-3 cultivated w/o GFs, were treated with target site blockers, that can shield the 4 retrieved sites at the 3'-UTR of the SSTR2 gene (723-729; 3001-3007 and 1008-1015; 2290-2260, respectively; Figure 24a). SSTR2 emerged to be upregulated, and TBS emerged to be the best inhibition strategies in these conditions (Figure 24 b, c)
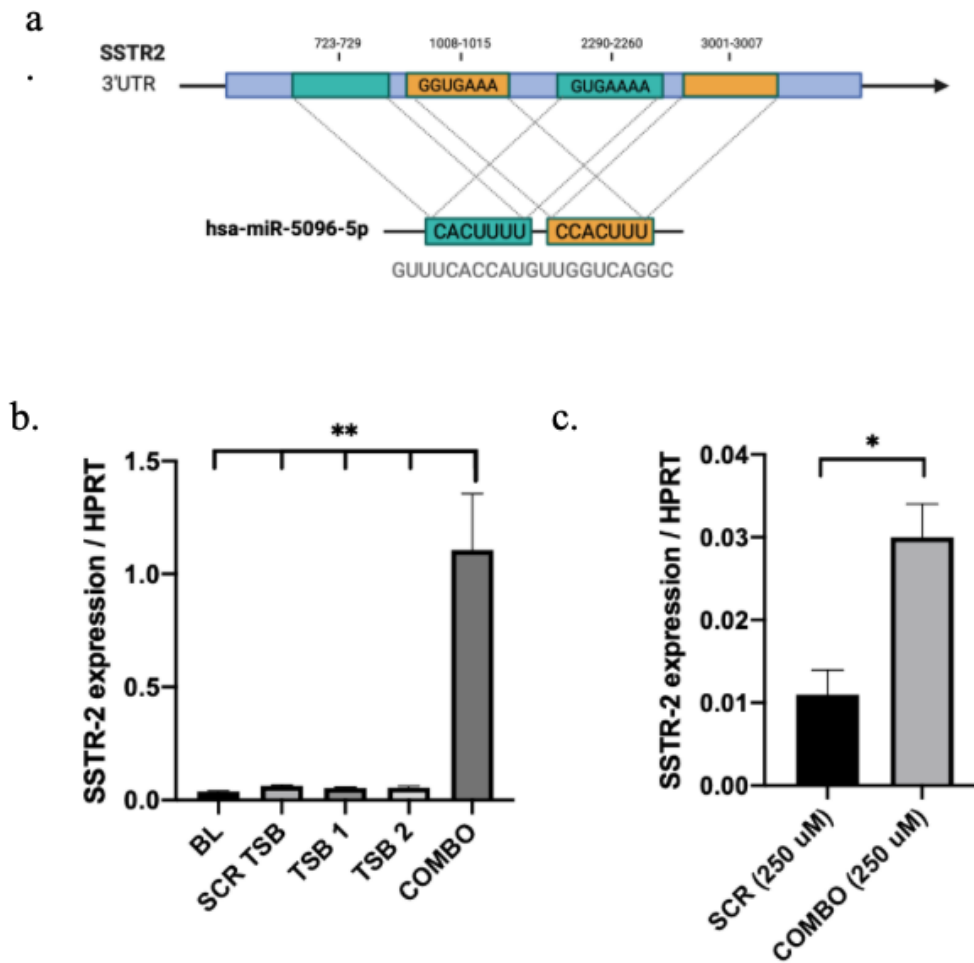
Figure 24 NT-3 and BON-1 treated with has-miR-5096 Target Site Blocker (TSB)

(a) Schematic representation of hsa-mir-5096 binding sites and their relative position on SSTR2 3'UTR; (b) SSTR2 expression level in low-grade NT-3 cell lines cultivated w/o growth factors and treated with single SSTR2 specific TSBs or in COMBO and scramble controls (c) SSTR2 expression level in BON-1 cell lines cultivated w/o growth factors and treated with control scrambled TSB or with COMBO SSTR2 specific TSBs.

5. Discussion

The absence of early-stage diagnosis, tumor heterogeneity and lack of validated companion circulating biomarkers delay therapeutic intervention of PanNET patients, ultimately impacting on survival. Imaging is complex and based on sophisticated invasive technologies, often failing to predict clinical outcome. Standard CT/MRI bear well-described sensitivity limitations and may lead to false negative results compared to functional imaging 68Ga-SSA-PET/CT. Furthermore, imaging can be invasive as it exposes patients to repetitive radiation sessions. Both clinical and imaging are operator-dependent strategies having high intra-observer variability (2). On the other hand, blood biomarkers represent easy-to-detect and non-invasive tools to evaluate disease with quantitative and parametric measurements (2). The advent of more sensitive technologies revolutionized the concept of biopsy, shifting from tumor tissue oriented to a systemic snapshot of the disease. Liquid biopsy allows the detection of specific nucleic acids in body fluids, and it has particularly benefited from NGS and quantitative PCR approaches, partially overcoming the limit of tumor biopsy heterogeneity (2). Application of those analyses to blood samples has clear advantages, by allowing multiple and consecutive measurements to follow disease recurrence and clinical management outcomes. The multinational, multidisciplinary Delphi consensus encouraged multi-analyte measurements usage to provide more accurate information on the proliferative, metabolic, and metastatic features of NETs (4). In this context, the combination of *in vivo* spatial and functional imaging of the tumor with measurable circulating transcripts (mRNAs and ncRNAs) should be preferred and could represent a key strategy for real-time disease monitoring and prognostication in the near future (9). In addition, regarding the blood based multianalyte tests (e.g mRNA transcripts), the Food and Drug Administration provides guidelines for *in vitro* diagnostic (IVD) tools development. Indeed, FDA defines as IVD "any reagent, instrument, and/or system intended for use in diagnosis of disease or other conditions, including a determination of the state of health, in order to cure, mitigate, treat, or liquid biomarkers include circulating cell-free DNA (cfDNA), circulating tumor cells (CTCs), small-non-coding molecules, as microRNAs (miRNAs) or long non-coding RNAs (lncRNA), blood transcripts (e.g., NETest) and proteins (**Table 6**).

In this context, this PhD study has focused on advanced, metastatic, and inoperable well-differentiated PanNETs, often routed to PRRT, targeting SSTRs with radiolabelled somatostatin analogues (SSAs). Nonetheless, while ^{68}Ga-DOTATOC PET/CT SUV$_{max}$ functional imaging is used to drive eligibility to PRRT and to predict its efficacy, the heterogeneous expression of SSTR2 in PanNETs affects PRRT sensitivity and accuracy. Indeed, despite ^{68}Ga-DOTATOC PET/CT SUV$_{max}$

helps to stratify PanNET patients, about 60% of patients do not respond to SSTR-based PRRT. Of note, PanNETs often display an increased glucose metabolism and an aggressive behavior which correlate with ^{18}F-FDG-PET/CT positivity and with poor PFS when treated with PRRT, suggesting a key role of tumor metabolism in the development of a PRRT refractory tumor phenotype (1, 24-28). Both ^{18}F-FDG PET/CT and ^{68}Ga-DOTATOC PET/CT have shown to be prognostic and predictive, but with some limitations, such as the difficulty of quantification and the lack of standardization of the uptake from multiple lesions. In this framework, it is still of clinical relevance to *i)* better understand the biology of these tumors, investigating molecular mechanisms leading to a PRRT refractory phenotype; *ii)* improve prognostic and predictive algorithms and provide better stratification of PanNETs undergoing PRRT. Currently, the only approved *in vitro diagnostic* (IVD) tool for NETs is the NETest. Recently, NETest was combined with grading and used to generate a PRRT predictive quotient (PPQ) for NETs. However, the NETest does not consider neither the contribution of tumor metabolism nor a direct correlation with ^{18}F-FDG-PET/CT status (38-42). Our results suggest a potential role of hsa-miR-5096-5p alone and combined into predictor P2 as oligo-analyte indicators for ^{18}F-FDG/PET positivity in PanNET patients (**Table 10**). In this context, *Predictors* may be useful to build a multi-analyte assay, given the possibility to mathematically combine the prognostic power of two or more miRNAs within a single blood withdrawal. In addition, ROC curve and KM analysis revealed that hsa-miR-5096-5p is an accurate and independent predictor of PFS in PanNET patients treated with ^{177}Lu-DOTATATE PRRT with 90% accuracy. In our retrospective study, our assay exhibits a metric comparable with the NETest (38). Of clinical relevance, the combination of 18F-FDG PET/CT positivity with a value of hsa-miR-5096-5p>70 identifies a novel prognostic category characterized by the poorest PFS after 177Lu-DOTATATE PRRT. Cut-off of 70 shows similar performance to LIU/Yuden standard computed cut-off but it avoids false positives at 18F-FDG PET/CT, preventing overtreatment of negative patients (hsa-miR-5096-5p <70). Of clinical relevance, the same cut-off of 70 well performs for different endpoints, thus increasing the clinical utility of this marker and facilitating data interpretation. hsa-miR-5096-5p could be adopted as a companion biomarker of ^{18}F-FDG PET/CT to improve PanNET stratification and predictivity of PRRT efficacy. Interestingly, circulating hsa-miR-5096-5p showed a mild inverse correlation with 68Ga-DOTATOC PET/CT SUVmax, and this negative correlation is further associated with 18F-FDG-PET/CT positivity in patients displaying low and high levels of hsa-miR-5096-5p (cut-off:70; Figure 19b). Of clinical relevance hsa-miR-5096-5p levels intercept a subgroup of 18F-FDG-PET positive patients that do not benefit of PRRT. This observation suggests that 18F-FDG-PET status in combination with hsa-miR-5096 determination in the blood allows to spare PanNEN patients

ineffective PRRT and overtreatment. We further confirmed the inverse correlation of SSTR2 and hsa-miR-5096-5p expression also at the single cell level on PanNET tissue specimens. In this context, we set up the miR-Protein *in situ* protocol to detect on the same tissue section both markers, using a semi-automated and robust procedure which also allowed us to save valuable patient's material. Of note, the novel miR-Protein detection and dedicated AND-Tool software of analysis provided the simultaneous detection of miRNAs and proteins, followed by standardized, operator independent measurements, turning qualitative *in situ* revelation into a quantitative analysis. Specifically, our novel staining workflow allows the automatization and avoids antigen degradation which typically occurs when immunohistochemistry is performed prior to ISH. In addition, the usage of DAB-brown staining, in contrast to typical blue used for ISH labeling, was crucial to ensure miRNA staining stability and to discriminate DAB-brown positive from negative nuclei (counterstained with hematoxylin) allowing AND-Tool software-based analysis. We believe our results sustain hsa-miR-5096-5p direct involvement in SSTR2 turnover into PanNET cells. Indeed, hsa-miR-5096-5p ectopic overexpression in PanNET insulinoma NT-3 cells leads to a significant decrease of SSTR2 transcript quantity, while hsa-miR-5096-5p inhibition significantly boosted SSTR2 expression both in QGP-1 and NT-3 cells substantiating direct targeting and regulation in PanNETs characterized by SSTR2^{low}/hsa-miR-5096-5p^{high} phenotype. Notably, NT-3 cells treated with growth factors are characterized by increased ki-67%, hsa-miR-5096-5p induction and decreased SSTR2 level, consistent with a more aggressive phenotype and with data observed in patients. From this perspective hsa-miR-5096-5p seems to contribute to a metabolic switch leading to lineage differentiation in PanNET cells. Of note, hsa-miR-5096-5p has been involved in glioblastoma biology and reported to be overexpressed in breast cancer and binds with high affinity about 725 target genes (42-44).

Several limitations of our study must be acknowledged for correct interpretation of the results. In order to provide adequate statistical power, robustness and translatability for clinical management we encourage further validation on external, enlarged and independent prospective cohorts. Here, we assessed hsa-miR-5096-5p circulating levels at baseline, focusing on its performance as prognostic biomarker for patient stratification prior to PRRT treatment, alone or in combination with hsa-miR-let7i (P2, if multianalyte assessment is preferred) and on its functional role in PanNET biology and SSTR2 modulation, providing the proof of concept of potential therapeutic compounds. In this context, we performed in vitro experiments on NT-3 cells that are the most representative, and validated cell model for low grade PanNET studies. Indeed, NT-3 cells express SSTR1, 2, 3 and 5 (35) isoforms and our analysis focused on SSTR2 which contains multiple target sequences for hsa-miR-5096-5p in its 3'-UTR and because of its prevalence and clinical relevance in PanNETs, as target

of PRRT. Intriguingly, the 3'-UTR of SSTR3 harbors a single hsa-miR-5096-5p predicted target site (TargetScan_Vert source), which may also determine a modulation of SSTR turnover and signaling in NET disease. In addition, the observation on high grade PanNET BON-1 and QGP-1 cell lines further supported the existence of a hsa-miR-5096-5p/SSTR2 axis and the hsa-miR-5096-5p mediated interference on SSTR2 transcripts. Accordingly, hsa-miR-5096-5p inhibitor was more effective on QGP-1 cells in triggering a significant SSTR2 upregulation since QGP-1 displayed higher levels of hsa-miR-5096-5p and lower SSTR-2 amounts compared to BON-1 cells. Our results lay the conceptual basis for a novel therapeutic for PanNET management, in order to sensitize tumor cells to PRRT via the delivery of specific hsa-miR-5096-5p inhibitory molecules. We can hypothesize to select B or T lymphocytes as "CAR-go" for small-molecules delivery, in particular B lymphocytes are easy to cultivate, to transfect and they are naturally able to carry and shed different types of molecules, including miRNAs. In addition, B lymphocytes are very easy to "arm" with specific antibodies to increase therapeutic specificity and thus effectiveness andlimiting off-target effects since they constitutively express FCγRII receptor (CD32).
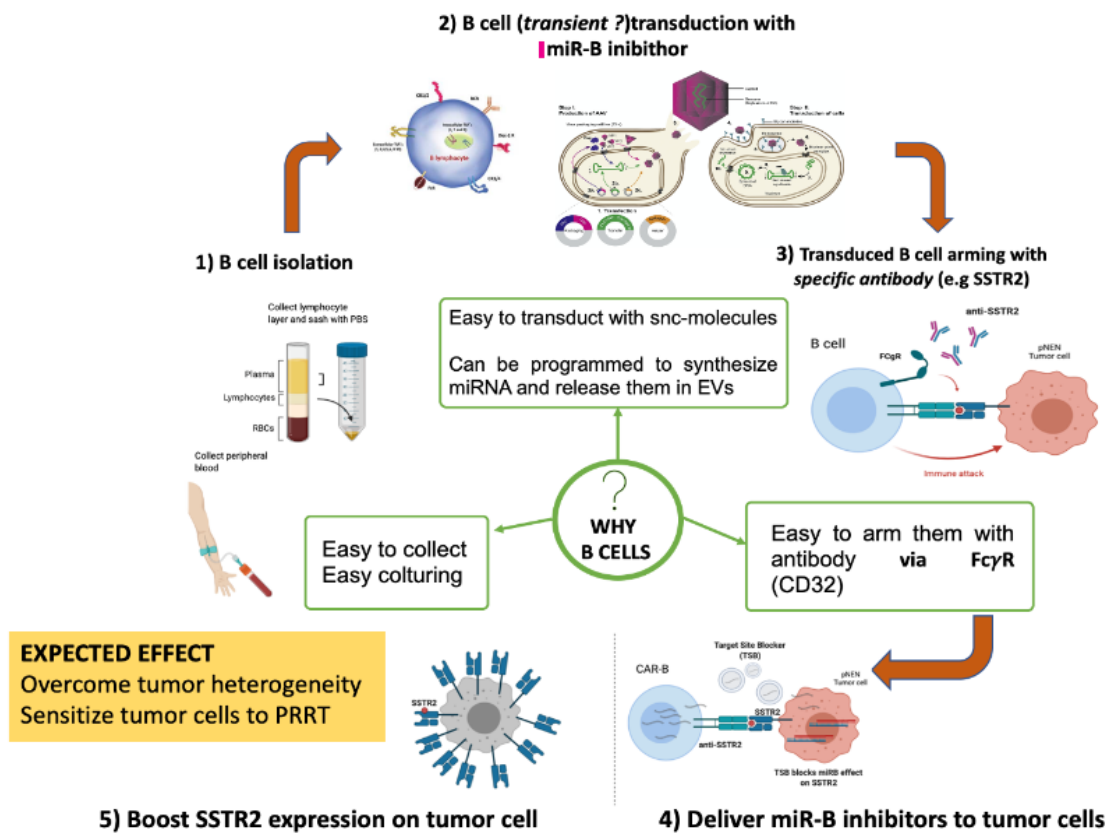

Figure 25 Potential cell therapy workflow for SSTR2 enhanced targeting
Schematic representation of hsa-mir-5096 inihibition based cell therapy. (1) B-cell isolation from whole blood; (2) B-cell transduction to produce hsa-mir-5096 ibhibitors; (3) Transducted B-cells

loading with specific tumor-targeting antibody; (4) Systemic delivery of autologous CAR-B-cell to tumor site; (5) CAR-B-cell targeting tumor cell to promote hsa-mir-5096 ibhibition and SSTR-2 upregulation at cell membrane, increasing their sensitivity to SSTR2 based treatments (e.g. PRRT).

6. Conclusions

Overall this PhD study has led to a candidate prognostic and low-complexity miRNA signature easily retrievable in plasma of PanNET patients. The potential clinical utility of hsa-miR-5096-5p alone or in combination with hsa-let-7i-3p relies on its prognostic power in predicting metabolic aggressiveness which will help in the stratification of PRRT-treated PanNET patients. Moreover, our findings suggest that hsa-miR-5096-5p can be expressed by tumor cells and released in biofluids through exosomes, which are vectors for miRNA signaling and can downmodulate SSTR2 expression in normal and tumor cells via a paracrine mechanism. This mechanism may contribute to tumor heterogeneity and to the development of a refractory phenotype and/or relapse to PRRT. Moving from this rationale we are now working on a therapeutic approach aimed at interfering with hsa-miR-5096-5p activity. Inhibiting its targeting of SSTR2 3'-UTR sequences, would enhance SSTRs expression and sensitize tumor cells to PRRT or other SSTR-targeted therapies. This could be achieved by exploiting nanoparticle delivery systems or microvesicles derived from immune cells as cargos for small molecules. To this aim B lymphocytes should be preferred, due to their inherent ability to synthesize and release high amounts of small-molecules. In this context, B lymphocytes could be transduced to produce hsa-miR-5096-5p inhibitors and then functionalized to deliver it towards a specific target at the tumor site.

References

1. Andreasi, V., Partelli, S., Muffatti, F., Manzoni, M.F., Capurso, G., Falconi, M., 2021. Update on gastroenteropancreatic neuroendocrine tumors. Dig.Liver Dis. 53, 171-182.

2. Bocchini, M., Nicolini, F., Severi, S., Bongiovanni, A., Ibrahim, T., Simonetti, G., Grassi, I., Mazza, M., 2020. Biomarkers for Pancreatic Neuroendocrine Neoplasms (PanNENs) Management-An Updated Review. Front.Oncol. 10, 831.

3. Halfdanarson TR, Rabe KG, Rubin J, Petersen GM. Pancreatic neuroendocrine tumors (PNETs): incidence, prognosis and recent trend toward improved survival. Ann Oncol. (2008) 19:1727–33. doi: 10.1093/annonc/mdn351

4. Dasari A, Shen C, Halperin D, Zhao B, Zhou S, Xu Y, et al. Trends in the incidence, prevalence, and survival outcomes in patients with neuroendocrine tumors in the united states. JAMA oncology. (2017) 3:1335– 42. doi: 10.1001/jamaoncol.2017.0589

5. Modlin IM, Öberg K, Chung DC, Jensen RT, de Herder WW, Thakker RV, et al. Gastroenteropancreatic neuroendocrine tumours. Lancet Oncol. (2008) 9:61–72. doi: 10.1016/S1470-2045(07)70410-2

6. Anlauf M, Garbrecht N, Bauersfeld J, Schmitt A, Henopp T, Komminoth P, et al. Hereditary neuroendocrine tumors of the gastroenteropancreatic system. *Virchows Arch.* (2007) 451 Suppl 1:S29–38. doi: 10.1007/s00428-007-0450-3

7. Falconi M, Eriksson B, Kaltsas G, Bartsch DK, Capdevila J, Caplin M, et al. ENETS consensus guidelines update for the management of patients with functional pancreatic neuroendocrine tumors and non- Functional pancreatic neuroendocrine tumors. *Neuroendocrinology.* (2016). 153–171. doi: 10.1159/000443171

8. Modlin IM, Gustafsson BI, Moss SF, Pavel M, Tsolakis AV, Kidd M. Chromogranin a–biological function and clinical utility in neuro endocrine tumor disease. *Ann Surg Oncol.* (2010) 17:2427– 43. doi: 10.1245/s10434-010-1006-3

9. Marx SJ, Simonds WF. Hereditary hormone excess: genes, molecular pathways, and syndromes. *Endocr Rev.* (2005) 26:615–61. doi: 10.1210/er.2003-0037

10. Lemmens I, Van de Ven WJ, Kas K, Zhang CX, Giraud S, Wautot V, et al. Identification of the multiple endocrine neoplasia type 1 (MEN1) gene. The European Consortium on MEN1. *Hum Mol Genet.* (1997) 6:1177– 83. doi: 10.1093/hmg/6.7.1177

11. Lemos MC, Thakker RV. Multiple endocrine neoplasia type 1 (MEN1): analysis of 1336 mutations reported in the first decade following identification of the gene. *Hum Mutat.* (2008) 29:22–32. doi: 10.1002/humu.20605

12. Perren A, Anlauf M, Henopp T, Rudolph T, Schmitt A, Raffel A, et al. Multiple endocrine neoplasia type 1 (MEN1): loss of one mEN1 allele in tumors and monohormonal endocrine cell clusters but not in islet hyperplasia of the pancreas. *J Clin Endocrinol Metab.* (2007) 92:1118– 28. doi: 10.1210/jc.2006-1944

13. Jiao Y, Shi C, Edil BH, de Wilde RF, Klimstra DS, Maitra A, et al. DAXX/ATRX, mEN1, and mTOR pathway genes are frequently altered in pancreatic neuroendocrine tumors. *Science.* (2011) 331:1199– 203. doi: 10.1126/science.1200609

14. Scarpa A, Chang DK, Nones K, Corbo V, Patch A-M, Bailey P, et al. Whole- genome landscape of pancreatic neuroendocrine tumours. *Nature.* (2017) 543:65–71. doi: 10.1038/nature21063

15. Crona J, Skogseid B. GEP- nETS uPDATE: genetics of neuroendocrine tumors. *Eur J Endocrinol.* (2016) 174:R275–90. doi: 10.1530/EJE-15-0972

16. Kreutzfeldt S, Apostolidis L, Oles M, Horak P, Heilig CE, Heining C, et al. Abstract 919: clinical relevance of comprehensive genomic analysis in patients with advanced-stage neuroendocrine neoplasms: results from the mASTER trial of the german cancer consortium. *Cancer Res.* (2019) 79:9191. doi: 10.1158/1538-7445.AM2019-919

17. Corbo V, Dalai I, Scardoni M, Barbi S, Beghelli S, Bersani S, et al. MEN1 in pancreatic endocrine tumors: analysis of gene and protein status in 169 sporadic neoplasms reveals alterations in the vast majority of cases. *Endocr Relat Cancer.* (2010) 17:771–83. doi: 10.1677/ERC-10-0028

18. Swarts DRA, Scarpa A, Corbo V, Van Criekinge W, van Engeland M, Gatti G, et al. MEN1 gene mutation and reduced expression are associated with poor prognosis in pulmonary carcinoids. *J Clin Endocrinol Metab.* (2014) 99:E374–8. doi: 10.1210/jc.2013-2782

19. Hessman O, Lindberg D, Einarsson A, Lillhager P, Carling T, Grimelius L, et al. Genetic alterations on 3p, 11q13, and 18q in nonfamilial and mEN 1-associated pancreatic endocrine tumours. *Genes Chromosomes Cancer.* (1999) 26:258–64.

20. Thakker RV. Multiple endocrine neoplasia type 1 (MEN1). *Best Pract Res Clin Endocrinol Metab.* (2010) 24:355–70. doi: 10.1016/j.beem.2010.07.003

21. Scarpa A. The landscape of molecular alterations in pancreatic and small intestinal neuroendocrine tumours. *Ann Endocrinol (Paris).* (2019) 80:153– 8. doi: 10.1016/j.ando.2019.04.010

22. Milne TA, Hughes CM, Lloyd R, Yang Z, Rozenblatt-Rosen O, Dou Y, et al. Menin and mLL cooperatively regulate expression of cyclin- dependent kinase inhibitors. Proc Natl Acad Sci USA. (2005) 102:749– 54. doi: 10.1073/pnas.0408836102

23. Wang Y, Ozawa A, Zaman S, Prasad NB, Chandrasekharappa SC, Agarwal SK, et al. The tumor suppressor protein menin inhibits aKT activation by regulating its cellular localization. *Cancer Res.* (2011) 71:371– 82. doi: 10.1158/0008-5472.CAN-10-3221

24. Fang M, Xia F, Mahalingam M, Virbasius C-M, Wajapeyee N, Green MR. MEN1 is a melanoma tumor suppressor that preserves genomic integrity by stimulating transcription of genes that promote homologous recombination-directed dNA repair. *Mol Cell Biol.* (2013) 33:2635– 47. doi: 10.1128/MCB.00167-13

25. Francis J, Lin W, Rozenblatt-Rosen O, Meyerson M. The menin tumor suppressor protein is phosphorylated in response to dNA damage. *PLoS ONE.* (2011) 6:e16119. doi: 10.1371/journal.pone.0016119

26. Borsari S, Pardi E, Pellegata NS, Lee M, Saponaro F, Torregrossa L, et al. Loss of p27 expression is associated with mEN1 gene mutations in sporadic parathyroid adenomas. *Endocrine.* (2017) 55:386– 97. doi: 10.1007/s12020-016-0941-6

27. Scarpa A. The landscape of molecular alterations in pancreatic and small intestinal neuroendocrine tumours. *Ann Endocrinol (Paris).* (2019) 80:153– 8. doi: 10.1016/j.ando.2019.04.010

28. Sorbye H, Baudin E, Borbath I, Caplin M, Chen J, Cwikla JB, et al. Unmet needs in high-Grade gastroenteropancreatic neuroendocrine neoplasms (WHO g3). *Neuroendocrinology.* (2019) 108:54–62. doi: 10.1159/000493318

29. Schmitt AM, Schmid S, Rudolph T, Anlauf M, Prinz C, Klöppel G, et al. VHL inactivation is an important pathway for the development of malignant sporadic pancreatic endocrine tumors. *Endocr Relat Cancer.* (2009) 16:1219– 27. doi: 10.1677/ERC-08-0297

30. Johannessen CM, Reczek EE, James MF, Brems H, Legius E, Cichowski K. The nF1 tumor suppressor critically regulates tSC2 and mTOR. *Proc Natl Acad Sci USA.* (2005) 102:8573–8. doi: 10.1073/pnas.0503224102

31. Missiaglia E, Dalai I, Barbi S, Beghelli S, Falconi M, Peruta della M, et al. Pancreatic endocrine tumors: expression profiling evidences a role for aKT-mTOR pathway. *J Clin Oncol.* (2010) 28:245–55. doi: 10.1200/JCO.2008.21.5988

32. Marinoni I, Kurrer AS, Vassella E, Dettmer M, Rudolph T, Banz V, et al. Loss of dAXX and aTRX are associated with chromosome instability and reduced survival of patients with pancreatic neuroendocrine tumors. *Gastroenterology.* (2014) 146:453–60.e5. doi: 10.1053/j.gastro.2013.10.020

33. Pea A, Yu J, Marchionni L, Noe M, Luchini C, Pulvirenti A, et al. Genetic analysis of small well-differentiated pancreatic neuroendocrine tumors identifies subgroups with differing risks of liver metastases. *Ann Surg.* (2020) 271:566–73. doi: 10.1097/SLA.0000000000003022

34. Starker LF, Carling T. Molecular genetics of gastroenteropancreatic neuroendocrine tumors. Curr Opin Oncol. (2009) 21:29– 33. doi: 10.1097/CCO.0b013e328319ea7b

35. Nagano Y, Kim DH, Zhang L, White JA, Yao JC, Hamilton SR, et al. Allelic alterations in pancreatic endocrine tumors identified by genome- wide single nucleotide polymorphism analysis. Endocr Relat Cancer. (2007) 14:483–92. doi: 10.1677/ERC-06-0090

36. Capurso G, Festa S, Valente R, Piciucchi M, Panzuto F, Jensen RT, et al. Molecular pathology and genetics of pancreatic endocrine tumours. J Mol Endocrinol. (2012) 49:R37–50. doi: 10.1530/JME-12-0069

37. Esposito I, Segler A, Steiger K, Klöppel G. Pathology, genetics and precursors of human and experimental pancreatic neoplasms: an update. Pancreatology. (2015) 15:598–610. doi: 10.1016/j.pan.2015.08.007

38. Kim DH, Nagano Y, Choi I-S, White JA, Yao JC, Rashid A. Allelic alterations in well-differentiated neuroendocrine tumors (carcinoid tumors) identified

39. Dreijerink KM, Hackeng WM, Singhi AD, Heaphy CM, Brosens LA (2022) Clinical implications of cell-of-origin epigenetic char- acteristics in non-functional pancreatic neuroendocrine tumors. J Pathol 256: 143-148.

40. **Rindi G,· Mete O.,· Uccella S. , Sylvia L. Asa Overview of the 2022 WHO Classification of Neuroendocrine Neoplasms. Endocrine Pathology (2022) 33:115–154**

41. Sadanandam A, Wullschleger S, Lyssiotis CA, Grötzinger C, Barbi S, Bersani S, et al. A cross-Species analysis in pancreatic neuroendocrine tumors reveals molecular subtypes with distinctive

clinical, metastatic, developmental, and metabolic characteristics. *Cancer Discov.* (2015) 5:1296–313. doi: 10.1158/2159-8290.CD-15-0068

42. Stefanoli M, La Rosa S, Sahnane N, Romualdi C, Pastorino R, Marando A, et al. Prognostic relevance of aberrant dNA methylation in g1 and g2 pancreatic neuroendocrine tumors. *Neuroendocrinology.* (2014) 100:26– 4. doi: 10.1159/000365449

43. Marinoni I, Wiederkeher A, Wiedmer T, Pantasis S, Di Domenico A, Frank R, et al. Hypo-methylation mediates chromosomal instability in pancreatic nET. *Endocr Relat Cancer.* (2017) 24:137–46. doi: 10.1530/ERC-16-0554

44. Di Domenico A, Wiedmer T, Marinoni I, Perren A. Genetic and epigenetic drivers of neuroendocrine tumours (NET). *Endocr Relat Cancer.* (2017) 24:R315–R34. doi: 10.1530/ERC-17-0012

45. Rindi G, Klöppel G, Couvelard A, Komminoth P, Körner M, Lopes JM, et al. TNM staging of midgut and hindgut (neuro) endocrine tumors: a consensus proposal including a grading system. Virchows Arch. (2007). 757–62. doi: 10.1007/s00428-007-0452-1

46. Coriat R, Walter T, Terris B, Couvelard A, Ruszniewski P. Gastroenteropancreatic well-Differentiated grade 3 neuroendocrine tumors: review and position statement. *Oncologist.* (2016) 21:1191–9. doi: 10.1634/theoncologist.2015-0476

47. Rindi G, Klöppel G, Alhman H, Caplin M, Couvelard A, De Herder WW, et al. TNM staging of foregut (neuro)endocrine tumors: a consensus proposal including a grading system. 395–401. doi: 10.1007/s00428-006-0250-1

48. Yachida S, Vakiani E, White CM, Zhong Y, Saunders T, Morgan R, et al. Small cell and large cell neuroendocrine carcinomas of the pancreas are genetically similar and distinct from well-differentiated pancreatic neuroendocrine tumors. *Am J Surg Pathol.* (2012) 36:173– 184. doi: 10.1097/PAS.0b013e3182417d36

49. Pizzi S, Azzoni C, Bassi D, Bottarelli L, Milione M, Bordi C. Genetic alterations in poorly differentiated endocrine carcinomas of the gastrointestinal tract. *Cancer.* (2003) 98:1273–82. doi: 10.1002/cncr.11621

50. Nassar H, Albores-Saavedra J, Klimstra DS. High-grade neuroendocrine carcinoma of the ampulla of vater: a clinicopathologic and immunohistochemical analysis of 14 cases. *Am J Surg Pathol.* (2005) 29:588–94. doi: 10.1097/01.pas.0000157974.05397.4f

51. Zhang H-Y, Rumilla KM, Jin L, Nakamura N, Stilling GA, Ruebel KH, et al. Association of dNA methylation and epigenetic inactivation of rASSF1A and beta-catenin with metastasis in small bowel carcinoid tumors. *Endocrine.* (2006) 30:299–306. doi: 10.1007/s12020-006-0008-1

52. Takizawa N, Ohishi Y, Hirahashi M, Takahashi S, Nakamura K, Tanaka M, et al. Molecular characteristics of colorectal neuroendocrine carcinoma; similarities with adenocarcinoma rather than neuroendocrine tumor. *Hum Pathol.* (2015) 46:1890–900. doi: 10.1016/j.humpath.2015.08.006

53. Makuuchi R, Terashima M, Kusuhara M, Nakajima T, Serizawa M, Hatakeyama K, et al. Comprehensive analysis of gene mutation and expression profiles in neuroendocrine carcinomas of the stomach. *Biomed Res.* (2017) 38:19–27. doi: 10.2220/biomedres.38.19

54. Nishikura K, Watanabe H, Iwafuchi M, Fujiwara T, Kojima K, Ajioka Y. Carcinogenesis of gastric endocrine cell carcinoma: analysis of histopathology and p53 gene alteration. *Gastric Cancer.* (2003) 6:203– 9. doi: 10.1007/s10120-003-0249-0

55. Vijayvergia N, Boland PM, Handorf E, Gustafson KS, Gong Y, Cooper HS, et al. Molecular profiling of neuroendocrine malignancies to identify prognostic and therapeutic markers: a fox chase cancer center pilot study. *Br J Cancer.* (2016) 115:564–70. doi: 10.1038/bjc.20 16.229

56. La Rosa S, Sessa F. *Pancreatic Neuroendocrine Neoplasms*. Berlin: Springer. (2015).

57. Scarpa A, Mantovani W, Capelli P, Beghelli S, Boninsegna L, Bettini R, et al. Pancreatic endocrine tumors: improved tNM staging and histopathological grading permit a clinically efficient prognostic stratification of patients. *Mod Pathol.* (2010) 23:824–33. doi: 10.1038/modpathol.2010.58

58. Scardoni M, Vittoria E, Volante M, Rusev B, Bersani S, Mafficini A, et al. Mixed adenoneuroendocrine carcinomas of the gastrointestinal tract: targeted next-generation sequencing suggests a monoclonal origin of the two components. *Neuroendocrinology.* (2014) 100:310–6. doi: 10.1159/000369071

59. Bergsland EK, Roy R, Stephens P, Ross JS, Bailey M, Olshen A. Genomic profiling to distinguish poorly differentiated neuroendocrine carcinomas arising in different sites. *J Clin Oncol.* (2016) 34:4020– 4020. doi: 10.1200/JCO.2016.34.15_suppl.4020

60. Tang LH, Basturk O, Sue JJ, Klimstra DS. A practical approach to the classification of who grade 3 (G3) well-differentiated neuroendocrine tumor (WD-NET) and poorly differentiated neuroendocrine carcinoma (PD-NEC) of the pancreas. *Am J Surg Pathol.* (2016) 40:1192–202. doi: 10.1097/PAS.0000000000000662

61. Modlin IM, Kidd M, Malczewska A, Drozdov I, Bodei L, Matar S, et al. The nETest: the clinical utility of multigene blood analysis in the diagnosis and management of neuroendocrine tumors. *Endocrinol Metab Clin North Am.* (2018) 47:485–504. doi: 10.1016/j.ecl.2018.05.002

62. Zikusoka MN, Kidd M, Eick G, Latich I, Modlin IM. The molecular genetics of gastroenteropancreatic neuroendocrine tumors. *Cancer.* (2005) 104:2292– 309. doi: 10.1002/cncr.21451

63. Heaphy CM, de Wilde RF, Jiao Y, Klein AP, Edil BH, Shi C, et al. Altered telomeres in tumors with aTRX and dAXX mutations. *Science.* (2011) 333:425. doi: 10.1126/science.1207313

64. Sposito T, Tu M-SN, Rutter GA, Novelli M, Thirlwell C, Salomoni P. Abstract 5294: the panNET-related histone h3.3 chaperone daxx regulates lineage specification and tissue homeostasis in the pancreas. *Cancer Res.* (2019) 79:5294. doi: 10.1158/1538-7445.AM2019-5294

65. de Wilde RF, Heaphy CM, Maitra A, Meeker AK, Edil BH, Wolfgang CL, et al. Loss of aTRX or dAXX expression and concomitant acquisition of the alternative lengthening of telomeres phenotype are late events in a small subset of mEN-1 syndrome pancreatic neuroendocrine tumors. *Mod Pathol.* (2012) 25:1033–9. doi: 10.1038/modpathol.2012.53

66. Fazio N, Milione M. Gastroenteropancreatic neuroendocrine carcinomas: the nET g3 subcategory is a reality. *Oncologist.* (2017) 22:359. doi: 10.1634/theoncologist.2016-0359

67. Ohmoto A, Rokutan H, Yachida S. Pancreatic neuroendocrine neoplasms: basic biology, current treatment strategies and prospects for the future. *IJMS.* (2017) 18:143. doi: 10.3390/ijms18010143

68. Crippa S, Partelli S, Belfiori G, Palucci M, Muffatti F, Adamenko O, et al. Management of neuroendocrine carcinomas of the pancreas (WHO g3): a tailored approach between proliferation and morphology. *WJG.* (2016) 22:9944–53. doi: 10.3748/wjg.v22.i45.9944

69. Swarts DRA, Ramaekers FCS, Speel E-JM. Biochimica et biophysica acta. *BBA - Reviews on Cancer.* (2012) 1826:255– 71. doi: 10.1016/j.bbcan.2012.05.001

70. Compton CC, Byrd DR, Garcia-Aguilar J, Kurtzman SH, Olawaiye A, Washington MK. *AJCC Cancer Staging Atlas*. Berlin: Springer Science & Business Media (2012).

71. International Agency for Research on Cancer. *WHO Classification of Tumours of Endocrine Organs*. Lyon: IARC Who Classification of Tum (2017).

72. Klöppel G. Neuroendocrine neoplasms: Dichotomy, origin and classifications. *Visc Med.* 2017;33:324–330. doi: 10.1159/000481390.

73. Klimstra DS, Kloppel G, La Rosa S, Rindi G. Digestive System Tumours. In: WHO Classification of Tumours. 5th edition. Vol 1. IARC, Lyon, 2019.

74. Cockburn A, Rege TA. Gastrointestinal neuroendocrine lesions. In: Fenoglio-Preiser' Gastrointestinal Pathology. 4th edition. Wolters Kluwer, Alphen aan den Rijn, pp3300-3512, 2017.

75. Rindi G, Klimstra DS, Abedi-Ardekani B, Asa SL, Bosman FT, Brambilla E, Busam KJ, de Krijger RR, Dietel M, El-Naggar AK, et al. A common classification framework for neuroendocrine neoplasms: An international agency for research on cancer (IARC) and World Health Organization (WHO) expert consensus proposal. *Mod Pathol.* 2018;31:1770–1786. doi: 10.1038/s41379-018-0110-y

76. Popa O, Taban SM, Pantea S, Plopeanu AD, Dema ALC. The new WHO classification of gastrointestinal neuroendocrine tumors and immunohistochemical expression of somatostatin receptor 2 and 5. Exp Ther Med. 2021 Oct;22(4):1179. doi: 10.3892/etm.2021.10613. Epub 2021 Aug 13. PMID: 34475969; PMCID: PMC8406677.

77. Drucker DJ, Asa SL, Henderson J, Goltzman D (1989) The parathyroid hormone-like peptide gene is expressed in the nor- mal and neoplastic human endocrine pancreas. Mol Endocrinol 3: 1589-1595.

78. Asa SL, Henderson J, Goltzman D, Drucker DJ (1990) Para- thyroid hormone-like peptide in normal and neoplastic human endocrine tissues. J Clin Endocrinol Metab 71: 1112-1118.

79. Ezzat S, Ezrin C, Yamashita S, Melmed S (1993) Recurrent acro- megaly resulting from ectopic growth hormone gene expression by a metastatic pancreatic tumor. Cancer 71: 66-70.

80. Oberg, K., Krenning, E., Sundin, A. et al., 2016. A Delphic consensus assessment: imaging and biomarkers in gastroenteropancreatic neuroendocrine tumor disease management. Endocr Connect. 5, 174-187.

81. Howe, J.R., Merchant, N.B., Conrad, C. et al., 2020. The North American Neuroendocrine Tumor Society Consensus Paper on the Surgical Management of Pancreatic Neuroendocrine Tumors. Pancreas. 49, 1-33.

82. Mafficini, A. and Scarpa, A., 2018. Genomic landscape of pancreatic neuroendocrine tumours: the International Cancer Genome Consortium. J.Endocrinol. 236, R161-R167.

83. Scarpa, A., Chang, D.K., Nones, K. et al., 2017. Corrigendum: Whole-genome landscape of pancreatic neuroendocrine tumours. Nature. 550, 548.

84. Partelli, S., Bartsch, D.K., Capdevila, J. et al., 2017. ENETS Consensus Guidelines for Standard of Care in Neuroendocrine Tumours: Surgery for Small Intestinal and Pancreatic Neuroendocrine Tumours. Neuroendocrinology. 105, 255-265.

85. Modlin, I.M., Moss, S.F., Chung, D.C., Jensen, R.T., Snyderwine, E., 2008. Priorities for

improving the management of gastroenteropancreatic neuroendocrine tumors. J.Natl.Cancer Inst. 100, 1282-1289.

86. Ahmed, M., 2020. Gastrointestinal neuroendocrine tumors in 2020. World J.Gastrointest.Oncol. 12, 791-807.

87. Nagtegaal, I.D., Odze, R.D., Klimstra, D., Paradis, V., Rugge, M., Schirmacher, P., Washington, K.M., Carneiro, F., Cree, I.A., WHO Classification of Tumours Editorial Board, 2020. The 2019 WHO classification of tumours of the digestive system. Histopathology. 76, 182-188.

88. Inzani, F., Petrone, G., Rindi, G., 2018. The New World Health Organization Classification for Pancreatic Neuroendocrine Neoplasia. Endocrinol.Metab.Clin.North Am. 47, 463-470.

89. Guenter R, Aweda T, Carmona Matos DM, Jang S, Whitt J, Cheng YQ, et al. Overexpression of somatostatin receptor type 2 in neuroendocrine tumors for improved Ga68-DOTATATE imaging and treatment. Surg (United States) . 2020;167(1):189–96.

90. Bodei, L., Ambrosini, V., Herrmann, K., Modlin, I., 2017. Current Concepts in (68)Ga-DOTATATE Imaging of Neuroendocrine Neoplasms: Interpretation, Biodistribution, Dosimetry, and Molecular Strategies. J.Nucl.Med. 58, 1718-1726.

91. Turner GB, Johnston BT, McCance DR, McGinty A, Watson RGP, Patterson CC, et al. Circulating markers of prognosis and response to treatment in patients with midgut carcinoid tumours. *Gut.* (2006) 55:1586– 91. doi: 10.1136/gut.2006.092320

92. Modlin IM, Gustafsson BI, Pavel M, Svejda B, Lawrence B, Kidd M. A nomogram to assess small-intestinal neuroendocrine tumor ("carcinoid") survival. *Neuroendocrinology.* (2010) 92:143–57. doi: 10.1159/000319784

93. Signore, A.; et al. Role of 18-F -FDG PET/CT in the managment of G1 gastenteropancreatic neuroendocrine tumors. *Endocrine* **2022**, *76*, 484–490.

94. Pape U-F, Böhmig M, Berndt U, Tiling N, Wiedenmann B, Plöckinger U. Survival and clinical outcome of patients with neuroendocrine tumors of the gastroenteropancreatic tract in a german referral center. *Ann N Y Acad Sci.* (2004) 1014:222–33. doi: 10.1196/annals.1294.025

95. Veenendaal LM, Borel Rinkes IHM, Lips CJM, van Hillegersberg R. Liver metastases of neuroendocrine tumours; early reduction of tumour load to improve life expectancy. *World J Surg Oncol.* (2006) 4:35. doi: 10.1186/1477-7819-4-35

96. Prosperi D, Gentiloni Silveri G, Panzuto F, Signore A. et al Nuclear Medicine and Radiological Imaging of Pancreatic Neuroendocrine Neoplasms: A Multidisciplinary Update. J Clin Med. 2022 Nov 18;11(22):6836. doi: 10.3390/jcm11226836.

97. Panzuto, F.; Pusceddu, S.; Faggiano, A.; Femia, D.; et al. Prognostic impact of tumour burden in stage IV neuroendocrine neoplasia: A comparison between pancreatic and gastrointestinal localizations. *Pancreatology* 2019, *19*, 1067–1073.

98. Staal, F.C.R.; Aalbersberg, E.A.; van der Velden, D.; Wilthagen, E.A.; Tesselaar, M.E.T.; Beets-Tan, R.G.H.; Maas, M. GEP-NET radiomics: A systematic review and radiomics quality score assessment. *Eur. Radiol.* 2022, *32*, 7278–7294.

99. Reisine, T.; Bell, G.I. Molecular biology of somatostatin receptors. Endocr. Rev. 1995, 16, 427–442.

100. Csaba, Z.; Dournaud, P. Cellular biology of somatostatin receptors. Neuropeptides 2001, 35, 1–23.

101. Reubi, J.C. Peptide receptors as molecular targets for cancer diagnosis and therapy. Endocr. Rev. 2003, 24, 389–427.

102. Reubi, J.C.; Waser, B.; Schaer, J.C.; Laissue, J.A. Somatostatin receptor sst1-sst5 expression in normal and neoplastic human tissues using receptor autoradiography with subtype-selective ligands. Eur. J. Nucl. Med. 2001, 28, 836–846.

103. Eychenne, R.; Bouvry, C.; Bourgeois, M.; Loyer, P.; Benoist, E.; Lepareur, N. Overview of Radiolabeled Somatostatin Analogs for Cancer Imaging and Therapy. Molecules 2020, 25, 4012.

104. Patel, Y.C. Somatostatin and its receptor family. *Front. Neuroendocrinol.* **1999**, *20*, 157–198.

105. Weckbecker, G.; Lewis, I.; Albert, R.; Schmid, H.A.; Hoyer, D.; Bruns, C. Opportunities in somatostatin research: Biological, chemical and therapeutic aspects. *Nat. Rev. Drug Discov.* **2003**, *2*, 999–1017.

106. Krenning, E.P.; Bakker, W.H.; Breeman, W.A.; Koper, J.W.; Kooij, P.P.; Ausema, L.; Lameris, J.S.; Reubi, J.C.; Lamberts, S.W. Localisation of endocrine-related tumours with radioiodinated analogue of somatostatin. *Lancet* **1989**, *1*, 242–244.

107. Heiman, M.L.; Murphy, W.A.; Coy, D.H. Differential binding of somatostatin agonists to somatostatin receptors in brain and adenohypophysis. *Neuroendocrinology* 1987, *45*, 429–436.

108. Mikołajczak, R.; Maecke, H.R. Radiopharmaceuticals for somatostatin receptor imaging. *Nucl. Med. Rev. Cent. East. Eur.* 2016, *19*, 126–132

109. Virgolini, I.; Ambrosini, V.; Bomanji, J.B.; Baum, R.P.; Fanti, S.; Gabriel, M.; Papathanasiou, N.D.; Pepe, G.; Oyen, W.;

110. De Cristoforo, C.; et al. Procedure guidelines for PET/CT tumour imaging with 68Ga-DOTA-conjugated peptides: 68Ga-DOTATOC, 68Ga-DOTA-NOC, 68Ga-DOTA-TATE. *Eur. J. Nucl. Med. Mol. Imaging* 2010, *37*, 2004–2010.

111. Hofmann, M.; Maecke, H.; Börner, R.; Weckesser, E.; Schöffski, P.; Oei, L.; Schumacher, J.; Henze, M.; Heppeler, A.; Meyer, J.; et al. Biokinetics and imaging with the somatostatin receptor PET radioligand (68) Ga-DOTATOC: Preliminary data. *Eur. J. Nucl. Med.* 2001, *28*, 1751–1757.

112. Hofman, M.S.; Lau, W.F.; Hicks, R.J. Somatostatin receptor imaging with 68Ga DOTATATE PET/CT: Clinical utility, normal patterns, pearls, and pitfalls in interpretation. *Radiographics* 2015, *35*, 500–516.

113. Wild, D.; Mäcke, H.R.; Waser, B.; Reubi, J.C.; Ginj, M.; Rasch, H.; Müller-Brand, J.; Hofmann, M. 68Ga-DOTANOC: A first compound for PET imaging with high affinity for somatostatin receptor subtypes 2 and 5. *Eur. J. Nucl. Med. Mol. Imaging* 2005, *32*, 724.

114. Bozkurt, M.F.; Virgolini, I.; Balogova, S.; Beheshti, M.; Rubello, D.; Decristoforo, C.; Ambrosini, V.; Kjaer, A.; Delgado-Bolton, R.; Kunikowska, J.; et al. Guideline for PET/CT imaging of neuroendocrine neoplasms with (68) Ga-DOTA-conjugated somatostatin receptor targeting peptides and (18)F-DOPA. *Eur. J. Nucl. Med. Mol. Imaging* 2017, *44*, 1588–1601.

115. Sundin, A.; Arnold, R.; Baudin, E.; Cwikla, J.B.; Eriksson, B.; Fanti, S.; Fazio, N.; Giammarile, F.; Hicks, R.J.; Kjaer, A.; et al. ENETS consensus guidelines for the standards of care in neuroendocrine tumors: Radiological, nuclear medicine and hybrid imaging. *Neuroendocrinology* 2017, *105*, 212–244.

116. Oberg, K.E., Reubi, J.C., Kwekkeboom, D.J., Krenning, E.P., 2010. Role of somatostatins in gastroenteropancreatic neuroendocrine tumor development and therapy. Gastroenterology. 139, 742-53, 753.e1.

117. Naji, M.; Al-Nahhas, A. ^{68}Ga-labelled peptides in the management of neuroectodermal tumours. *Eur. J. Nucl. Med. Mol. Imaging* 2012, *39* (Suppl. S1), S61–S67.

118. Sharma, P.; Arora, S.; Karunanithi, S.; Khadgawat, R.; Durgapal, P.; Sharma, R.; Kandasamy, D.; Bal, C.; Kumar, R. Somatostatin receptor-based PET/CT imaging with 68Ga-DOTA-Nal3-octreotide for localization of clinically and biochemically suspected insulinoma. *Q. J. Nucl. Med. Mol. Imaging* 2016, *60*, 69–76.

119. Christ, E.; Antwi, K.; Fani, M.; Wild, D. Innovative imaging of insulinoma: The end of sampling? A review. *Endocr. Relat. Cancer* 2020, *27*, R79–R92.

120. Prasad, V.; Sainz-Esteban, A.; Arsenic, R.; Plöckinger, U.; Denecke, T.; Pape, U.F.; Pascher, A.; Kühnen, P.; Pavel, M.; Blankenstein, O. Role of (68)Ga somatostatin receptor PET/CT in the detection of endogenous hyperinsulinaemic focus: An explorative study. *Eur. J. Nucl. Med. Mol. Imaging* 2016, *43*, 1593–1600.

121. Wild, D.; Christ, E.; Caplin, M.E.; Kurzawinski, T.R.; Forrer, F.; Brändle, M.; Seufert, J.; Weber, W.A.; Bomanji, J.; Perren, A.; et al. Glucagon-like peptide-1 versus somatostatin receptor targeting reveals 2 distinct forms of malignant insulinomas. *J. Nucl. Med.* 2011, *52*, 1073–1078.

122. Veltroni, A.; Cosaro, E.; Spada, F.; Fazio, N.; Faggiano, A.; Colao, A.; Pusceddu, S.; Zatelli, M.C.; Campana, D.; Piovesan, A.; et al. Clinico-pathological features, treatments and survival of malignant insulinomas: A multicenter study. *Eur. J. Endocrinol.* 2020, *182*, 439–446.

123. Pattison, D.A.; Hicks, R.J. Molecular imaging in the investigation of hypoglycaemic syndromes and their management. *Endocr. Relat. Cancer* 2017, *24*, R203–R221.

124. Boellaard, R.; Delgado-Bolton, R.; Oyen, W.J.; Giammarile, F.; Tatsch, K.; Eschner, W.; Verzijlbergen, F.J.; Barrington, S.F.; Pike, L.C.; Weber, W.A.; et al. FDG PET/CT: EANM procedure guidelines for tumour imaging: Version 2.0. *Eur. J. Nucl. Med. Mol. Imaging* 2015, *42*, 328–354.

125. Binderup, T.; Knigge, U.; Loft, A.; Federspiel, B.; Kjaer, A. 18F-fluorodeoxyglucose positron emission tomography predicts survival of patients with neuroendocrine tumors. *Clin. Cancer Res.* 2010, *16*, 978–985

126. Abdulrezzak, U.; Kurt, Y.K.; Kula, M.; Tutus, A. Combined imaging with 68Ga-DOTA-TATE and 18F-FDG PET/CT in the basis of volumetric parameters in neuroendocrine tumors. *Nucl. Med. Commun.* 2016, *37*, 874–881.

127. Rinzivillo, M.; Partelli, S.; Prosperi, D.; Capurso, G.; Pizzichini, P.; Iannicelli, E.; Merola, E.; Muffatti, F.; Scopinaro, F.; Schillaci, O.; et al. Clinical usefulness of 18F-fluorodeoxyglucose positron emission tomography in the diagnostic algorithm of advanced entero-pancreatic neuroendocrine neoplasms. *Oncologist* 2018, *23*, 186–192.

128. Ijichi, H.; Shirabe, K.; Taketomi, A.; Yoshizumi, T.; Ikegami, T.; Mano, Y.; Aishima, S.; Abe, K.; Honda, H.; Maehara, Y. Clinical usefulness of 18 F-fluorodeoxyglucose positron emission tomography/computed tomography for patients with primary liver cancer with special reference to rare histological types, hepatocellular carcinoma with sarcomatous change and combined hepatocellular and cholangiocarcinoma. Hepatol. Res. 2013, 43, 481–487.

129. Paiella, S.; Landoni, L.; Tebaldi, S.; Zuffanter, M.; Salgarello, M.; Cingarlini, S.; D'onofrio, M.; Parisi, A.; Deiro, G.; Manfrin, E.; et al. Dual tracer (68Ga-DOTATOC and 18F-FDG) PET/CT scan and G1–G2 nonfunctioning pancreatic neuroendocrine tumors: A single center retrospective evaluation of 124 nonmetastatic resected cases. Neuroendocrinology 2022, 112, 143–152.

130. Severi, S., Nanni, O., Bodei, L., Sansovini, M., Ianniello, A., Nicoletti, S., Scarpi, E.,

Matteucci, F., Gilardi, L., Paganelli, G., 2013. Role of 18FDG PET/CT in patients treated with 177Lu-DOTATATE for advanced differentiated neuroendocrine tumours. Eur.J.Nucl.Med.Mol.Imaging. 40, 881-888.

131.   Chbat J, Amer L, Akirov A, Ezzat S (2021) The diagnosis of neu- roendocrine neoplasms. In: Asa SL, La Rosa S, Mete O, editors. The Spectrum of Neuroendocrine Neoplasia. Cham, Switzerland: Springer Nature. pp. 15–28.

132.   Hofland J, Zandee WT, de Herder WW. Role of biomarker tests for diagnosis of neuroendocrine tumours. *Nat Rev Endocrinol.* (2018) 14:656–9. doi: 10.1038/s41574-018-0082 Kanakis G, Kaltsas G. Biochemical markers for gastroenteropancreatic neuroendocrine tumours (GEP-NETs). *Best Pract Res Clin Gastroenterol.* (2012) 26:791–802. doi: 10.1016/j.bpg.2012.12.006

133.   Tony JC. The chromogranin-secretogranin family. *N Engl J Med.* (2003) 348:2579–80. doi: 10.1056/NEJMra021405

134.   Kanakis G, Kaltsas G. Biochemical markers for gastroenteropancreatic neuroendocrine tumours (GEP-NETs). *Best Pract Res Clin Gastroenterol.* (2012) 26:791–802. doi: 10.1016/j.bpg.2012.12.006

135.   Nobels FR, Kwekkeboom DJ, Coopmans W, Schoenmakers CH, Lindemans J, De Herder WW, et al. Chromogranin a as serum marker for neuroendocrine neoplasia: comparison with neuron-specific enolase and the alpha-subunit of glycoprotein hormones. *J Clin Endocrinol Metab.* (1997) 82:2622–8. doi: 10.1210/jcem.82.8.4145

136.   van Adrichem RCS, Kamp K, Vandamme T, Peeters M, Feelders RA, De Herder WW. Serum neuron-specific enolase level is an independent predictor of overall survival in patients with gastroenteropancreatic neuroendocrine tumors. Ann Oncol. (2016) 27:746–7. doi: 10.1093/annonc/mdv626

137.   Baudin E, Gigliotti A, Ducreux M, Ropers J, Comoy E, Sabourin JC, et al. Neuron-specific enolase and chromogranin a as markers of neuroendocrine tumours. Br J Cancer. (1998) 78:1102–7. doi: 10.1038/bjc.1998.635

138.   Öberg K, Knigge U, Kwekkeboom D, Perren A, ESMO Guidelines Working Group. Neuroendocrine gastro-entero-pancreatic tumors: ESMO Clinical Practice Guidelines for diagnosis, treatment and follow-up. *Ann Oncol.* (2012) 23 Suppl 7:vii124–30. doi: 10.1093/annonc/mds295

139.   Walter T, Chardon L, Chopin-laly X, Raverot V, Caffin A-G, Chayvialle J- A, et al. Is the combination of chromogranin and pancreatic polypeptide serum determinations of interest in the

diagnosis and follow-up of gastro- entero-pancreatic neuroendocrine tumours? *Eur J Cancer.* (2012) 48:1766– 73. doi: 10.1016/j.ejca.2011.11.005

140. Panzuto F, Severi C, Cannizzaro R, Falconi M, Angeletti S, Pasquali A, et al. Utility of combined use of plasma levels of chromogranin a and pancreatic polypeptide in the diagnosis of gastrointestinal and pancreatic endocrine tumors. *J Endocrinol Invest.* (2004) 27:6–11. doi: 10.1007/bf03350903

141. Tsai HK, Hornick JL, Vivero M (2020) INSM1 expression in a subset of thoracic malignancies and small round cell tumors: rare potential pitfalls for small cell carcinoma. Mod Pathol 33: 1571-1580.

142. Kanitra JJ, Hardaway JC, Soleimani T, Koehler TJ, McLeod MK, Kavuturu S (2018) Adrenocortical oncocytic neoplasm: A systematic review. Surgery 164: 1351-1359.

143. 47. Ohara Y, Oda T, Hashimoto S, Akashi Y, Miyamoto R, Enomoto T, Satomi K, Morishita Y, Ohkohchi N (2016) Pancreatic neuroendo- crine tumor and solid-pseudopapillary neoplasm: Key immunohis- tochemical profiles for differential diagnosis. World J Gastroenterol 22: 8596-8604.

144. Morimoto M, Nishinakamura R, Saga Y, et al. Different assemblies of Notch receptors coordinate the distribution of the major bronchial Clara, ciliated and neuroendocrine cells. Development. 2012;139 (23):4365–4373.

145. Bray SJ. Notch signalling in context. Nat Rev Mol Cell Biol. 2016;17 (11):722–735.

146. Sabari JK, Lok BH, Laird JH, et al. Unravelling the biology of SCLC: implications for therapy. Nat Rev Clin Oncol. 2017;14(9):549–561.

147. Saunders LR, Bankovich AJ, Anderson WC, et al. A DLL3-targeted antibody-drug conjugate eradicates high-grade pulmonary neu- roendocrine tumor-initiating cells in vivo. Sci Transl Med. 2015;7 (302):302ra136.

148. Puca L, Gavyert K, Sailer V, et al. Delta-like protein 3 expression and therapeutic targeting in neuroendocrine prostate cancer. Sci Transl Med. 2019;11(484).

149. Ranallo N, Bocchini M, Menis J, Bongiovanni A. et al Delta-like ligand 3 (DLL3): an attractive actionable target in tumors with neuroendocrine origin. Expert Rev Anticancer Ther. 2022 Jun;22(6):597-603.

150. Bocchini M, Mazza M, Foca F, Nicolini F, Calogero RA, Severi S, et al. 1385PDNew circulating biomarkers in gastro- entero-pancreatic-neuroendocrine-tumours. Annonc. (2019) 30. doi: 10.1093/annonc/mdz256.005

151.   Hofland J, Kaltsas G, de Herder WW (2020) Advances in the Diagnosis and Management of Well-Differentiated Neuroendocrine Neoplasms. Endocr Rev 41: 5573926.

152.   Akirov A, Larouche V, Alshehri S, Asa SL, Ezzat S (2019) Treat- ment Options for Pancreatic Neuroendocrine Tumors Cancers (Basel) 11

153.   Leon, S., Shapiro, B., Sklaroff, D., Yaros, M., 1977. Free DNA in the serum of cancer patients and the effect of therapy. Cancer Res. 37 (3), 646–650.

154.   Mouliere, F., Rosenfeld, N., 2015. Circulating tumor-derived DNA is shorter than somatic DNA in plasma. Proc. Natl. Acad. Sci. 112 (11), 3178–3179.

155.   Zakka, K., Nagy, R., Drusbosky, L., Akce, M., Wu, C., Alese, O.B., El-Rayes, B.F., Kasi, P. M., Mody, K., Starr, J., 2020. Blood-based next-generation sequencing analysis of neuroendocrine neoplasms. Oncotarget 11 (19), 1749.

156.   Mafficini, A., Scarpa, A., 2018. Genomic landscape of pancreatic neuroendocrine tumours: the international cancer genome consortium. J. Endocrinol. 236 (3), R161–R167.

157.   Rizzo, F.M., Meyer, T., 2018. Liquid biopsies for neuroendocrine tumors: circulating tumor cells, DNA, and MicroRNAs. Endocrinology and Metabolism. Clinics 47 (3), 471–483.

158.   **Smolkova B, Kataki A, Earl J, Ruz-Caracuel I, Cihova M, Urbanova M, Buocikova V, Tamargo S, Rovite V, Niedra H, Schrader J, Kohl Y. Liquid biopsy and preclinical tools for advancing diagnosis and treatment of patients with pancreatic neuroendocrine neoplasms. Crit Rev Oncol Hematol. 2022.**

159.   Mandair, D., Khan, M.S., Lopes, A., Furtado O'Mahony, L., Ensell, L., Lowe, H., Hartley, J.A., Toumpanakis, C., Caplin, M., Meyer, T., 2021. Prognostic threshold for circulating tumor cells in patients with pancreatic and midgut neuroendocrine tumors. J. Clin. Endocrinol. Metab. 106 (3), 872–882.

160.   Puliani, G., Di Vito, V., Feola, T., Sesti, F., Centello, R., Pandozzi, C., Tarsitano, M.G., Verrico, M., Lenzi, A., Isidori, A.M., Giannetta, E., Faggiano, A., 2022. NETest: a systematic review focusing on the prognostic and predictive role. Neuroendocrinology 112 (6), 523–536.

161.   Blázquez-Encinas R, Moreno-Montilla MT, Castaño JP et al. The uprise of RNA biology in neuroendocrine neoplasms: altered splicing and RNA species unveil translational opportunities. Rev Endocr Metab Disord. 2022 Nov 24:1–16.

162.   Havasi, A.; Sur, D.; Cainap, S.S.; Lungulescu, C.-V.; Gavrilas, L.-I.; Cainap, C.; Vlad, C.; Balacescu, O. Current and New Challenges in the Management of Pancreatic Neuroendocrine Tumors: The Role of miRNA-Based Approaches as New Reliable Biomarkers. Int. J. Mol. Sci. 2022, 23, 1109.

163. Weber,J.A.;Baxter,D.H.;Zhang,S.;Huang,D.Y.;HowHuang,K.;JenLee,M.;Galas,D.J.;Wang, K.TheMicroRNASpectrumin Body Fluids. Clin. Chem. 2010, 56, 1733–1741.

164. DiLeva, G.; Garofalo, M.; Croce,C.M. MicroRNAs in Cancer. Annu.Rev.Pathol.Mech.Dis.2014,9,287–314.

165. Krichevsky,A.M.;Gabriely,G.miR-21:A small multifaceted RNA. J.Cell.Mol.Med.2008,13,39–53